GeoArabia, v. 15, no. 1, 2010, p. 49-90
Gulf PetroLink, Bahrain

The sabkha sequence at Mussafah Channel (Abu Dhabi, United Arab Emirates): Facies stacking patterns, microbial-mediated dolomite and evaporite overprint

Christian J. Strohmenger, Abdulla Al-Mansoori, Omar Al-Jeelani, Ali Al-Shamry, Ismail Al-Hosani, Khalil Al-Mehsin and Hesham Shebl

ABSTRACT

The Mussafah Channel is a man-made canal cut perpendicular to the coastline, located to the southwest of the city of Abu Dhabi, United Arab Emirates, and is ideal for studying coastal depositional processes in an arid environment. The channel walls reveal a few meters of Pleistocene reworked dune deposits, unconformably overlain by Holocene carbonates and sabkha evaporites. The Holocene succession consists of intertidal to shallow subtidal sediments that vary significantly along depositional strike direction. Bladed gypsum crystals, gypsum rosettes, and nodular to highly contorted, discontinuous bands of classic sabkha anhydrite are present along the channel walls. Sedimentology, petrography, SEM, X-ray diffraction, and radiocarbon age-dating analyses of the sabkha sequence show the following profile from base to top: (1) non-bedded carbonate-rich sand: reworked aeolianite with an approximate (ca.) radiocarbon age in years (yrs) before present (BP) ca. 26,800 ^{14}C yrs BP; (2) cross-bedded to non-bedded carbonate-rich sand: aeolianite/reworked aeolianite (ca. 24,000–23,500 ^{14}C yrs BP); (3) crinkly-laminated stromatolitic bindstone: intertidal, low-energy microbial mat (ca. 6,600–6,200 ^{14}C yrs BP); (4) lower, discontinuous and in places reworked hardground: cemented channel-lag deposits (ca. 6,400 ^{14}C yrs BP); (5) peloid-skeletal packstone with rootlets or microbial-laminated peloid-skeletal packstone, laterally grading into fine- to coarse-grained, cross-bedded, cerithid-rich, bioclastic packstone, grainstone, and rudstone: lowermost intertidal to shallow subtidal, low-energy, mud-rich rooted and microbial-laminated lagoonal deposits and moderate- to high-energy, intertidal to shallow subtidal tidal-channel, tidal-delta, and tidal-bar deposits (ca. 6,200–5,200 ^{14}C yrs BP); (6) upper discontinuous and shingled hardground: cemented beach rock (ca. 5,700 ^{14}C yrs BP); (7) cross-bedded, bioclastic rudstone/grainstone, grading laterally into intervals displaying bladed gypsum crystals and nodular to enterolithic anhydrite: intertidal to shallow subtidal, high-energy longshore beach bar and beach spit deposits; overprinted by sabkha gypsum and anhydrite (ca. 5,000 ^{14}C yrs BP).

Significant amounts of dolomite were found within the rooted and microbial-laminated mud-rich lagoonal carbonates, some of the tidal-channel/lagoonal deposits, the buried crinkly-laminated microbial mats, and within some of the Pleistocene carbonate-rich sands. The dolomite is very fine-crystalline and displays spherical morphologies as well as subhedral to euhedral dolomite rhombohedra. The formation of dolomite is interpreted to be related to dolomite-mediating microbial organisms which form the widespread microbial mat along the Abu Dhabi coastline. Microbial organisms are also present within the rooted and microbial-laminated lagoonal carbonates and, most probably, within all the other studied carbonates and the Pleistocene carbonate-rich sands. Biopolymers of microbial origin, referred to as Extracellular Polymeric Substances (EPS), are interpreted to play a key role in primary dolomite formation.

The sabkha sequence at Mussafah Channel formed during the post-glacial Flandrian transgression, resulting in the reworking of the Pleistocene aeolian dunes and the deposition of intertidal to shallow subtidal carbonates. Recent find of whale bones within tidal-channel deposits overlying the microbial mat further document the initial Holocene transgression. During a subsequent slight sea-level fall (regression), these carbonates were overprinted by gypsum and anhydrite.

The observed lateral and vertical facies variations reflect primary reservoir quality variations, an important aspect to be considered for geological facies and reservoir quality modeling.

INTRODUCTION

Studies of recent sediments are a fundamental tool in interpretation of features observed in ancient cores and outcrops. The modern arid carbonate-evaporite depositional environments along the Abu Dhabi coastline and offshore Abu Dhabi, United Arab Emirates, are among the few areas of the world where geoscientists can observe the interplay between carbonate and evaporite sedimentation. Geoscientists from all over the world have studied the famous Abu Dhabi sabkha since the early 1960s (Wells, 1962; Curtis et al., 1963; Kendall and Skipwith, 1968, 1969; Evans et al., 1969; Kinsman, 1969; Butler, 1969, 1970; Purser, 1973; Schneider, 1975; Kinsman and Park, 1976; Leeder and Zeidan, 1977; Park, 1977; Patterson and Kinsman, 1977, 1981, 1982; McKenzie et al., 1980; McKenzie, 1981; Butler et al., 1982; Shearman, 1983; Shinn, 1983; Warren and Kendall, 1985; Kendall and Warren, 1988; Kenig et al., 1990; Müller et al., 1990; Kenig, 1991; Wenk et al., 1993; Alsharhan and Kendall, 1994; Baltzer et al., 1994; Kendall et al., 1994, 2002; Evans, 1995; Peebles et al., 1995; Kirkham, 1997, 1998; Alsharhan et al., 1998; Sanford and Wood, 2001; Alsharhan and Kendall, 2002; Wood and Sanford, 2002; Wood et al., 2002, 2005; Evans and Kirkham, 2002; Strohmenger et al., 2004, 2007, 2008a, 2008b, 2008c, 2010; Bontognali, 2008; Jameson et al., 2008; Kening, 2010; Bontognali et al., 2010).

One much-visited locality is the Mussafah Channel, a man-made canal, dredged into the sabkha near the Mussafah Industrial Area to the southwest of the city of Abu Dhabi (N24°18′43.62″; E54°31′27.88″; Figures 1a, 1b, and 1c). At Mussafah Channel, vertical sections displaying c. 2 m of Holocene sabkha-overprinted intertidal to shallow subtidal lagoonal sediments are well exposed (Kirkham, 1997). The channel was dredged in 1985 and 1986 and runs west-east perpendicular to the coastline. The studied eastern and southern walls of the channel are over 7 km inland from the landward reach of the restricted lagoon and c. 25 km from the open Arabian Gulf waters (Figures 1a and 1b). The Mussafah Channel crosses the so-called "Evans line" (Figure 1b), a transect where modern sabkha attributes were studied initially (Evans et al., 1969).

Starting at the base, the channel walls show cross-bedded and reworked Pleistocene carbonate-rich aeolian sands being unconformably overlain by a well developed Holocene microbial mat. The latter is overlain by rooted and microbial-laminated lagoonal, tidal-channel, tidal-delta, tidal-bar, and longshore beach-bar and beach spit deposits that are partly to completely overprinted by gypsum and anhydrite. As a good example of Walther's law (Walter 1893-1894), the exposed sabkha sequence at Mussafah Channel represents vertically stacked facies successions that reflect the modern day lateral facies variability along the arid Abu Dhabi coastline (Strohmenger et al., 2004, 2007, 2008a, 2008b, 2008c, 2010; Figure 1b). The stacking patterns of the carbonates and evaporites at Mussafah Channel record the post-glacial Flandrian Holocene sea-level rise (transgression: microbial mat and carbonate deposition) and subsequent sea-level fall (regression: evaporitic overprint).

The sabkha sequence at Mussafah Channel was studied along the eastern and adjacent southern margin of the channel over a lateral distance of c. 700 m. Five vertical sections were studied in greater detail (location 1: MC-1, location 2: MC-2, location 3: MC-3A and MC-3B, and location 4: MC-4; Figures 1c and 2). In addition, lateral changes in facies (location 1a) and evaporitic overprint (location 3a), as well as the site where large bones of a whale have recently been found (location 4a; Figures 1c and 2) were closely examined.

Our detailed studies show that the "classical" sabkha sequence at Mussafah Channel represents a stranded Holocene sea-level highstand of marine deposits, altered by evaporites that most likely precipitated around paleo-groundwater tables during a subsequent 2–3 meter slight sea-level fall.

Methods

A total of 50 samples have been collected for thin section and 44 samples for whole rock and clay fraction X-ray diffraction (XRD) analyses. Fourteen samples were sampled for radiocarbon age-dating.

Thin sections and outcrop sections were described using Dunham classification/sedimentary texture (Dunham, 1962) with supplements by Embry and Klovan (1971). For each sample the facies type

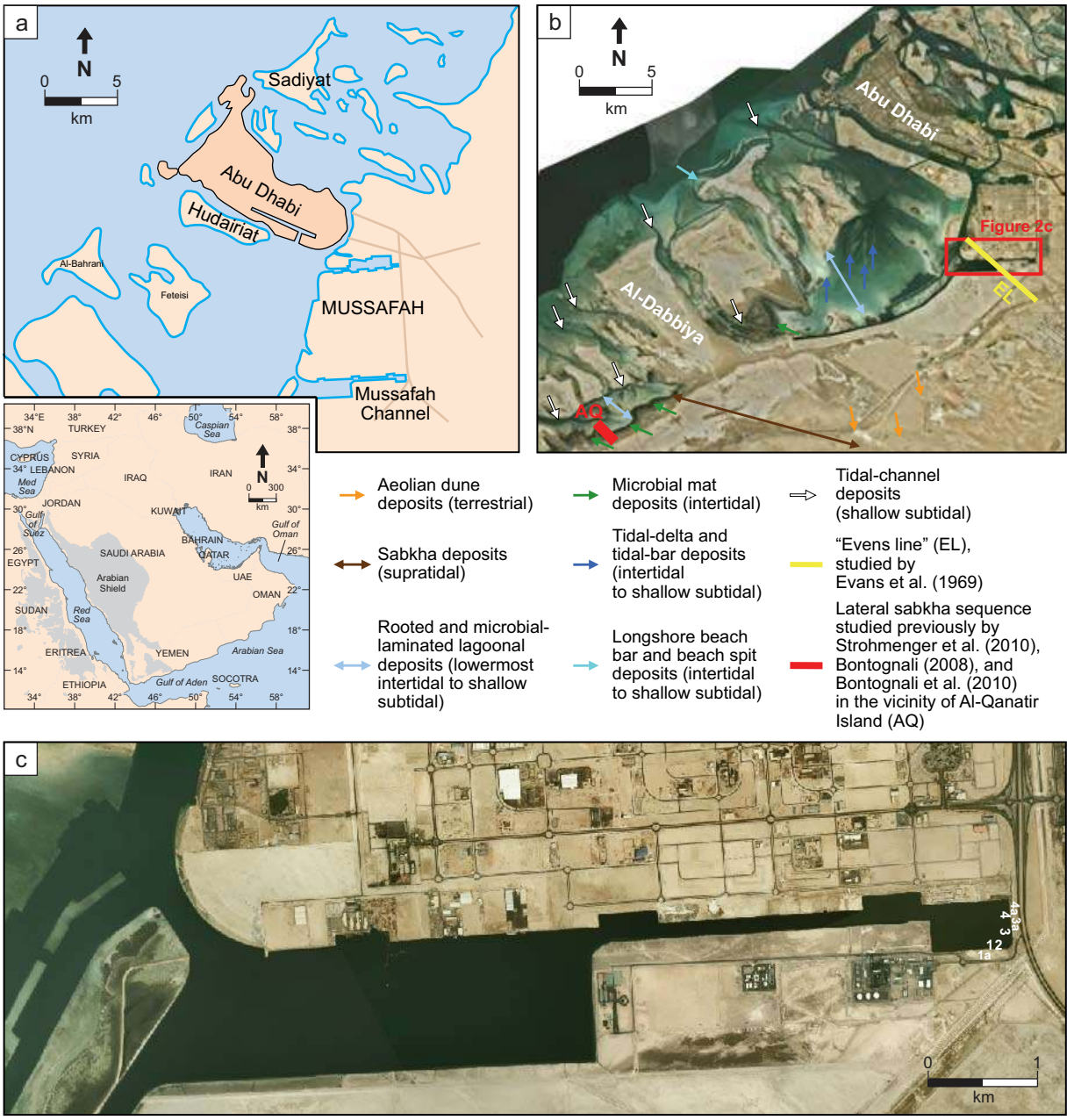

Figure 1: (a) Location map showing the Arabian Peninsula and the United Arab Emirates (inset) the city of Abu Dhabi and the location of the Mussafah Channel.

(b) Satellite image showing the Mussafah Channel southwest of the city of Abu Dhabi (red box) and modern day carbonate depositional environments along the Abu Dhabi coastline. The modern day carbonate depositional environments are marked by arrows and compared with the vertically stacked sediments at the southern and eastern walls of the Mussafah Channel (Figure 1c). Digitalglobe Quickbird satellite imagery, vintage 2006. Image processing by maps geosystems.

(c) Close-up of the Mussafah Channel (red box, Figure 1b) showing the locations of the four measured vertical sections MC-1 to MC-4 (location 1: MC-1, location 2: MC-2, location 3: MC-3, and location 4: MC-4). Facies transitions along the southern wall (location 1a), and diagenetic (evaporite) features along the eastern wall of the channel (location 3a), as well as the location of the whale excavation site (location 4a) are also shown. Digitalglobe Quickbird satellite imagery, vintage 2006. Image processing by maps geosystems.

and its depositional environment was interpreted using microscopic (sedimentary textures and grain types) and macroscopic (sedimentary structures) criteria. Facies and depositional environment of the samples correspond to the modern day facies associations, forming under arid conditions along the Abu Dhabi coastline (Figure 1b).

The cumulative weight percentages of non-clay minerals are shown along each photograph of the vertical sections MC-1 to MC-4. The mineralogical data given for each of the 44 analyzed samples are relative, not absolute. The weight percentage of a mineral within a given sample may vary considerably depending on the location of the sample. The presence/absence of minerals and their relative proportions are better guides than the absolute concentration. The XRD results were compared to petrographic thin section analyses and adjusted where needed. The seven analyzed carbonate-rich sand samples (MC1-1, MC-1-2, MC-1-3, MC-2-1, MC-3A-1, MC-3B-1, and MC4-1) showed c. 30–50% siliciclastic grains (quartz, plagioclase, and feldspar) with c. 50–70% carbonate material (predominantly foraminifera and red algal clasts). It should be noted that grain frequency and XRD derived weight percentages may differ in poly-mineralic sediment samples due to differences in grain density between solid clastic grains and porous carbonate grains. Carbonate grains that are hydraulically equivalent to clastic grains are significantly larger (Wanless et al., 1981). The slightly larger grain size of the carbonate material (foraminifera and red algal clasts: very fine upper to fine upper, vfU-fU) compared to the clastic material (quartz, plagioclase, and feldspar: very fine lower to fine lower, vfL-fL) may have contributed to a slight overrepresentation of carbonate grain weight percentages of the carbonate-rich sand samples. The bimodal grain size distribution within the aeolian deposits can be explained by the relatively lower density of the carbonate material (foraminifera and red algal clasts), compared to the siliciclastic grains. Abundant microporosity within the foraminifera and the red algal clasts (micro-intraparticle porosity) is interpreted to allow bigger (but lighter) carbonate grains to be transported together with smaller (but heavier) siliciclastic grains. In any case, the high amount of carbonate material indicates that the Pleistocene aeolian dunes formed relatively close to the shoreline. With the "Shamal" winds blowing mainly from the north-northwest, carbonate material was constantly wind-transported landward and incorporated into the aeolian dunes; similar processes happen today along the Abu Dhabi coastline. XRD results also showed that the clay fraction of the samples was very low, below measurement in 21 samples and less than 10% in 23 samples.

Radiocarbon age-dating was carried out on bulk samples of four carbonate-rich sand samples (MC1-1, MC-1-2, MC-2-1, and MC-3A-1), four microbial mat samples (MC-1-4, MC-2-2, MC-3A-2, and MC-4-2) and two hardground samples (MC-3A-7 and MC-3B-2). In addition, radiocarbon age-dating has been carried out on selected shells from three cross-bedded, cerithid-rich, bioclastic grainstone, grainstone/rudstone, and rudstone/grainstone samples (MC-3A-5, MC-3B-6, and MC-3B-11), and one fine-grained/coarse-grained, bioclastic grainstone sample (MC-4-4). Standard radiometric analysis was used for the six carbonate samples (MC-3A-5, MC-3A-7, MC-3B-2, MC-3B-6, MC-3B-11, and MC-4-4). The ^{14}C ages of the four carbonate-rich sand samples (MC1-1, MC-1-2, MC-2-1, and MC-3A-1) and the four microbial mat samples (MC-1-4, MC-2-2, MC-3A-2, and MC-4-2) were determined using the accelerator-mass-spectrometer (AMS) technique, where only the organic matter is used for age-dating after removal of the carbonate fraction. The radiocarbon age-dating results are given as the delta ^{13}C-corrected, un-calibrated conventional ^{14}C age in years before present (^{14}C yrs BP). Carbon-isotopic values are reported in delta (δ) ‰ PDB (international standard: Pee Dee Belemnite). The radiocarbon age-dating was carried out by Beta Analytic Inc., Miami. The samples show a range from ca. 26,800 ^{14}C yrs BP (Pleistocene: carbonate-rich sand, sample MC-1-1) to ca. 5,000 ^{14}C yrs BP (Holocene: gypsum-rich, cross-bedded, bioclastic rudstone/grainstone, sample MC-3B-11).

Scanning electron microcopy (SEM) together with energy-dispersive X-ray spectrometer (EDX) analysis on dolomite samples were performed by Tomaso Bontognali (ETH Zurich, Switzerland). Images and EDX analyses were obtained with a backscatter detector, an accelerating voltage of 12 kV, and a working distance of 10 mm.

THE SABKHA SEQUENCE AT MUSSAFAH CHANNEL

The following is a detailed description of the six studied locations along the southern (locations 1, 1a, and 2) and eastern (locations 3, 3a, 4, and 4a) channel walls (Figures 1c and 2).

Location 1: Vertical Section MC-1

Approximately 1.80 m of vertical section of Pleistocene carbonate-rich sand and unconformably overlying Holocene carbonates and sabkha evaporites are described at location 1 (vertical section MC-1) along the southern channel wall (Figures 1c, 2, and 3a). In the following account, the encountered facies types, their key sedimentary structures and evaporitic overprint, as well as their interpreted depositional environments are listed from base to top:

Fine-grained, carbonate-rich sand (sample MC-1-1)

- sedimentary structure: un-bedded to wavy-bedded
- siliciclastic grain size: very fine lower to very fine upper (vfL-vfU: 60–100 µ)
- carbonate grain size: very fine lower to very fine upper (vfL-vfU: 60–120 µ)
- depositional environment: reworked aeolian dunes (aeolianite; Figures 3a and 3b)

Fine-grained, high-angle cross-bedded, carbonate-rich sand (sample MC-1-2)

- sedimentary structure: high-angle cross-bedded
- siliciclastic grain size: very fine upper to fine lower (vfU-fL: 100–150 µ)
- carbonate grain size: very fine upper to fine upper (vfU-fU: 100–220 µ)
- depositional environment: aeolian dunes (aeolianite; Figures 3a and 3c)

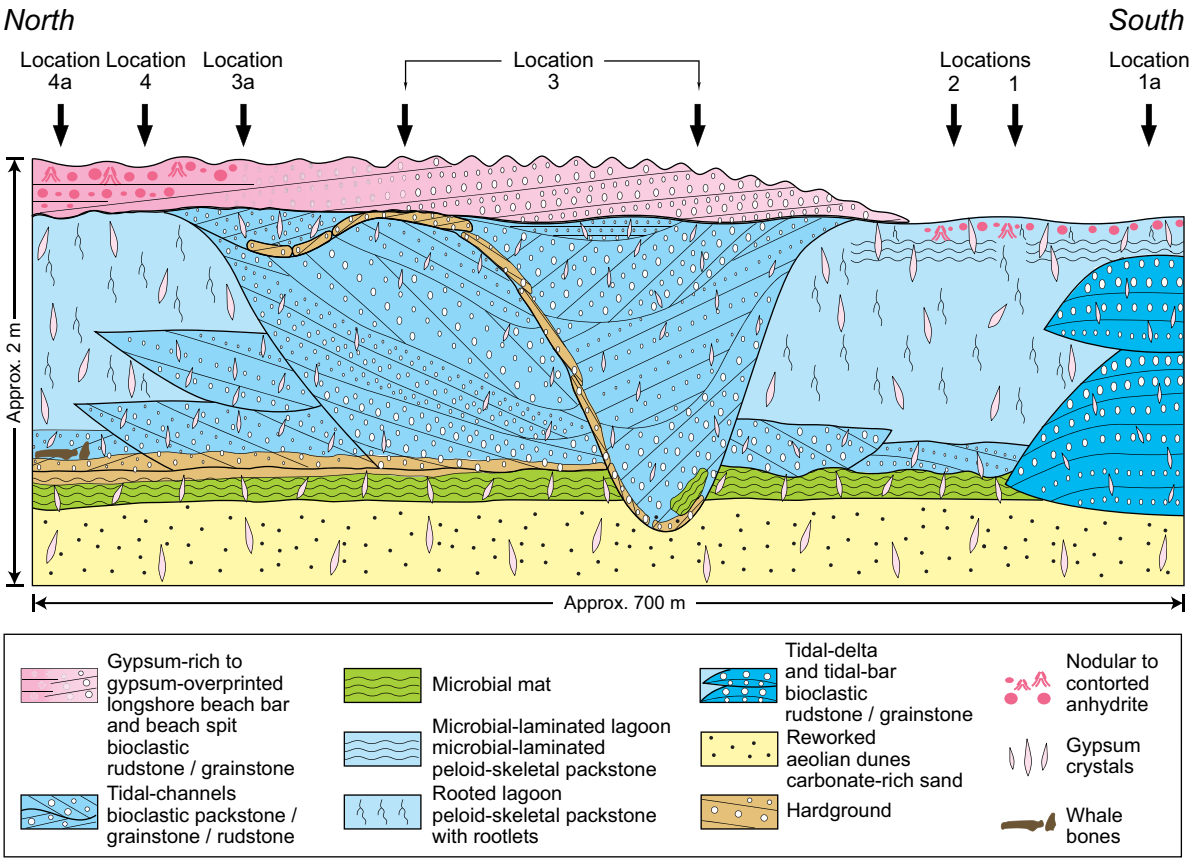

Figure 2: Sketch showing the observed lateral and vertical variations in texture, facies, depositional environment, and diagenetic overprint (hardgrounds, gypsum, and anhydrite) along the studied Mussafah Channel exposures. Also shown are the six studied locations 1: vertical section MC-1, 1a: tidal-delta and tidal-bar deposits, 2: vertical section MC-2, 3: vertical section MC-3, 3a: lateral replacement of gypsum by anhydrite, 4: vertical section MC-4, and 4a: site of whale bone exposure. Locations 1a, 1, and 2, studied at the southern wall of the channel cut (see Figure 1c) are schematically projected onto the eastern wall (locations 3, 3a, 4, and 4a).

Fine-grained, carbonate-rich sand (sample MC-1-3)
- sedimentary structure: un-bedded to wavy-bedded
- siliciclastic grain size: very fine upper (vfU: 100)
- carbonate grain size: very fine upper to fine upper (vfU-fU: 100–220 µ)
- depositional environment: reworked aeolian dunes (aeolianite; Figures 3a and 3d)

Crinkly-laminated stromatolitic bindstone (sample MC-1-4)
- sedimentary texture: boundstone/bindstone
- sedimentary structure: dark organic, crinkly laminated
- depositional environment: intertidal, low-energy microbial mat (Figure 3a)

Cerithid-rich, bioclastic packstone (sample MC-1-5)
- sedimentary texture: mud-lean to mud-rich packstone
- sedimentary structure: low-angle cross-bedded
- depositional environment: shallow subtidal, moderate- to low-energy tidal-channel grading into lowermost intertidal to shallow subtidal, low-energy, mud-rich lagoonal deposits (Figure 3a)

Fine-grained, bioclastic packstone (sample MC-1-6)
- sedimentary texture: mud-lean to mud-rich packstone
- sedimentary structure: low-angle cross-bedded to un-bedded
- depositional environment: shallow subtidal, moderate- to low-energy tidal-channel grading into lowermost intertidal to shallow subtidal, low-energy, mud-rich lagoonal deposits (Figure 3a)

Peloid-skeletal packstone with rootlets (sample MC-1-7)
- sedimentary texture: mud-rich packstone
- sedimentary structure: rootlets
- depositional environment: lowermost intertidal to shallow subtidal, low-energy, mud-rich, rooted lagoonal deposits (Figure 3a)

Anhydrite-rich, peloid-skeletal packstone (sample MC-1-8)
- sedimentary texture: mud-rich packstone
- sedimentary structure: altered by replacive/displacive growth of anhydrite
- depositional environment: lowermost intertidal to shallow subtidal, low-energy, mud-rich, lagoonal deposits; overprinted by sabkha anhydrite (Figures 3a and 3e)

The facies succession observed at Mussafah vertical section MC-1 corresponds to some of the lateral facies variations along the Abu Dhabi coastline, as illustrated by arrows on Figure 1b.

The peloid-skeletal packstone with rootlets (sample MC-1-7: 49%), but also the fine-grained, bioclastic packstone (sample MC-1-6: 24%), the cerithid-rich, bioclastic packstone (sample MC-1-5: 15%), and the microbial mat (sample MC-1-4: 12%), as well as the reworked Pleistocene carbonate-rich sand (sample MC-1-3: 19%) are rich in dolomite (Figure 3a).

Eight samples (MC-1-1 to MC-1-8) were selected for thin section and XRD analyses (Figure 3a). Radiocarbon age-dating carried out on two carbonate-rich sand samples (^{14}C accelerator-mass-spectrometer technique, bulk samples) and one microbial mat sample (^{14}C accelerator-mass-spectrometer technique, bulk sample) showed an age of 26,760 ± 180 ^{14}C yrs BP for the lower, reworked carbonate-rich sand sample (MC-1-1), 23,490 ± 130 ^{14}C yrs BP for the middle, cross-bedded carbonate-rich sand sample (MC-1-2), and 6,180 ± 50 ^{14}C yrs BP for the microbial mat sample (MC-1-4). The microbial mat sample showed a distinctively more negative delta ^{13}C value (-10.1‰ PDB; Figure 3a), due to its high organic content.

The lowermost fine-grained, carbonate-rich sand is slightly finer-grained (sample MC-1-1: 60–100 µ/60–120 µ, vfL-vfU) than the overlying high-angle cross-bedded (sample MC-1-2: 100–150 µ/100–220 µ, vfU-fL/vfU-fU) and the reworked fine-grained, carbonate-rich sands (sample MC-1-3: 100 µ/100–220 µ, vfU/ vfU-fU; Figures 3a to 3d, and 4a). The high-angle cross-bedded, carbonate-rich

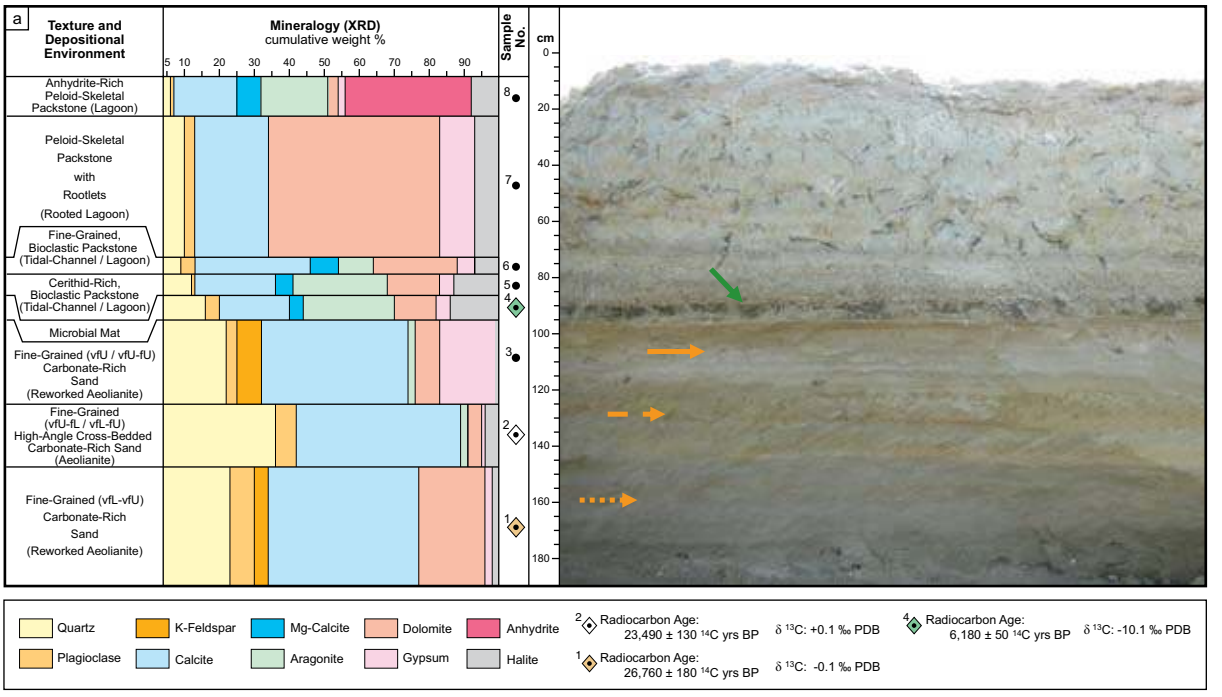

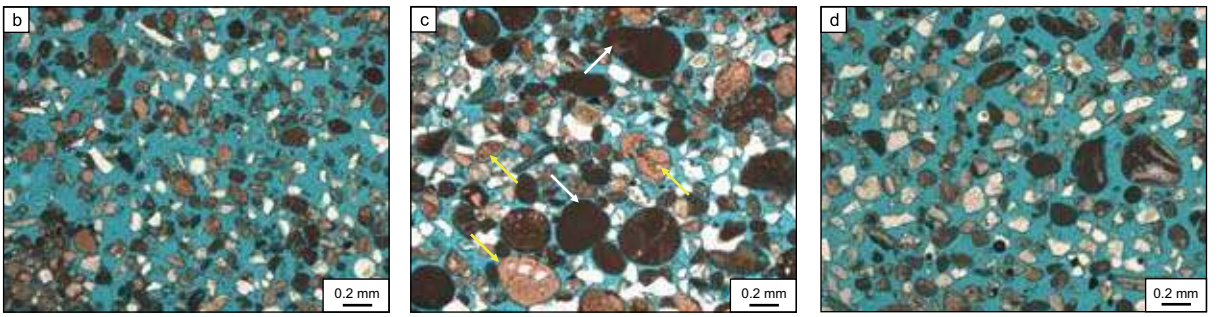

Figure 3: (a) Vertical section MC-1 (location 1; Figures 1c and 2) showing Holocene sediments (transgressive microbial mat: green arrow) overlying Pleistocene fine-grained, carbonate-rich sand (younger reworked aeolian dune deposits: orange arrow with solid line, cross-bedded aeolian dune deposits: orange arrow with dashed line, and older reworked aeolian dune deposits: orange arrow with dotted line). Mineralogical composition from XRD (cumulative weight %). Radiocarbon and carbon-isotope results are for two carbonate-rich sands (MC-1-1 and MC-1-2) and microbial mat (MC-1-4).

(b-e) Thin section photomicrographs.

(b-e) Plane polarized light.

(b and c) Stained with Alizarin red-S.

(b) Reworked, carbonate-rich sand (MC-1-1). The siliciclastic (60 to 100 µ) and the carbonate material (60 to 120 µ) are both very fine lower to very fine upper (vfL-vfU).

(c) Cross-bedded, carbonate-rich sand (MC-1-2) showing abundant rotalid foraminifera (*Ammonia* sp.: yellow arrows) and red algal clasts (white arrows). The siliciclastic material (100 to 150 µ) is very fine upper to fine lower (vfU-fL), whereas the carbonate material (100 to 220 µ) is very fine upper to fine upper (vfU-fU).

(d) Reworked, carbonate-rich sand (MC-1-3). The siliciclastic material (100 µ) is very fine upper (vfU), whereas the carbonate material (100 to 220 µ) is very fine upper to fine upper (vfU-fU).

(e) Anhydrite-rich, peloid- skeletal packstone (MC-1-8) showing miliolid foramninifera (*Triloculina* sp.: red arrow).

sand (sample MC-1-2; Figures 3c and 4a) is rich in rounded red algal clasts and rotalid foraminifera (*Ammonia* sp.). Miliolid foramninifera (*Triloculina* sp.) are found in the anhydrite-rich, peloid-skeletal packstone (sample MC-1-8; Figure 3e).

The transgressive microbial mat, overlying the reworked Pleistocene aeolian dune deposits, shows burrowing and/or erosion on top (Figures 4a and 4b).

The dark grey-greenish, peloid-skeletal packstone with rootlets (sample MC-1-7) shows oxidized vertical seaweed rootlets (*Halodule uninervis*) as well as large bladed gypsum crystals (Figure 4b).

Shell samples derived from the cerithid-rich, bioclastic packstone (sample MC-1-5: tidal-channel/lagoonal deposits), directly overlying the transgressive microbial mat, are rich in gastropods: *Cerithidea*

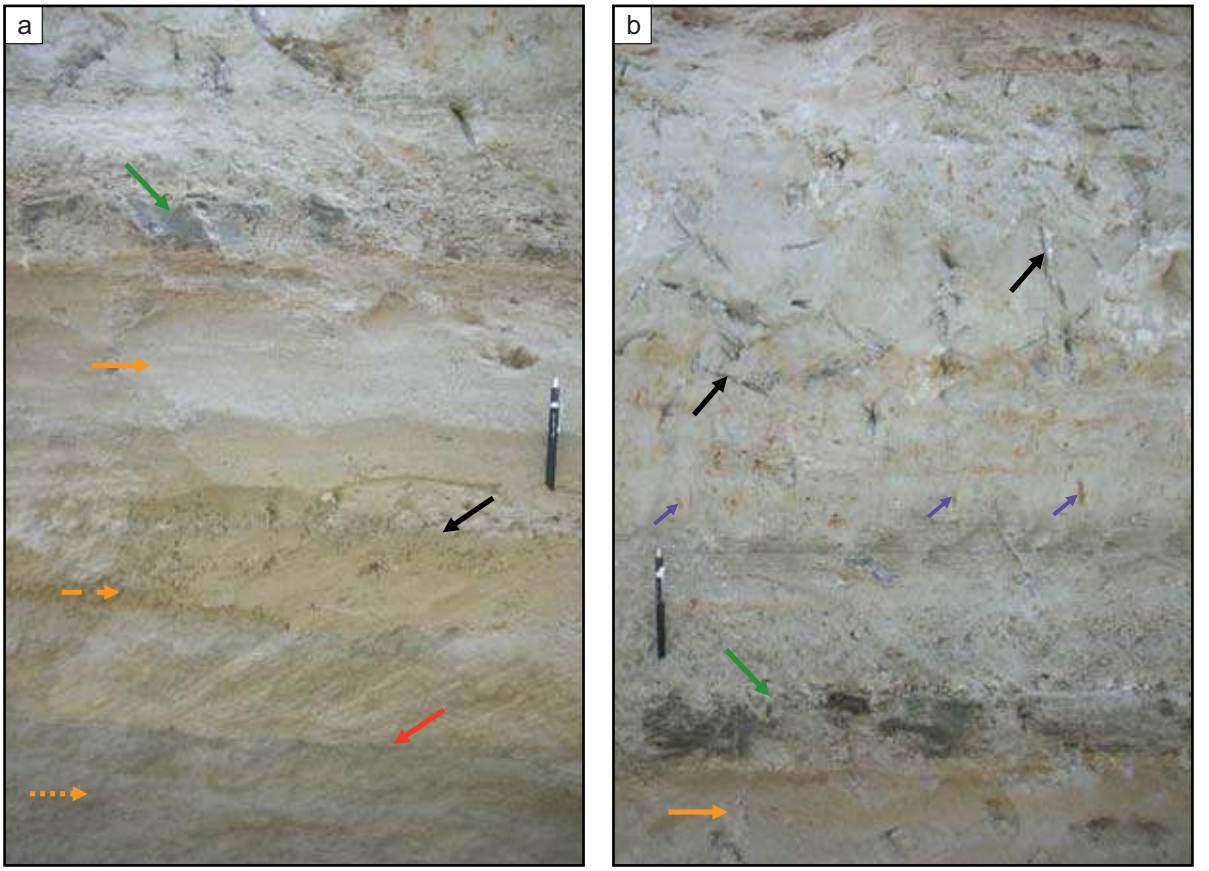

Figure 4: Close-ups of the MC-1 section shown on Figure 3a. Length of pencil is 12 cm.

(a) Displayed are, from base to top: un-bedded to wavy-bedded, Pleistocene fine-grained, carbonate-rich sand (older reworked aeolian dune deposits: orange arrow with dotted line), followed by high-angle cross-bedded, Pleistocene fine-grained, carbonate-rich sand (aeolian dune deposits: orange arrow with dashed line), un-bedded to wavy-bedded, Pleistocene fine-grained, carbonate-rich sand (younger reworked aeolian dune deposits: orange arrow with solid line), and microbial mat (transgressive microbial mat: green arrow). Sharp to erosive contacts are present between the lower, reworked aeolian dune deposits and the high-angle cross-bedded dune deposits (red arrow), as well as between the high-angle cross-bedded dune deposits and the upper reworked aeolian dune deposits (black arrow).

(b) Microbial mat showing burrowing and erosion (green arrow) overlies reworked aeolian dune deposits (orange arrow), indicating the transgression of the Holocene sea between 6,600–6,200 ^{14}C yrs BP. Above the microbial mat the sediments show a fining-upward trend towards fine-grained, grey-greenish colored, rooted lagoonal carbonates. The latter are rich in oxidized root marks, probably corresponding to seaweed *Halodule uninervis* (blue arrows) and large bladed gypsum crystals (black arrows).

cingulata (Gmelin; Figure 5a), *Cerithium rueppeli* (Phillipi; Figure 5b), *Potamides conicus* (Blainville; Figure 5c), and *Priotrochus obscurus* (Wood; Figure 5d), as well as pelecypods: *Mysia* cf. *elegans* (H. Adams; Figure 5e). The biota suggests that elevated seawater salinity probably characterizes the initial Holocene transgression. This can be inferred from the occurrence of the transgressive, intertidal microbial mat, but also from the occurrence of *Potamides* gastropods (tolerating high water salinity; Kenig, 2009); found within the cerithid-rich, bioclastic packstone (tidal-channel/lagoonal deposits) directly overlying the microbial mat.

The Holocene vertical section MC-1 represents a transgressive (deepening-upward) facies succession from intertidal (microbial mat) to lowermost intertidal to shallow subtidal (rooted lagoonal-dominated) deposits, with a marine flooding surface on top of the Pleistocene carbonate-rich sands (reworked aeolian dune deposits). The regressive phase of the sea level is represented by the diagenetic (evaporitic) sabkha-overprint, resulting in the growths of gypsum and anhydrite (Figure 2).

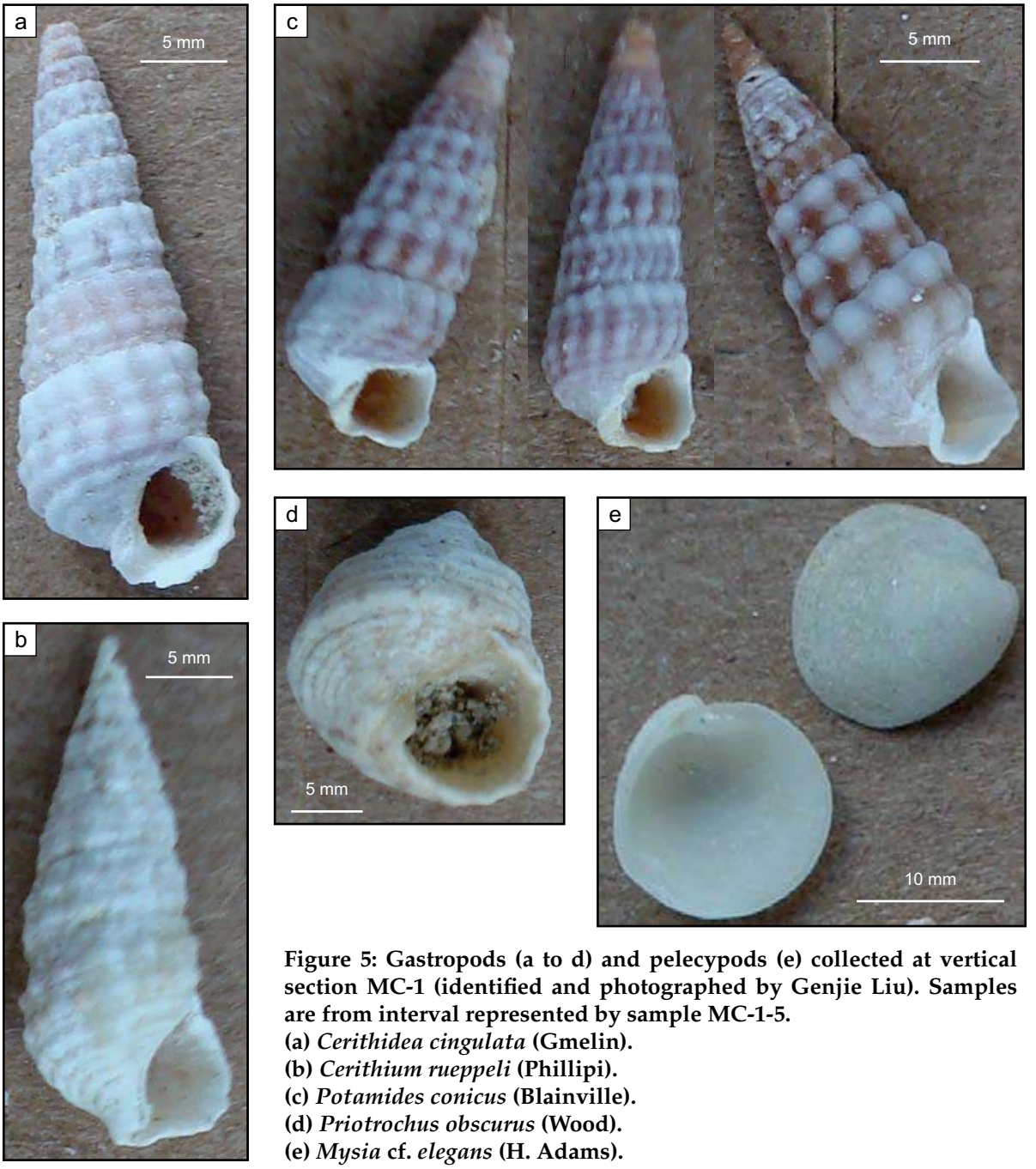

Figure 5: Gastropods (a to d) and pelecypods (e) collected at vertical section MC-1 (identified and photographed by Genjie Liu). Samples are from interval represented by sample MC-1-5.
(a) *Cerithidea cingulata* (Gmelin).
(b) *Cerithium rueppeli* (Phillipi).
(c) *Potamides conicus* (Blainville).
(d) *Priotrochus obscurus* (Wood).
(e) *Mysia* cf. *elegans* (H. Adams).

Location 1a: Tidal-Delta and Tidal-Bar Deposits

A couple of meters to the west, the low-energy, mud-rich, lagoonal-dominated carbonates of section MC-1 grade into high-energy, cross-bedded, coarse-grained, bioclastic rudstones and grainstones (Figures 1c, 2 and 6a). Relatively steep forset beds are clear to see (clinoforms or accretion wedges), showing iron staining along the inclined bedding planes (Figures 6a and 6b) and inclined to sigmoid bedding (foreset beds: tidal bundles) towards the top (Figure 6c) of the section. The described sedimentary textures and structures allow to interpret the cross-bedded, bioclastic rudstones and grainstones as corresponding to high-energy intertidal to shallow subtidal, tidal-delta and tidal-bar deposits, similar

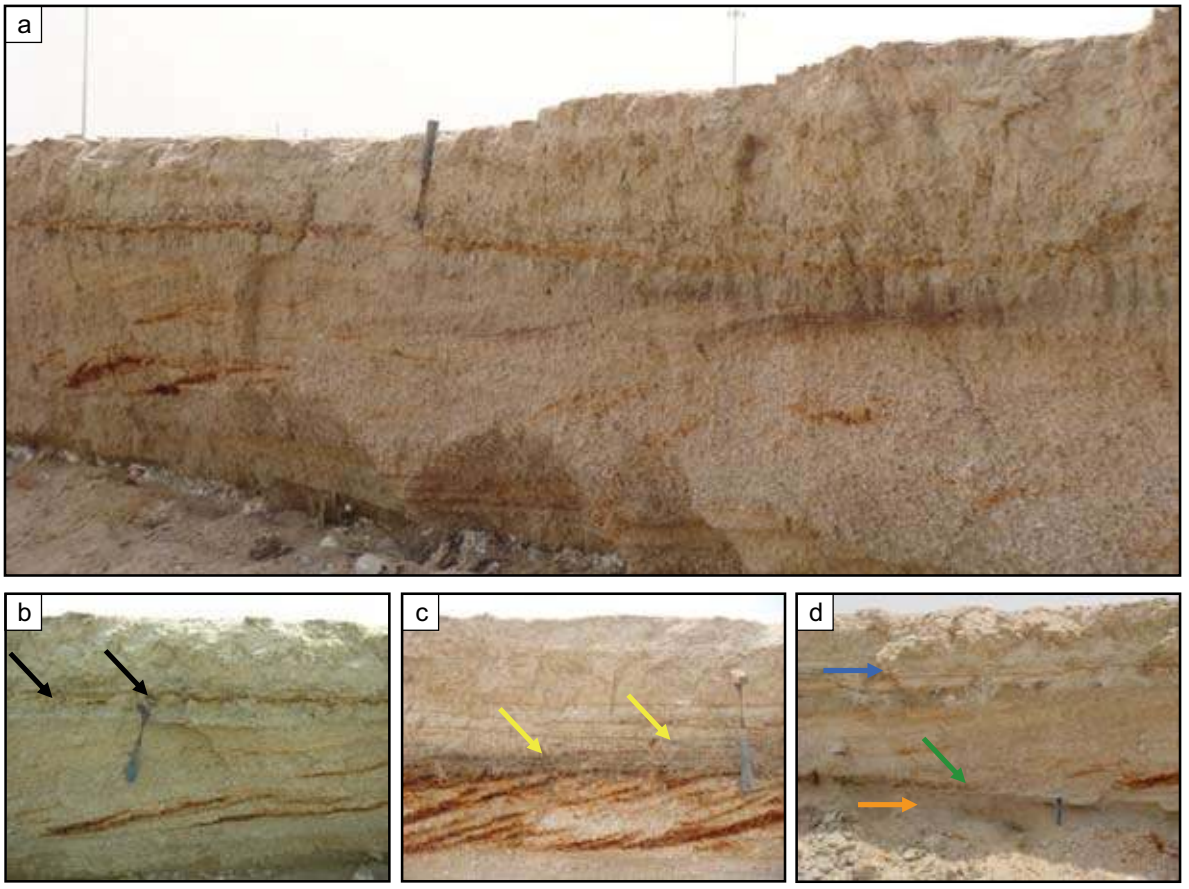

Figure 6: View of channel wall west to the measured vertical section MC-1 (location 1a; Figures 1c and 2). Length of hammer is 27.7 cm. Length of permanent marker is 13 cm.

(a) Tidal-delta and tidal-bar deposits (cerithid-rich, bioclastic rudstone/grainstone) showing festoon cross-bedding and iron-staining along inclined bedding-planes. Horizontal reddish band (below hammer) corresponds to oxidized horizon interpreted as paleo-groundwater table (see text for further explanation).

(b) Close-up of tidal-delta deposits, displaying iron-staining along inclined bedding-planes (clinoforms or accretion wedges). Also shown are bladed gypsum crystals (black arrows) within overlying fine-grained, rooted lagoonal carbonates. Horizontal reddish band (above black arrows) corresponds to oxidized horizon marking paleo-groundwater table.

(c) Close-up of tidal-bar showing inclined to sigmoid cross-bedding (foreset beds: tidal bundles), typical for high-energy tidal-bar deposits, as well as iron-staining along bedding planes. Some dark coloration is due to black pebbles within overlying, microbial-laminated lagoonal deposits (yellow arrows). Horizontal reddish bands (above yellow arrows) correspond to oxidized horizons interpreted as paleo-groundwater tables.

(d) Close-up of tidal-delta deposits cutting into underlying Holocene microbial mat (green arrow) and Pleistocene fine-grained, carbonate-rich sand (reworked aeolian dune deposits: orange arrow). The tidal-delta deposits grade upwards into fine-grained, rooted lagoonal carbonates (peloid-skeletal packstone with rootlets; blue arrow). Horizontal reddish bands (below blue arrow) correspond to oxidized horizons interpreted as paleo-groundwater tables.

to those that dominate the lagoonal environment behind the barrier islands along the present-day Abu Dhabi coastline (as illustrated by arrows on Figure 1b). Tidal-bars characterize the top of the tidal-channel/tidal-bar system and are overlain by microbial-laminated lagoonal carbonates, rich in black pebbles (Figure 6c). At location 1a (Figure 2), the tidal-delta deposits cut through the microbial mat into the Pleistocene, carbonate-rich sands (reworked aeolian dune deposits), and are overlain by mud-rich, rooted lagoonal deposits (Figure 6d).

Location 2: Vertical Section MC-2

Approximately 1.30 m of vertical section of Pleistocene carbonate-rich sands and unconformably overlying Holocene carbonates and sabkha evaporites are described at location 2 (vertical section MC-2) along the southern channel wall (Figures 1c, 2 and 7a). In the following account, the encountered facies types, their key sedimentary structures and evaporitic overprint, as well as their interpreted depositional environments are listed from base to top:

Fine-grained, carbonate-rich sand (sample MC-2-1)
- sedimentary structure: un-bedded to wavy-bedded
- siliciclastic grain size: very fine upper (vfU: 100 μ)
- carbonate grain size: very fine upper to fine upper (vfU-fU: 100–220 μ)
- depositional environment: reworked aeolian dunes (aeolianite; Figures 7a and 7b)

Crinkly-laminated stromatolitic bindstone (sample MC-2-2)
- sedimentary texture: boundstone/bindstone
- sedimentary structure: dark organic, crinkly laminated
- depositional environment: intertidal, low-energy microbial mat (Figures 7a, 7c and 8a)

Cerithid-rich, bioclastic grainstone/packstone (sample MC-2-3)
- sedimentary texture: grainstone to mud-lean packstone
- sedimentary structure: low-angle cross-bedded
- depositional environment: shallow subtidal, high- to moderate-energy tidal-channel deposits (Figures 7a and 7d)

Peloid-skeletal packstone with rootlets (samples MC-2-4 and MC-2-5)
- sedimentary texture: mud-rich packstone
- sedimentary structure: rootlets
- depositional environment: lowermost intertidal to shallow subtidal, low-energy, mud-rich, rooted lagoonal deposits (Figures 7a, 7e and 8b)

Microbial-laminated peloid-skeletal packstone (sample MC-2-6)
- sedimentary texture: mud-rich packstone
- sedimentary structure: irregular, diffuse, dark organic, crinkly-laminated
- depositional environment: lowermost intertidal to shallow subtidal, low-energy, mud-rich microbial-laminated lagoonal deposits (Figures 7a, 8c, and 8d)

Anhydrite-rich, peloid-skeletal packstone (sample MC-2-7)
- sedimentary texture: mud-rich packstone
- sedimentary structure: destroyed by replacive/displacive growth of anhydrite and halite
- depositional environment: lowermost intertidal to shallow subtidal, low-energy, mud-rich lagoonal deposits; overprinted by sabkha anhydrite and halite (Figures 7a, 7d and 8c)

The facies succession observed at Mussafah vertical section MC-2 corresponds to some of the lateral facies variations along the Abu Dhabi coastline, as illustrated by arrows on Figure 1b.

The microbial-laminated peloid-skeletal packstone (sample MC-2-6: 42%), the peloid-skeletal packstone with rootlets (MC-2-5 and MC-2-4: 41% – 33%), and the microbial mat (MC-2-2: 12%) are very rich in dolomite (Figure 7a).

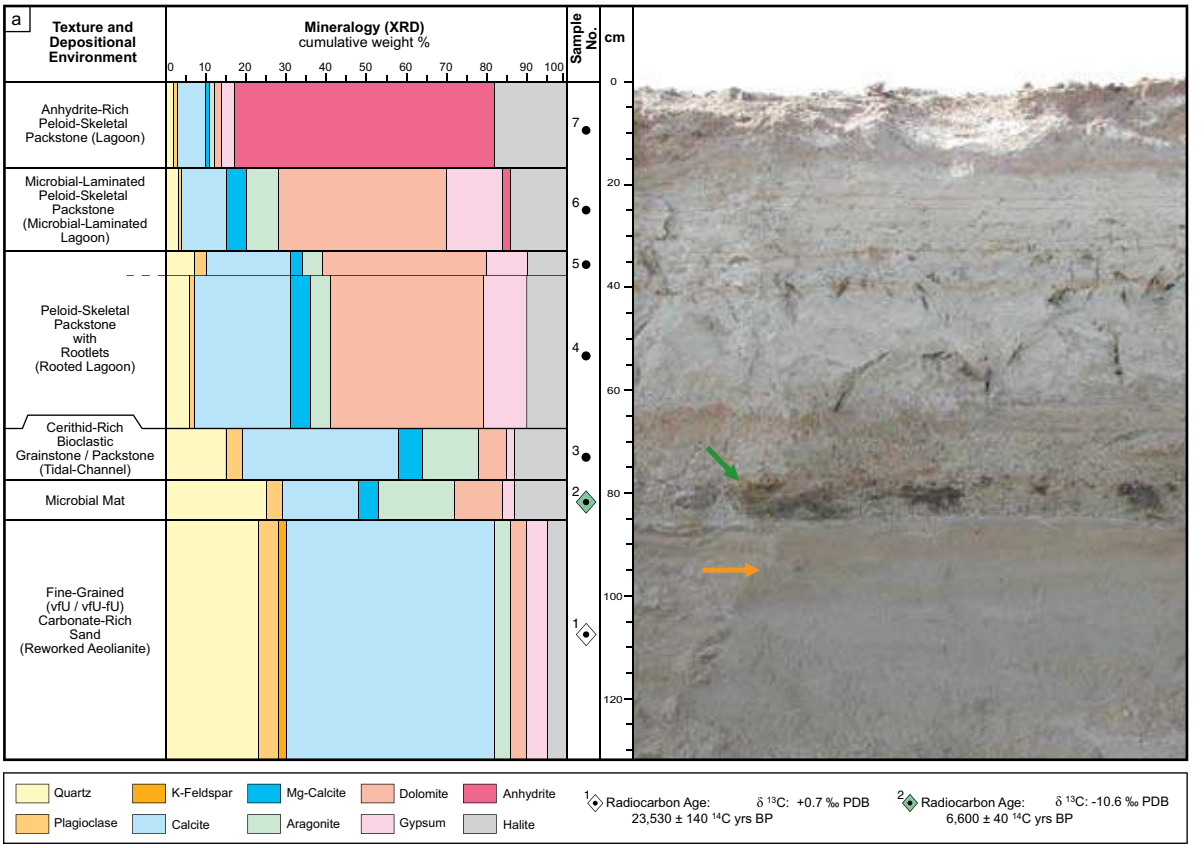

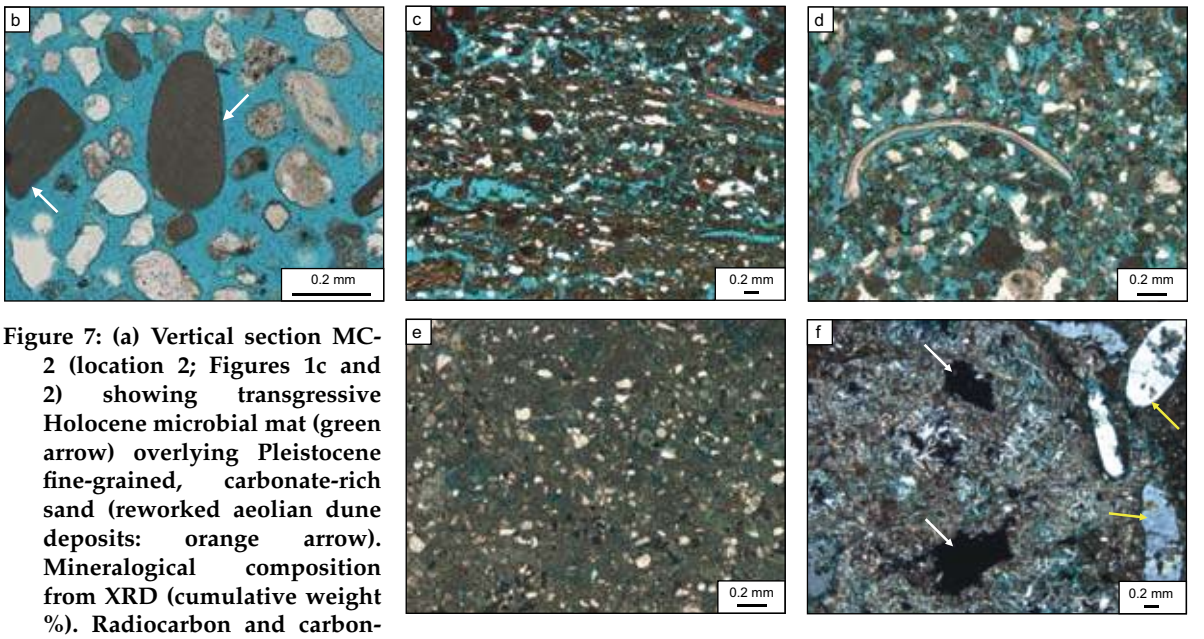

Figure 7: (a) Vertical section MC-2 (location 2; Figures 1c and 2) showing transgressive Holocene microbial mat (green arrow) overlying Pleistocene fine-grained, carbonate-rich sand (reworked aeolian dune deposits: orange arrow). Mineralogical composition from XRD (cumulative weight %). Radiocarbon and carbon-isotope results are for carbonate-rich sand (MC-2-1) and microbial mat (MC-2-2). Horizontal reddish bands correspond to oxidized horizons interpreted as paleo-groundwater tables.

(b-f) Thin section photomicrographs.

(b-e) Plane polarized light.

(f) Crossed polarized light.

(c) Stained with Alizarin red-S.

(b) Reworked, carbonate-rich sand (MC-2-1). The siliciclastic material (100 µ) is very fine upper (vfU), whereas the carbonate material (100 to 220 µ) is very fine upper to fine upper (vfU-fU). Carbonate grains are commonly red algal grains (white arrows). (c) Microbial mat (MC-2-2). (d) Cerithid-rich, bioclastic grainstone/packstone (MC-2-3). (e) Peloid-skeletal packstone (MC-2-4). (f) Anhydrite-rich peloid-skeletal packstone (MC-2-7) showing replacive, lath shaped anhydrite crystals exhibiting felted texture, as well as lenticular gypsum crystals (yellow arrows) and halite crystals (white arrows).

Seven samples (MC-2-1 to MC-2-7) were selected for thin section and XRD analyses (Figure 7a). Radiocarbon age-dating carried out on one carbonate-rich sand sample (^{14}C accelerator-mass-spectrometer technique, bulk sample) and one microbial mat sample (^{14}C accelerator-mass-spectrometer technique, bulk sample) showed an age of 23,530 ± 140 ^{14}C yrs BP for the reworked carbonate-rich sand sample (MC-2-1) and 6,600 ± 40 ^{14}C yrs BP for the microbial mat sample (MC-2-2). The microbial mat sample showed a distinctively more negative delta ^{13}C value (-10.6‰ PDB; Figure 7a), due to its high organic content.

Like the high-angle cross-bedded, carbonate-rich sand present at vertical section MC-1 (sample MC-1-2; Figures 4a and 4c) the upper reworked carbonate-rich sand of vertical section MC-2 (sample MC-2-1) is rich in rounded red algal fragments (red algal intraclasts; Figure 7b).

The transgressive microbial mat, overlying the reworked Pleistocene aeolian dune deposits shows burrowing and/or erosion on top (Figure 8a).

The dark grey-greenish peloid-skeletal packstone with rootlets shows vertical oxidized seaweed rootlets (*Halodule uninervis*) and possible molds of mangrove roots (*Avicennia marina*), as well as large bladed gypsum crystals (Figure 8b). The dark grey-greenish, microbial-laminated peloid-skeletal packstone displays diffuse, irregular, dark organic, crinkly laminations (Figures 8c and 8d) as well as secondary reddish horizontal bands, the latter corresponding to paleo-groundwater tables.

The microbial-laminated peloid-skeletal packstone was described as a regressive microbial mat by Kening et al. (1990) and Kening (1991, 2010), interpreted to represent a falling sea level. However, the microbial-laminated peloid-skeletal packstone grades laterally (location 1: vertical section MC-1; Figures 2 and 3a) and vertically (location 1a and location 2: vertical section MC-2; Figures 2, 6 and 7a) into a peloid-skeletal packstone with rootlets. This favors the interpretation of lateral facies variations or short term sea-level/seasonal fluctuations. In addition, bioclastic rudstone/grainstone (high-energy longshore beach bar and beach spit deposits, see vertical sections MC-3 and MC-4) are interpreted to have originally been deposited on top of the low-energy lagoonal sediments at vertical sections MC-1 and MC-2 (Figure 2). The observed vertical change from low-energy (lagoonal deposits) to high-energy (longshore beach bar and beach spit deposits) conditions requires the barrier islands offshore the Abu Dhabi coastline to be flooded (Figure 1a); thus indicating a still rising sea level above the rooted lagoonal and microbial-laminated lagoonal deposits.

Vertical section MC-2 is interpreted as having formed during the Holocene transgression, showing a deepening-upward facies succession from intertidal (microbial mat) to lowermost intertidal to shallow subtidal (rooted and microbial-laminated lagoonal-dominated) deposits, as previously described from vertical section MC-1 (location 1; Figures 1c and 2). Like at vertical section MC-1, the regressive phase of the sea level is represented by the diagenetic (evaporitic) sabkha-overprint, resulting in the growths of gypsum and anhydrite.

Location 3: Vertical Section MC-3

Approximately 2.20 m of vertical section of Pleistocene carbonate-rich sands and overlying Holocene carbonates are exposed at location 3 (vertical section MC-3) along the eastern channel wall (Figures 1c, 2, and 9). Vertical section MC-3 displays a compound tidal-channel cutting into Holocene carbonates and Pleistocene fine-grained, carbonate-rich sands (Figure 9). Stratigraphic truncation and shingled hardgrounds along the channel-fill, similar to those described by Shinn (1973) from northeast Qatar, can be observed (Figure 9). Radiocarbon age-dating results confirm that the channel-fill deposits are slightly younger than the incised carbonate sediments (Figure 9).

In contrast to vertical sections MC-1 and MC-2, which are dominated by low-energy, mud-rich, rooted and microbial-laminated lagoonal carbonates (Figures 3, 4, 7, and 8), vertical section MC-3 predominantly consists of low- to high-energy tidal-channel deposits, overlain by gypsum rich, cross-bedded bioclastic rudstone/grainstone, interpreted as longshore beach bar and beach spit deposits (Figures 2 and 9). Similar longshore beach bar and beach spit deposits can be observed along the southern coast of the Bar Al-Hikman peninsula in Oman (Homewood et al., 2007) and also resemble those described by Shinn (1973, 2008) from Qatar as "chenier" beaches.

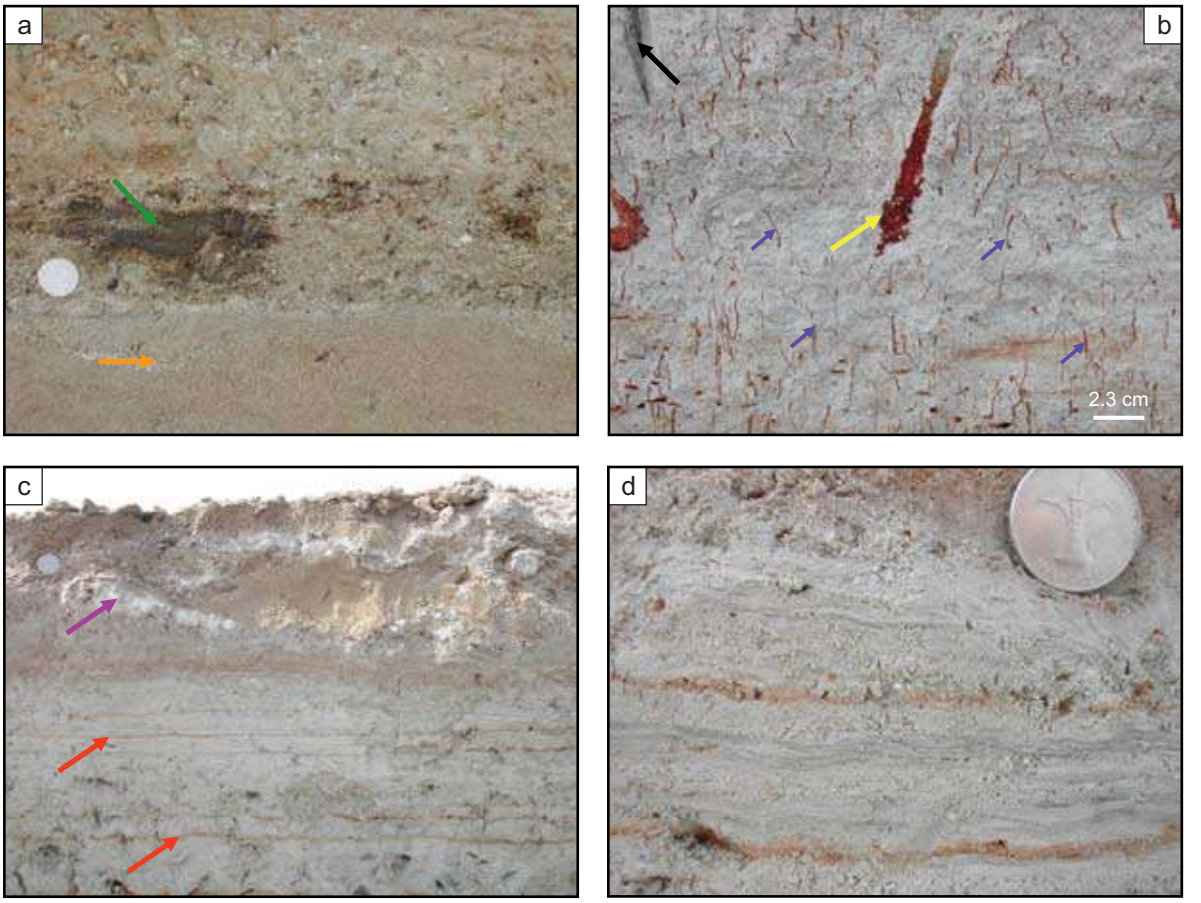

Figure 8: Close-ups of vertical section MC-2 shown on Figure 7a. Diameter of coin is 2.3 cm (scale on Figure 2b).

(a) Transgressive microbial mat (green arrow) overlying Pleistocene fine-grained, carbonate-rich sand (reworked dune deposits: orange arrow). Microbial mat displays burrowing and/or erosion.

(b) Grey-greenish, fine-grained, peloid-skeletal packstone (rooted lagoonal deposits) displaying oxidized root marks, probably corresponding to seaweed *Halodule uninervis* (blue arrows). Also shown is oxidized possible mold of mangrove root (*Avicennia marina*, yellow arrow) and large bladed gypsum crystal (black arrow).

(c) Microbial-laminated, fine-grained, peloid-skeletal packstone (microbial-laminated lagoonal deposits) overlain by anhydrite-rich (purple arrow) peloid-skeletal packstone (lagoonal deposits), also containing relatively high amounts of halite (18%; see Figure 8a). Horizontal reddish bands (red arrows) correspond to oxidized horizons interpreted as paleo-groundwater tables.

(d) Close-up of microbial-laminated, fine-grained, peloid-skeletal packstone (microbial-laminated lagoonal deposits) displaying dark organic, diffuse to crinkly laminations. Horizontal reddish bands correspond to oxidized horizons interpreted as paleo-groundwater tables.

It could be argued that the longshore beach bar and beach spit deposits already represent a falling sea level. However, as mentioned above, to form high-energy longshore beach bar and beach spit deposits above low- to high-energy lagoonal and tidal-channel deposits (see vertical sections MC-3A, MC-3B, and MC-4) requires the barrier islands offshore the Abu Dhabi coastline to be flooded. This favors the interpretations of the longshore beach bar and beach spit deposits representing the turn around point from transgression (establishing of high-energy condition) to still stand/regression (longshore beach bar and beach spit progradation and evaporite precipitation).

Vertical section MC-3A gives a detailed description of the older, pre-channel-cut deposits (Figures 10 and 11) and vertical section MC-3B describes in detail the younger channel-fill deposits (Figures 12 and 13).

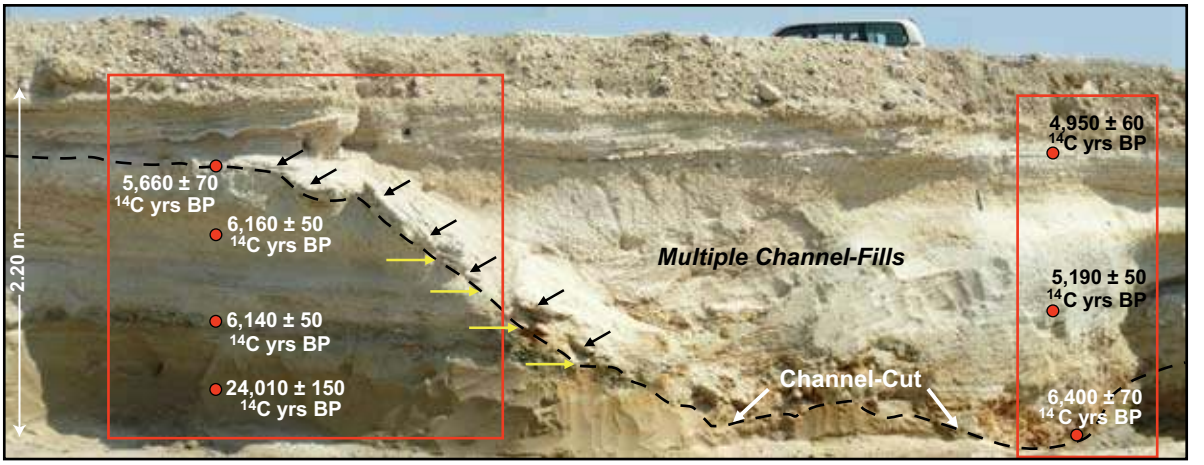

Figure 9: Vertical section MC-3 (location 3; Figures 1c and 2) showing compound Holocene channel cutting into Holocene carbonates and Pleistocene fine-grained, carbonate-rich sand (reworked aeolian dune deposits). Stratigraphic truncation (yellow arrows) and shingled hardgrounds (black arrows) are present on the left (north) side of the channel. Details of the measured sections MC-3A and MC-3B marked by red boxes are shown on Figures 10 and 12. Radiocarbon ages in ^{14}C years before present (^{14}C yrs BP). Thickness of the studied in-place deposits is 2.20 m at white double arrow on the left. The top of the section is erosive and overlain by construction-fill rubble.

Location 3: Vertical Section MC-3A

Approximately 1.90 m of vertical section of Pleistocene carbonate-rich sands and unconformably overlying Holocene carbonates and sabkha evaporites are described at vertical section MC-3A; the latter representing slightly older, pre-channel-cut deposits (Figures 2 and 10a). In the following account, the encountered facies types, their key sedimentary structures and evaporitic overprint, as well as their interpreted depositional environments are listed from base to top:

Fine-grained, carbonate-rich sand (sample MC-3A-1)

- sedimentary structure: un-bedded to wavy-bedded
- siliciclastic grain size: very fine upper (vfU: 100 µ)
- carbonate grain size: very fine upper to fine upper (vfU-fU: 100–220 µ)
- depositional environment: reworked aeolian dunes (aeolianite; Figure 10a)

Crinkly-laminated stromatolitic bindstone (sample MC-3A-2)

- sedimentary texture: boundstone/bindstone
- sedimentary structure: dark organic, crinkly laminated
- depositional environment: intertidal, low-energy microbial mat (Figure 10a)

Hardground (sample MC-3A-3)

- cemented cerithid-rich, bioclastic grainstone
- patchy, fibrous aragonite cement
- cemented channel-lag (Figures 10a and 10b)

Cerithid-rich, bioclastic grainstone (sample MC-3A-3)

- sedimentary texture: grainstone
- sedimentary structure: low-angle cross-bedded
- depositional environment: shallow subtidal, high-energy tidal-channel deposits (Figure 10a)

Fine-grained, bioclastic packstone (sample MC-3A-4A)

- sedimentary texture: mud-lean to mud-rich packstone
- sedimentary structure: low-angle cross-bedded
- depositional environment: shallow subtidal, moderate- to low-energy tidal-channel grading into lowermost intertidal to shallow subtidal, low-energy, mud-rich lagoonal deposits (Figure 10a).

Fine-grained/coarse-grained, bioclastic packstone/grainstone (sample MC-3A-4B)

- sedimentary texture: mud-lean packstone (fine-grained layers) to grainstone (coarse-grained layers)
- sedimentary structure: low-angle cross-bedded
- depositional environment: shallow subtidal, moderate- to high-energy tidal-channel deposits (Figure 10a)

Cross-bedded, cerithid-rich, bioclastic grainstone/rudstone (sample MC-3A-5)

- sedimentary texture: grainstone and rudstone
- sedimentary structure: high-angle cross-bedded
- depositional environment: shallow subtidal, high-energy tidal-channel deposits (Figures 10a and 10c)

Fine-grained, bioclastic packstone (sample MC-3A-6)

- sedimentary texture: mud-lean to mud-rich packstone
- sedimentary structure: low-angle cross-bedded to un-bedded
- depositional environment: shallow subtidal, moderate- to low-energy tidal-channel grading into lowermost intertidal to shallow subtidal, low-energy, mud-rich lagoonal deposits (Figure 10a)

Hardground (sample MC-3A-7)

- cemented, bioclastic grainstone
- patchy, fibrous aragonite cement
- cemented beach rock (Figures 10a and 10d)

Gypsum-rich, cross-bedded, bioclastic rudstone/grainstone (samples MC-3A-8 and MC-3A-9)

- sedimentary texture: rudstone and grainstone.
- sedimentary structure: low-angle cross-bedded to parallel-bedded
- depositional environment: shallow subtidal to intertidal, high-energy longshore beach bar and beach spit deposits; overprinted by sabkha gypsum (Figures 10a and 10e).

As with previous sections, the facies succession observed at Mussafah vertical section MC-3A corresponds to some of the lateral facies variations along the Abu Dhabi coastline illustrated by arrows on Figure 1b.

The fine-grained, bioclastic packstone (sample MC-3A-4A: 20%), and the cerithid-rich, bioclastic grainstone (MC-3A-3: 13%), as well as the microbial mat (sample MC-3A-2: 17%) are rich in dolomite (Figure 10a).

Nine samples (MC-3A-1 to MC-3A-9) were selected for thin section and XRD analyses (Figure 10a). Radiocarbon age-dating carried out on one carbonate-rich sand sample (^{14}C accelerator-mass-spectrometer technique, bulk sample), one microbial mat sample (^{14}C accelerator-mass-spectrometer technique, bulk sample), one unconsolidated carbonate sample (selected shell sample) and one hardground sample (^{14}C radiometric dating technique, bulk sample) showed an age of 24,010 ± 150 ^{14}C yrs BP for the reworked carbonate-rich sand sample (MC-3A-1), 6,140 ± 50 ^{14}C yrs BP for the microbial mat sample (MC-3A-2), 6,160 ± 50 ^{14}C yrs BP for the cross-bedded, cerithid-rich, bioclastic grainstone/rudstone sample (MC-3A-5), and 5,660 ± 70 ^{14}C yrs BP for the upper hardground sample (MC-3A-7). As with previous samples, the microbial mat sample showed a distinctively more negative delta ^{13}C value (-9.9‰ PDB; Figure 10a), due to its high organic content.

Shell samples derived from the cross-bedded, cerithid-rich, bioclastic grainstone/rudstone (tidal-channel deposits, sample MC-3A-5) are rich in gastropods: *Cerithium rueppeli* (Phillipi; Figure 11a), *Potamides conicus* (Blainville; Figure 11b), *Mitrella bland* (Sowerby; Figure 11c), *Lunella* sp. (Figure 11d), and *Priotrochus obscurus* (Wood; Figure 11e). Like at vertical MC-1, the biota indicates elevated seawater salinity during the initial Holocene transgression.

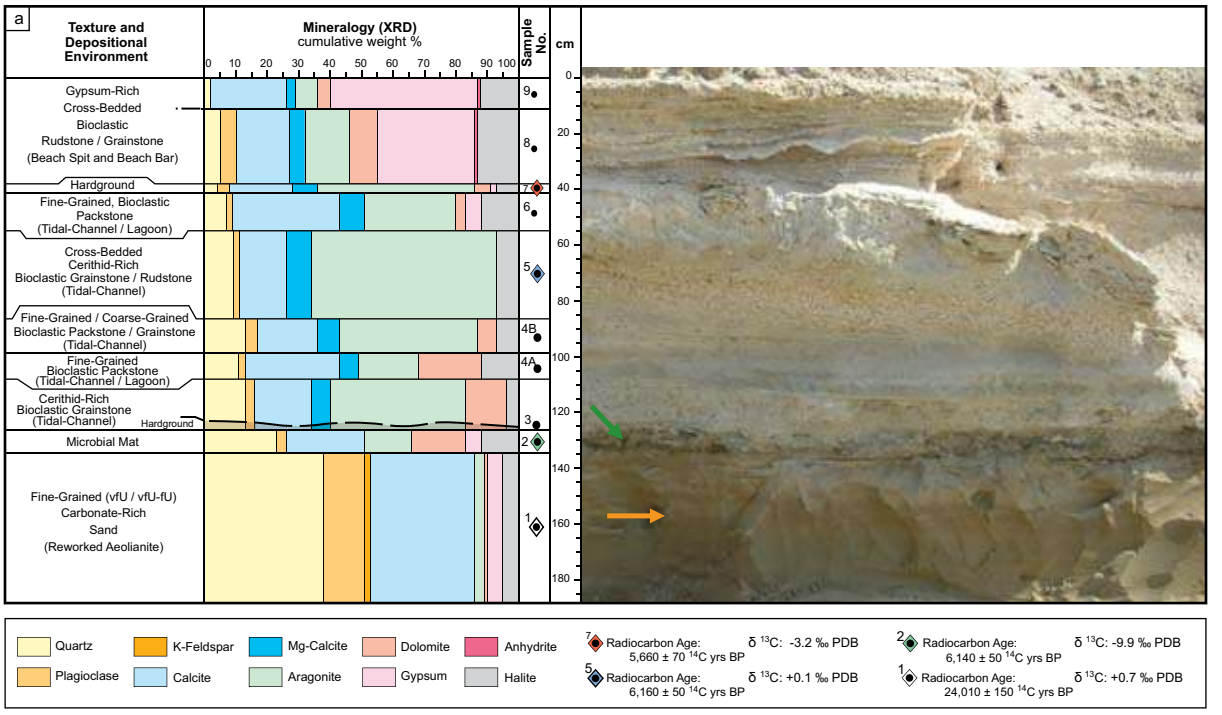

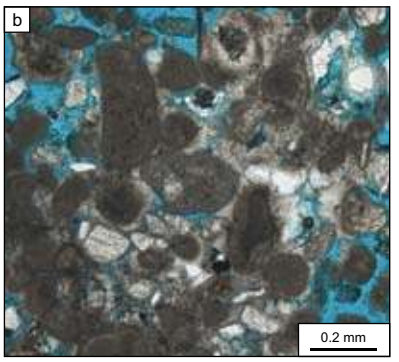

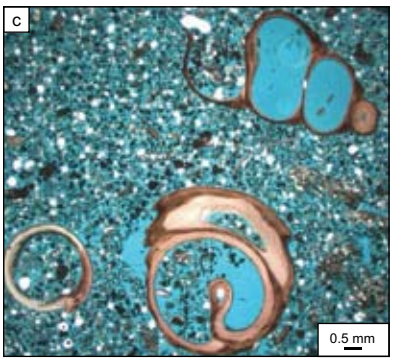

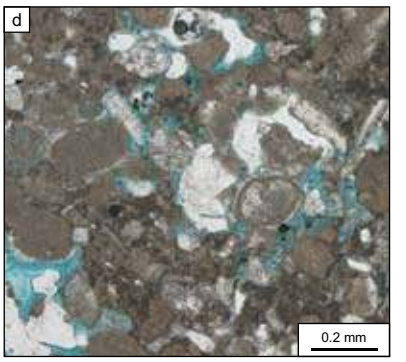

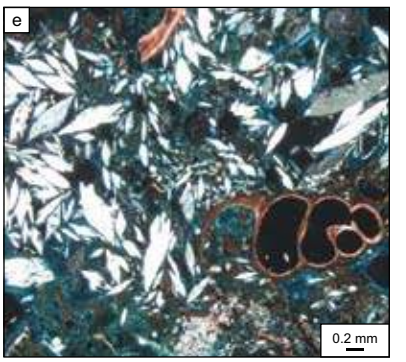

Figure 10: (a) Vertical section MC-3A showing transgressive Holocene microbial mat (green arrow) overlying Pleistocene fine-grained, carbonate-rich sand (reworked aeolian dune deposits: orange arrow). Mineralogical composition from XRD (cumulative weight %). Radiocarbon and carbon-isotope results for carbonate-rich sand (MC-3A-1), microbial mat (MC-3A-2), cross-bedded, cerithid-rich grainstone (MC-3A-5), and hardground (MC-3A-7).

(b-e) Thin section photomicrographs.

(b-d) Plane polarized light.

(e) Partly crossed polarized light.

(c and e) Stained with Alizarin red-S.

(b) Patchy fibrous aragonite cemented cerithid-rich, bioclastic grainstone (older hardground, MC-3A-3).

(c) Cerithid-rich, bioclastic grainstone/rudstone (MC-3A-5) showing longitudinal and median sections of cerithid gastropods.

(d) Younger hardground (MC-3A-7) exhibiting patchy, isopachous, fibrous aragonite cement fringes around carbonate grains. Aragonite rim cement is absent around quartz grains.

(e) Gypsum-rich, cross-bedded, bioclastic rudstone/grainstone (MC-3A-9) showing lenticular gypsum crystals and cerithid gastropod.

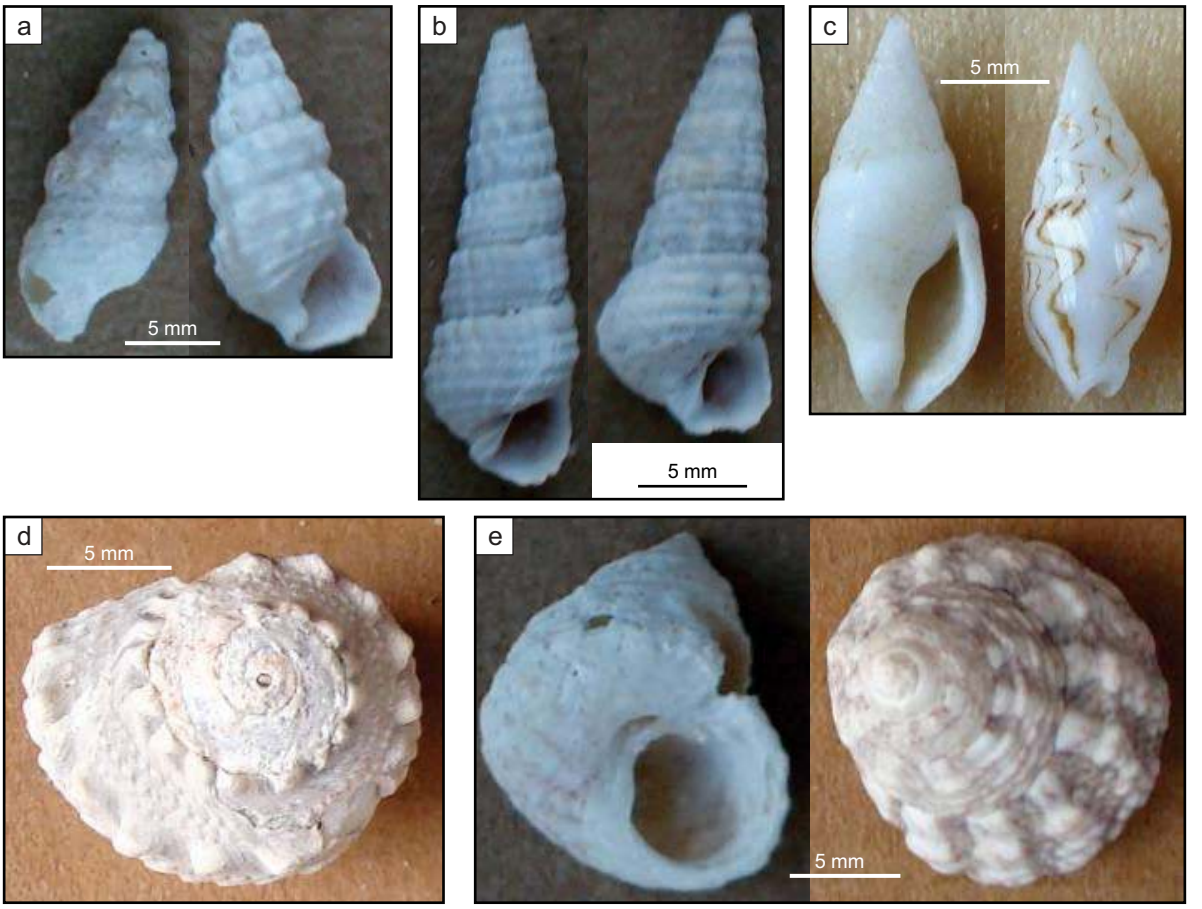

Figure 11: Gastropods collected at vertical section MC-3A. Samples are from interval represented by sample MC-3A-5 (identified and photographed by Genjie Liu).
(a) ***Cerithium rueppeli*** **(Phillipi). (b)** ***Potamides conicus*** **(Blainville). (c)** ***Mitrella bland*** **(Sowerby). (d)** ***Lunella*** **sp. (e)** ***Priotrochus obscurus*** **(Wood).**

The Holocene vertical section MC-3A represents a transgressive (deepening-upward) facies succession from intertidal (microbial mat) to shallow subtidal to intertidal (tidal-channel and minor lagoonal) deposits, with a marine flooding surface on top of the Pleistocene carbonate-rich sands (reworked aeolian dune deposits). The slow rising/still stand and regressive phase of the sea level is represented by the prograding longshore beach bar and beach spit deposits and the diagenetic (evaporitic) sabkha-overprint, resulting in the growths of gypsum crystals (Figure 2).

Location 3: Vertical Section MC-3B

Approximately 2.20 m of vertical section of incised Pleistocene carbonate-rich sands and unconformably overlying Holocene carbonates and sabkha evaporites are described at vertical section MC-3B; the latter representing slightly younger channel-fill deposits (Figures 2 and 12a). In the following account, the encountered facies types, their key sedimentary structures and evaporitic overprint, as well as their interpreted depositional environments are listed from base to top:

Fine-grained, carbonate-rich sand (sample MC-3B-1)

- sedimentary structure: un-bedded to wavy-bedded
- siliciclastic grain size: very fine upper (vfU: 100 µ)
- carbonate grain size: very fine upper to fine upper (vfU-fU: 100–220 µ)
- depositional environment: reworked aeolian dunes (aeolianite; Figure 12a)

Hardground (Sample MC-3B-2)

- cemented, bioclastic grainstone
- fibrous to botryoidal aragonite cement
- cemented channel-lag (Figures 12a and 12b)

Reworked crinkly-laminated stromatolitic bindstone (Sample MC-3B-3)
- sedimentary texture: boundstone/bindstone
- sedimentary structure: dark organic, crinkly laminated
- depositional environment: intertidal, low-energy microbial mat (Figure 12a)

Cerithid-rich, bioclastic grainstone (sample MC-3B-4)
- sedimentary texture: grainstone
- sedimentary structure: low-angle cross-bedded
- depositional environment: shallow subtidal, high-energy tidal-channel deposits (Figures 12a and 12c)

Fine-grained/coarse-grained, bioclastic packstone/grainstone (sample MC-3B-5)
- sedimentary texture: mud-lean packstone (fine-grained layers) to grainstone (coarse grained layers)
- sedimentary structure: low-angle cross-bedded
- depositional environment: shallow subtidal, moderate- to high-energy tidal-channel deposits (Figure 12a)

Cross-bedded, cerithid-rich, bioclastic grainstone (sample MC-3B-6)
- sedimentary texture: grainstone
- sedimentary structure: high- to low-angle cross-bedded
- depositional environment: shallow subtidal, high-energy tidal-channel deposits (Figures 12a and 12d)

Cross-bedded, fine-grained, bioclastic grainstone/packstone (samples MC-3B-7 and MC-3B-8)
- sedimentary texture: grainstone to mud-lean packstone
- sedimentary structure: high- to low-angle cross-bedded
- depositional environment: shallow subtidal, high- to moderate-energy tidal-channel deposits (Figure 12a)

Cross-bedded, bioclastic grainstone (sample MC-3B-9)
- sedimentary texture: grainstone
- sedimentary structure: low-angle cross-bedded
- depositional environment: shallow subtidal, high-energy tidal-channel deposits (Figures 12a and 12e)

Gypsum-rich, cross-bedded, bioclastic rudstone/grainstone (samples MC-3B-10, MC-3B-11, and MC-3B-12)
- sedimentary texture: rudstone and grainstone.
- sedimentary structure: low-angle cross-bedded
- depositional environment: shallow subtidal to intertidal, high-energy longshore beach bar and beach spit deposits; overprinted by sabkha gypsum (Figures 12a and 12f)

For comparison of the facies succession observed at Mussafah vertical section MC-3B with the lateral facies distribution along the Abu Dhabi coastline see Figure 1b.

The microbial mat (sample MC-3B-3: 10%) and the reworked Pleistocene carbonate-rich sand (sample MC-3B-1: 13%) are rich in dolomite (Figure 12a).

Twelve samples (MC-3B-1 to MC-3A-12) were selected for thin section and XRD analyses (Figure 12a). Radiocarbon age-dating carried out on one hardground sample (^{14}C radiometric dating technique, bulk sample) and two unconsolidated carbonate samples (^{14}C radiometric dating technique, selected shell samples) show an age of 6,400 ± 70 ^{14}C yrs BP for the hardground sample (MC-3B-2), 5,190 ± 50 ^{14}C yrs BP for the cross-bedded, cerithid-rich, bioclastic grainstone sample (MC-3B-6), and 4,950 ± 60 ^{14}C yrs BP for the gypsum-rich, cross-bedded, bioclastic rudstone/grainstone sample (MC-3B-11; Figure 12a).

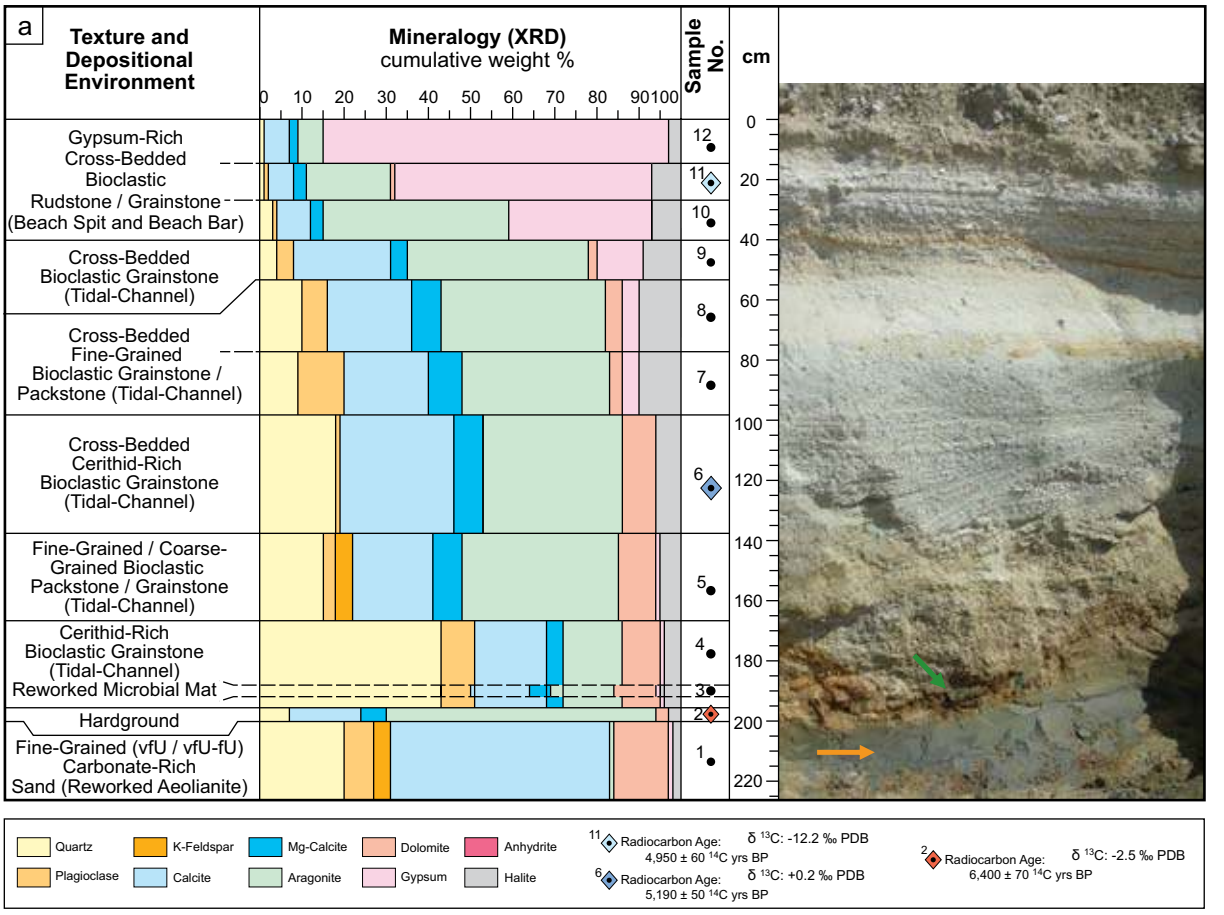

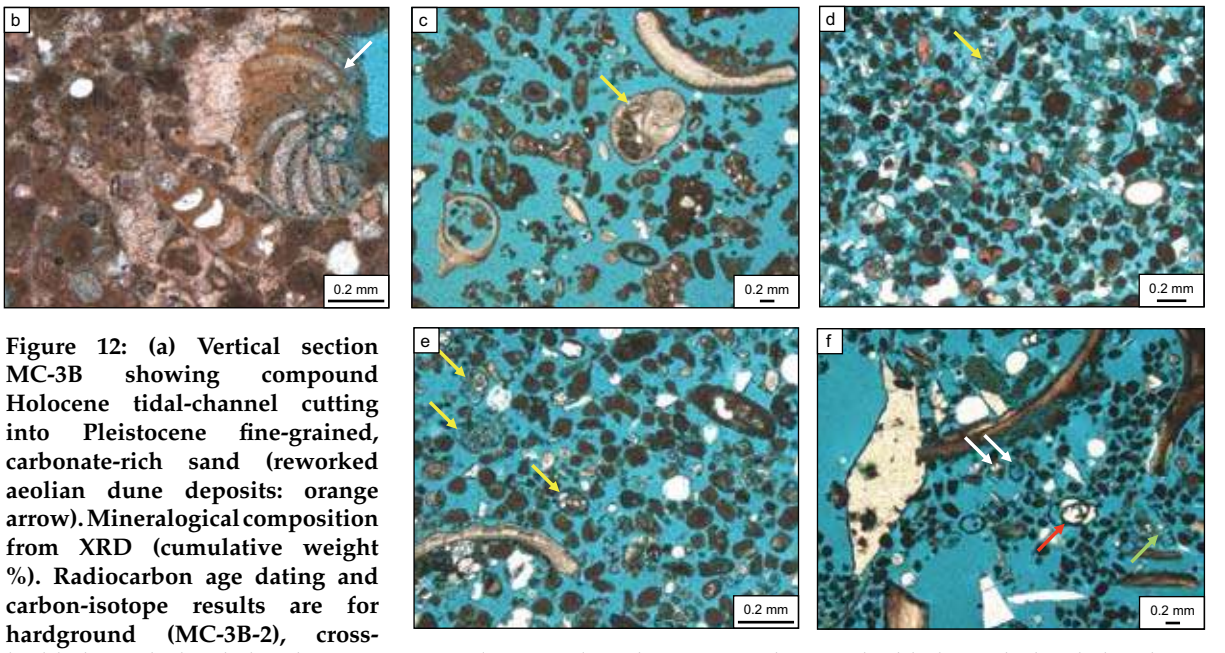

Figure 12: (a) Vertical section MC-3B showing compound Holocene tidal-channel cutting into Pleistocene fine-grained, carbonate-rich sand (reworked aeolian dune deposits: orange arrow). Mineralogical composition from XRD (cumulative weight %). Radiocarbon age dating and carbon-isotope results are for hardground (MC-3B-2), cross-bedded, cerithid-rich, bioclastic grainstone (MC-3B-6), and gypsum-rich, cross-bedded, cerithid-rich, bioclastic rudstone/grainstone (MC-3B-11). Horizontal reddish bands correspond to oxidized horizons interpreted as paleo-groundwater tables. (b-f) Thin section photomicrographs. (b-e) Plane polarized light. (f) Partly crossed polarized light. (b) Stained with Alizarin red-S. (b) Hardground (MC-3B-2) exhibiting patchy, fibrous to botryoidal aragonite cement and miliolid foraminifera (*Peneroplis* sp.: white arrow). (c) Cerithid-rich, bioclastic grainstone (MC-3B-4) showing shell fragments and rotalid foraminifera (*Ammonia* sp.: yellow arrow). (d) Cross-bedded, cerithid-rich, bioclastic grainstone (MC-3B-6) showing abundant quartz grains and rotalid foraminifera (*Ammonia* sp., yellow arrow). (e) Cross-bedded, bioclastic grainstone (MC-3B-9) showing shell fragments and abundant rotalid foraminifera (*Ammonia* sp.: yellow arrows). (f) Gypsum-rich, cross-bedded, bioclastic rudstone/grainstone (MC-3B-10) showing lenticular gypsum crystals, shell fragments and abundant miliolid foraminifera (*Peneroplis* sp., *Quinqueloculina* sp., and *Spirolina* sp.: white, red, and green arrows, respectively).

The hardground (sample MC-3B-2) exhibits patchy, fibrous to botryoidal aragonite cement and miliolid foraminifera (*Peneroplis* sp.; Figure 112b). Rotalid foraminifera (*Ammonia* sp) are abundant in the cerithid-rich, bioclastic grainstone (sample MC-3B-4, Figure 12c), the cross-bedded, cerithid-rich, bioclastic grainstone (sample MC-3B-6; Figure 12d), and the cross-bedded, bioclastic grainstone (sample Mc-3B-9; Figure 12e). The gypsum-rich, cross-bedded, bioclastic rudstone/grainstone (sample MC-3B-10) shows bladed gypsum crystals, shell fragments, and abundant miliolid foraminifera (*Peneroplis* sp., *Quinqueloculina* sp., and *Spirolina* sp.; Figure 12f).

Shell samples derived from the cross-bedded, cerithid-rich, bioclastic grainstone (tidal-channel deposits, sample MC-3B-6) are rich in gastropods: *Cerithidea cingulata* (Gmelin; Figure 13a). *Mitrella*

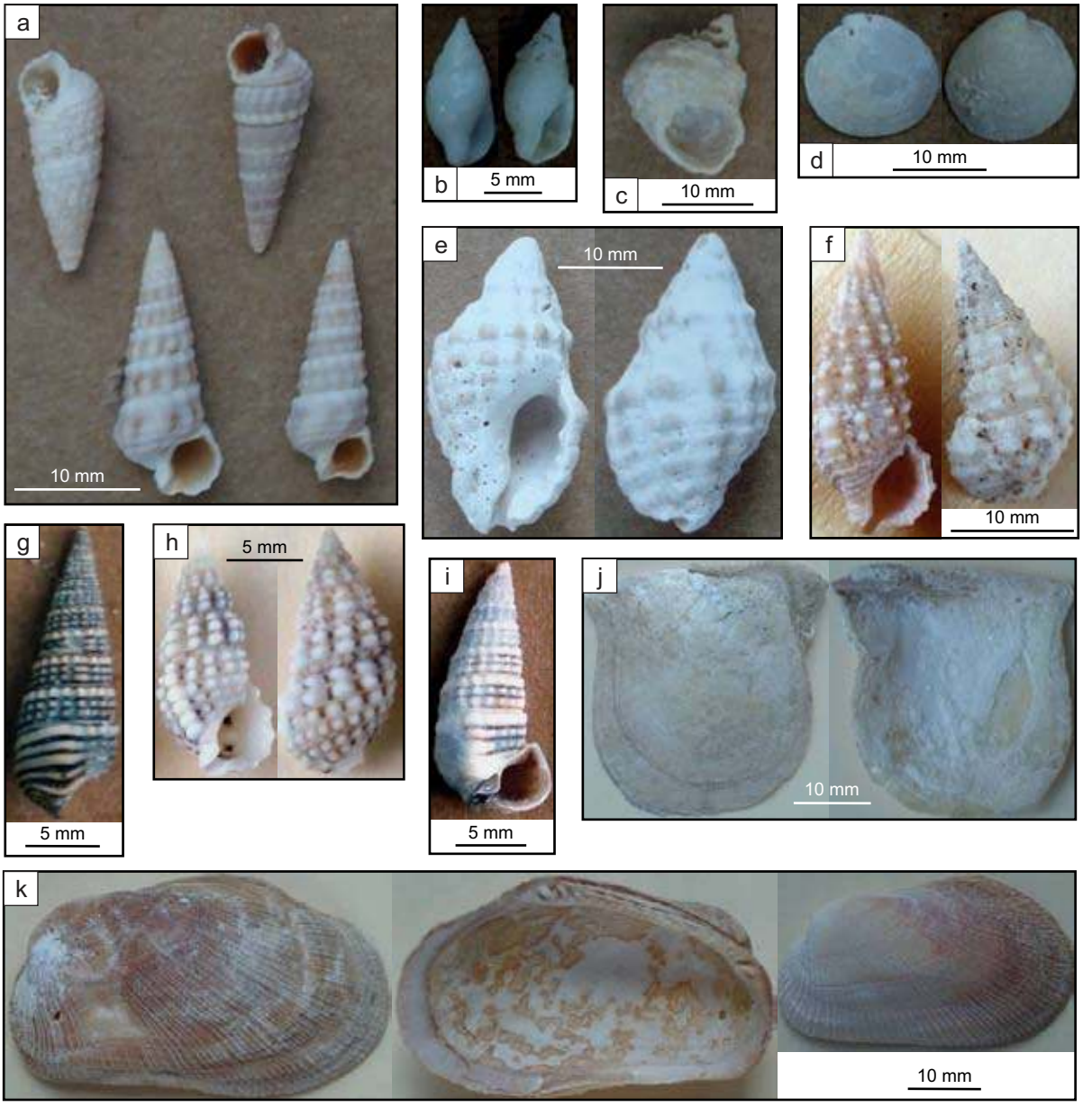

Figure 13: Gastropods (a to c and e to i) and pelecypods (d, j, and k) collected at vertical section MC-3B (identified and photographed by Genjie Liu). Samples are from intervals represented by sample MC-3B-6 (a to d) and samples MC-3B-10 and MC-3B-11 (e to k).
(a) *Cerithidea cingulata* (Gmelin). (b) *Mitrella bland* (Sowerby). (c) *Priotrochus obscurus* (Wood). (d) *Mysia* cf. *elegans* (H. Adams). (e) *Cronia konkanensis* (Melvill). (f) *Cerithium rueppeli* (Phillipi). (g) *Cerithidea cingulata* (Gmelin). (h) *Clypeomorus bifasciatus persicus* (Houbrick). (i) *Potamides conicus* (Blainville). (j) *Pinctada radiata* (Leach). (k) *Barbaria setigera* (Reeve).

bland (Sowerby; Figure 13b), *Priotrochus obscurus* (Wood, Figure 13c), as well as in pelecypods: *Mysia* cf. *elegans* (H. Adams; Figure 13d). Shell samples derived from the gypsum-rich, cross-bedded, bioclastic rudstone/grainstone (longshore beach bar and beach spit deposits, samples MC-3B-10 and MC-3B-11) are rich in gastropods: *Cronia konkanensis* (Melvill; Figure 13e), *Cerithium rueppeli* (Phillipi; Figure 13f), *Cerithidea cingulata* (Gmelin; Figure 13g), *Clypeomorus bifasciatus persicus* (Houbrick; Figure 13h), and *Potamides conicus* (Blainville; Figure 13i), as well as in pelecypods: *Pinctada radiata* (Leach; Figure 13j) and *Barbaria setigera* (Reeve; Figure 13k). The shell assemblages correspond to the ones found along the present-day Abu Dhabi coastline (beaches).

The Holocene vertical section MC-3B corresponds to channel-fills of multiple tidal-channels that incised older Holocene tidal-channels, a microbial mat (vertical section 3A), and Pleistocene reworked carbonate-rich sand (Figures 2 and 9). Radiocarbon age dating show that the youngest channel-fill carbonates at vertical section MC-3B are ca. 1,000 years younger than the tidal-channel deposits at vertical section MC-3A (sample MC-3B-6: ca. 5,200 ^{14}C yrs BP *versus* sample MC-3A-5: ca. 6,200 ^{14}C yrs BP), and ca. 500 years younger than the upper hardground of vertical section MC-3A (sample MC-3B-6: ca. 5,200 ^{14}C yrs BP *versus* sample MC-3A-7: ca. 5,700 ^{14}C yrs BP; Figures 9, 10, and 12). While cutting into the Holocene carbonates of vertical section MC-3A, the tidal-channels have excavated and eroded the previously formed upper hardground (sample MC-3A-7: beach rock, radiocarbon age: ca. 5,700 ^{14}C yrs BP; Figures 9 and 10a), now lining the channel-fill wall as shingled slabs and, subsequently, the lower hardground (sample MC-3A-3 corresponding to sample MC-3B-2: channel-lag, radiocarbon age: ca. 6,400 ^{14}C yrs BP; Figures 10a and 12a), now lining the base of the cannel-cut. The radiocarbon age of the eroded/reworked hardground (sample MC-3B-2: 6,400 ^{14}C yrs BP) which is interpreted to correspond to the in-place hardground of vertical section MC-3A (sample MC-3A-3; Figure 10a) is slightly "too old" compared to the radiocarbon age of the microbial mat (sample MC-3A-2: 6,140 ^{14}C yrs BP; Figure 10a). Like the tidal-channel of vertical section MC-3B, the tidal-channel of vertical section MC-3A (Figures 9 and 10a) might have cut into Pleistocene carbonate-rich sands elsewhere. This could have let to the incorporation of "older" carbonate material, resulting in the slightly "too old" radiocarbon age of the reworked hardground (sample MC-3B-2: bulk sample analysis). Alternatively, the radiocarbon age of the microbial mat sample of vertical section MC-3A (sample MC-3A-2) might be anomalously young compared with the analyzed radiocarbon ages of the microbial mat samples from vertical sections MC-2 and MC-4 (samples MC-2-4 and MC-4-2: both ca. 6,600 ^{14}C yrs BP). The latter interpretation is supported by the radiocarbon age of the cross-bedded, cerithid-rich, bioclastic grainstone sample (sample MC-3A-5: 6,160 ^{14}C yrs BP) which shows a similar radiocarbon age as the underlying microbial mat sample (MC-3A-2: 6,140 ^{14}C yrs BP; Figures 9 and 10a).

Location 3a: Lateral Replacement of Gypsum by Anhydrite

Along the eastern channel wall between studied sections MC-3 and MC-4, the longshore beach bar and beach spit deposits become more gypsum- and anhydrite-rich, until finally being completely overprinted by gypsum and anhydrite (Figures 2, 14a, 14b, and 14c).

The gypsum-rich, cross-bedded, bioclastic rudstone/grainstone (longshore beach bar and beach spit deposits) is rich in gastropods (cerithids) and pelecypods (*Pinctada* sp.; Figure 15a). In addition, encrusting coralline red algae (*Goniolithon*; Figure 15b) and, rarely, coral debris can be found.

Large gypsum crystals, showing a poikilotopic fabric are growing within cross-bedded, fine-grained, bioclastic grainstone/packstone (tidal-channel deposits); mimicking the cross-bedding (Figure 15c). Relatively small bladed gypsum crystals are nearly completely overprinting/replacing the longshore beach bar and beach spit deposits (Figure 15b). Further north, towards studied vertical section MC-4, anhydrite is growing replacive/displacive within the gypsum-overprinted, cross-bedded, bioclastic rudstone/grainstone (longshore beach bar and beach spit deposits; Figure 2). The anhydrite clearly post-dates the gypsum growths and displays a nodular to contorted (enterolithic/ptygmatic) fabric (Figures 14a, 14b, and 15d), in places also showing teepee-like structures (Figure 14c).

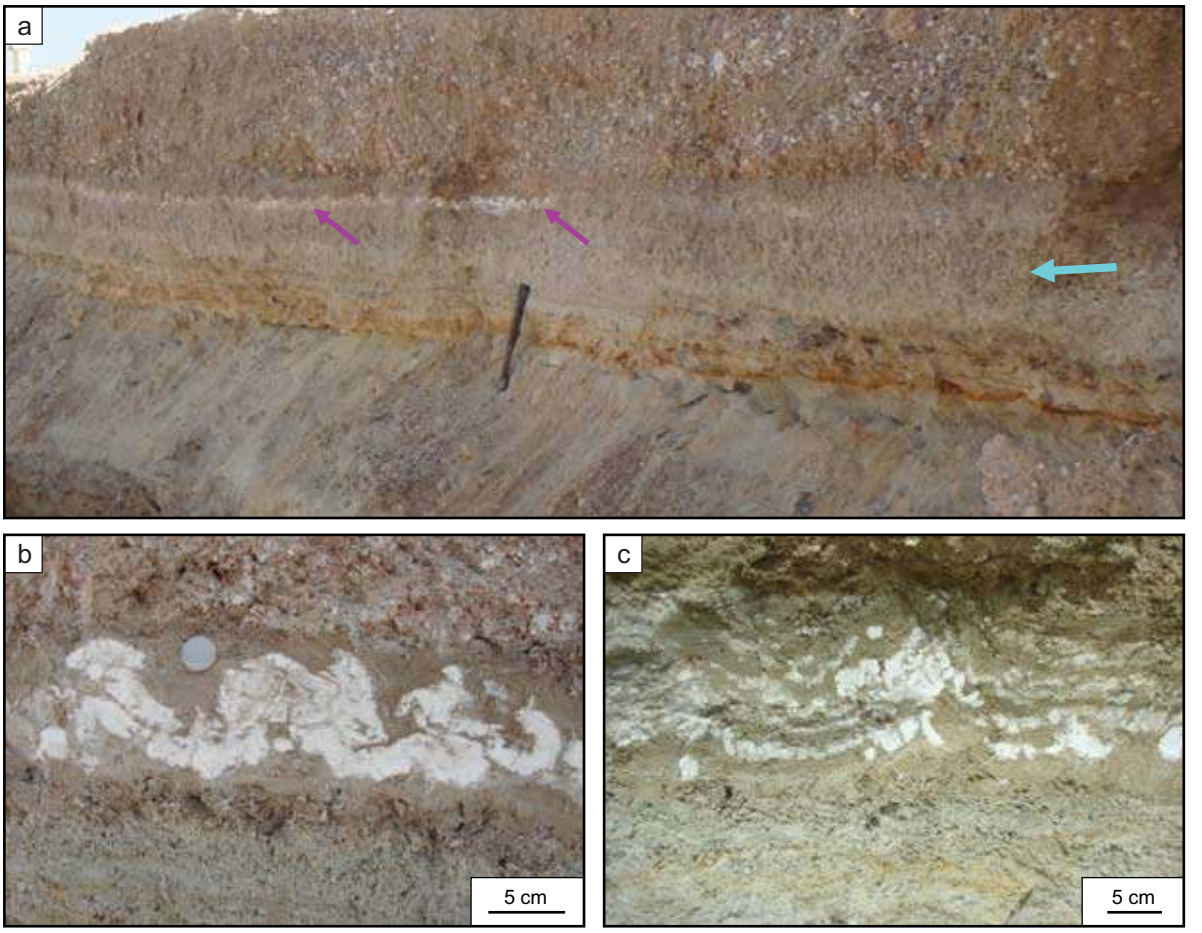

Figure 14: (a) East wall of channel between measured vertical sections MC-3 and MC-4 (location 3a; Figures 1c and 2) showing lateral increase in discontinuous nodular to contorted (enterolithic/ptygmatic) anhydrite (purple arrows) replacing gypsum-overprinted, cross-bedded, bioclastic rudstone/grainstone (longshore beach bar and beach spit deposits: cyan arrow). Horizontal reddish bands (around hammer) correspond to oxidized horizons interpreted as paleo-groundwater tables. Length of hammer is 27.7 cm.
(b) Close-up of replacive/displacive, discontinuous nodular to contorted (enterolithic/ptygmatic) anhydrite (measured section MC-4; Figure 16). See Figures 1c and 2 for location.
(c) Discontinuous nodular to contorted anhydrite showing teepee structure (close to whale excavation site; Figure 17). See Figures 1c and 2 for location.

Location 4: Vertical Section MC-4

Approximately 1.30 m of vertical section of Pleistocene carbonate-rich sands and unconformably overlying Holocene carbonates and sabkha evaporites are described at location 4 (vertical section MC-4) along the eastern channel wall (Figures 1c, 2, and 16a). In the following account, the encountered facies types, their key sedimentary structures and evaporitic overprint, as well as their interpreted depositional environments are listed from base to top:

Fine-grained, carbonate-rich sand (sample MC-4-1)

- sedimentary structure: un-bedded to wavy-bedded
- siliciclastic grain size: very fine upper (vfU: 100 µ)
- carbonate grain size: very fine upper to fine upper (vfU-fU: 100–220 µ)
- depositional environment: reworked aeolian dunes (aeolianite; Figures 16a and 16b)

Crinkly-laminated stromatolitic bindstone (sample MC-4-2)

- sedimentary texture: boundstone/bindstone
- sedimentary structure: dark organic, crinkly laminated
- depositional environment: intertidal, low-energy microbial mat (Figure 16a)

Hardground (sample MC-4-3)

- cemented, cerithid-rich, bioclastic grainstone
- isopachous, fibrous aragonite cement
- cemented microbial mat and cemented channel-lag (Figure 16c)

Cerithid-rich, bioclastic grainstone (sample MC-4-3)

- sedimentary texture: grainstone
- sedimentary structure: low-angle cross-bedded
- depositional environment: shallow subtidal, high-energy tidal-channel deposits (Figure 16a)

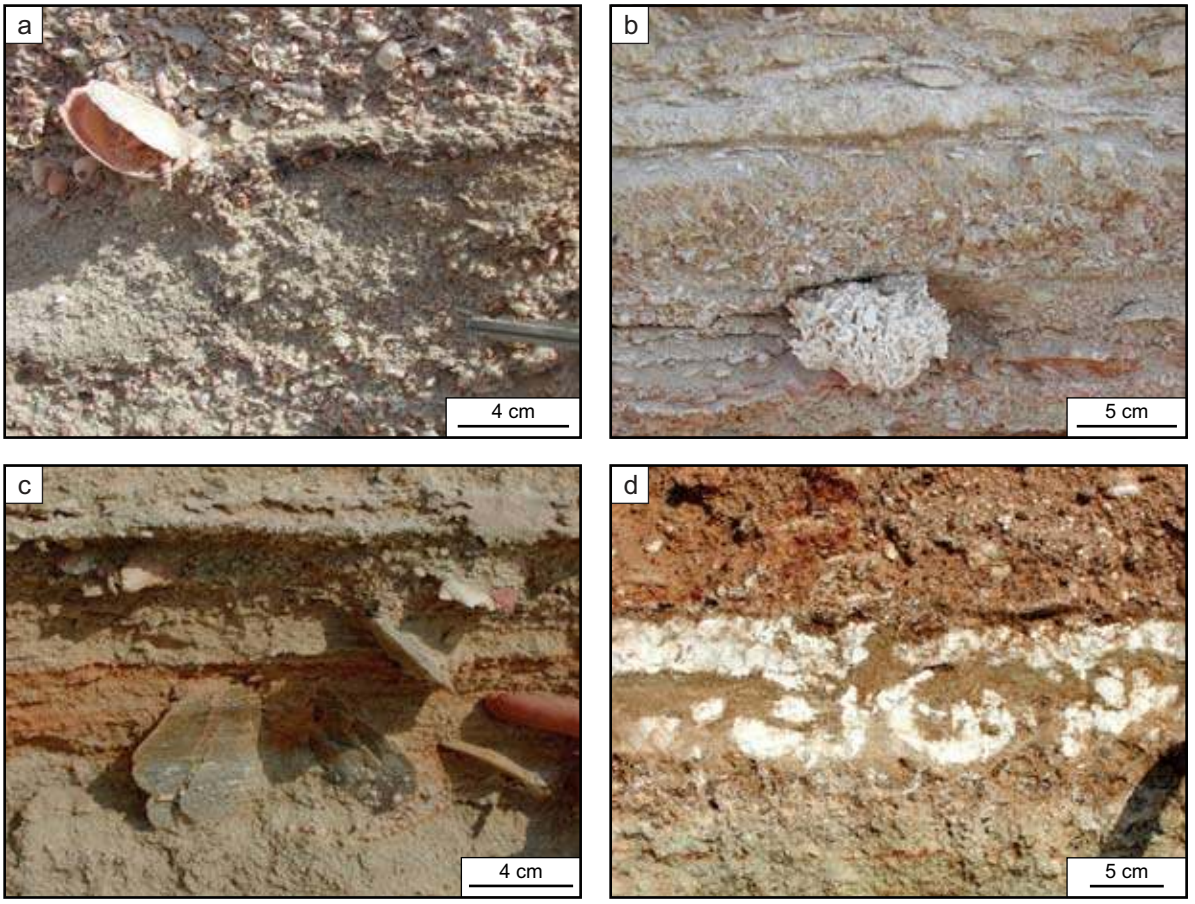

Figure 15: Sedimentary structures along the east wall of the channel, between vertical sections MC-3 and MC-4 (location 3a; Figures 1c and 2).

(a) Gypsum-rich, cross-bedded, bioclastic rudstone/grainstone (longshore beach bar and beach spit deposits), rich in cerithid gastropods and bivalves (*Pinctata* sp.).

(b) Encrusting coralline red algae (*Goniolithon*) within gypsum-rich (small, bladed gypsum crystals), cross-bedded, bioclastic rudstone/grainstone.

(c) Gypsum crystals (gypsum rosettes) poikilotopically enclosing grains of cross-bedded, fine-grained, bioclastic grainstone. Cross-bedding and iron staining is still visible within the gypsum crystals.

(d) Replacive/displacive growth of nodular to contorted (enterolithic/ptygmatic) anhydrite within gypsum-overprinted, cross-bedded, bioclastic rudstone/grainstone.

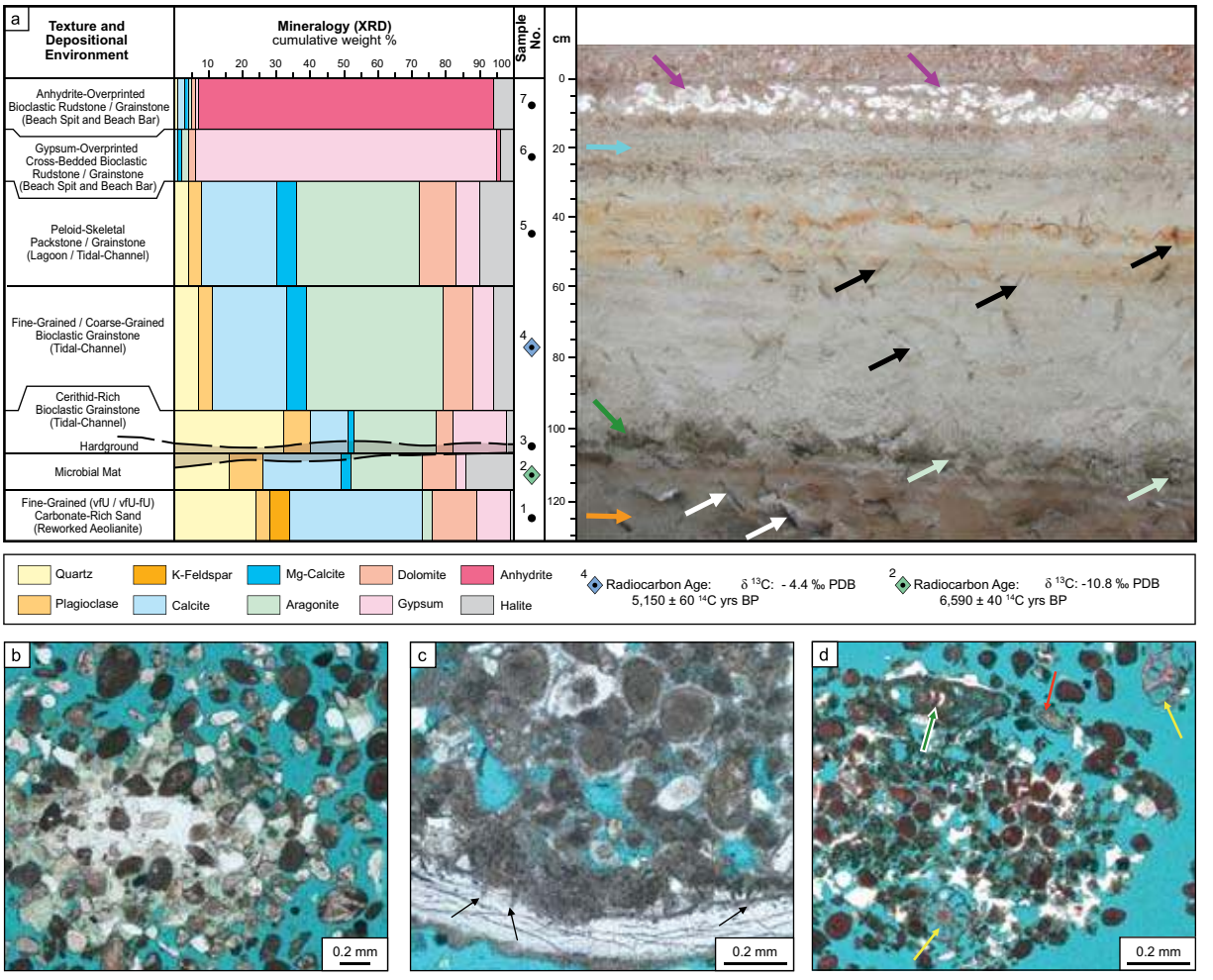

Figure 16: (a) Vertical section MC-4 (location 4; Figures 1c and 2) showing Holocene sediments (transgressive microbial mat; green arrow) overlying Pleistocene fine-grained, carbonate-rich sand (reworked aeolian dune deposits: orange arrow). Mineralogical composition from XRD (cumulative weight %). Radiocarbon age dating and carbon-isotope results are for microbial mat (MC-4-2) and fine-grained to coarse-grained, bioclastic grainstone (MC-4-4). Large bladed gypsum crystals are present within the Pleistocene fine-grained, carbonate-rich sand (white arrows), the microbial mat (light green arrows), and the fine-grained, grey-greenish interval displaying oxidized horizons (black arrows). The cross-bedded, bioclastic rudstone/grainstone is overprinted by small, bladed gypsum crystals (cyan arrow), and is overlain by an interval showing replacive/displacive growth of discontinuous, nodular and contorted (enterolithic/ptygmatic) anhydrite (purple arrows). Horizontal reddish bands correspond to oxidized horizons interpreted as paleo-groundwater tables. (b-e) Thin section photomicrographs. (b-d) Plane polarized light. (e) Partly crossed polarized light. (d) Stained with Alizarin red-S. (b) Pleistocene fine-grained, carbonate-rich sand (MC-4-1) showing poikilotopic gypsum cementation (whitish and greenish crystals) around siliciclastic and carbonate grains. The siliciclastic material (100 µ) is very fine upper (vfU), whereas the carbonate material (100 to 220 µ) is very fine upper to fine upper (vfU-fU). (c) Cemented cerithid-rich, bioclastic grainstone (hardground, MC-4-3) showing shell fragment with borings (black arrows) and isopachous, fibrous aragonite cement around carbonate grains. (d) Fine-grained, peloid-skeletal packstone/grainstone (MC-4-5) showing rotalid foraminifera (*Ammonia* sp.: yellow arrows) and miliolid foraminifera (*Quinqueloculina* sp. and *Dentritina* sp.: red and green arrows, respectively). Whitish patches are halite. (e) Anhydrite-overprinted bioclastic rudstone/grainstone showing felted anhydrite texture (MC-4-7).

Fine-grained/coarse-grained, bioclastic grainstone (sample MC-4-4)

- sedimentary texture: grainstone
- sedimentary structure: low-angle cross-bedded
- depositional environment: shallow subtidal, moderate- to high-energy tidal-channel deposits (Figure 16a)

Peloid-skeletal packstone/grainstone (sample MC-4-5)

- sedimentary texture: packstone to grainstone
- sedimentary structure: low-angle cross-bedded to un-bedded and rootlets
- depositional environment: shallow subtidal moderate-energy tidal-channel grading into lowermost intertidal to shallow subtidal, low-energy, mud-rich, rooted lagoonal deposits (Figure 16d)

Gypsum-overprinted, cross-bedded, bioclastic rudstone/grainstone (sample MC-4-6)

- sedimentary texture: rudstone and grainstone (destroyed by gypsum overprint).
- sedimentary structure: low-angle cross-bedded to parallel-bedded
- depositional environment: shallow subtidal to intertidal, high-energy longshore beach bar and beach spit deposits; overprinted by sabkha gypsum (Figure 16a)

Anhydrite-overprinted, bioclastic rudstone/grainstone (sample MC-4-7)

- sedimentary texture: rudstone and grainstone (destroyed by gypsum and anhydrite overprint)
- sedimentary structure: low-angle cross-bedded to parallel-bedded
- depositional environment: shallow subtidal to intertidal, high-energy longshore beach bar and beach spit deposits; overprinted by sabkha anhydrite-after-gypsum (Figures 16a and 16e)

The facies succession observed at Mussafah vertical section MC-4 corresponds to some of the lateral facies variations along the Abu Dhabi coastline, as illustrated by arrows on Figure 1b.

The fine-grained, peloid-skeletal packstone/grainstone (sample MC-4-5: 11%), the microbial mat (sample MC-4-2: 10%) and the reworked Pleistocene carbonate-rich sand (sample MC-4-1: 13%) are rich in dolomite (Figure 16a).

Seven samples (MC-4-1 to MC-4-7) were selected for thin section and XRD analyses (Figure 12a). Radiocarbon age-dating carried out on one microbial mat sample (^{14}C accelerator-mass-spectrometer technique, bulk sample) and one unconsolidated carbonate sample (^{14}C radiometric dating technique, selected shell samples) show an age of 6,590 ± 40 ^{14}C yrs BP for the microbial mat sample (MC-4-2) and 5,150 ± 60 ^{14}C yrs BP for the fine-grained/coarse-grained, bioclastic grainstone sample (MC-4-4). The microbial mat sample shows a distinctively more negative delta ^{13}C value (-10.8‰ PDB; Figure 16a), due to its high organic content.

The whole section, including the Pleistocene carbonate-rich sand and the microbial mat is rich in bladed gypsum crystals (Figure 16a). The reworked carbonate-rich sand (sample MC-4-1) shows gypsum cementation of siliciclastic and carbonate grains (Figure 16b). The hardground (sample MC-4-3) exhibits shell fragments with borings and isopachous, fibrous aragonite cement around carbonate grains (Figure 16c). Abundant rotalid foraminifera (*Ammonia* sp.) and miliolid foraminifera (*Quinqueloculina* sp. and *Dentritina* sp.) were found within the fine-grained, peloid-skeletal packstone/grainstone (sample MC-4-5; Figure 16d). Thin sections reveal the felted micro-structure of the nodular to contorted (enterolithic/ptygmatic) anhydrite (sample MC-4-7; Figure 16e).

The Holocene vertical section MC-4 represents a transgressive (deepening-upward) facies succession from intertidal (microbial mat) to shallow subtidal to intertidal (predominantly tidal-channel and rooted lagoon deposits, with a marine flooding surface on top of the Pleistocene carbonate-rich sands (reworked aeolian dune deposits). The slow rising/still stand and regressive phase of the sea level is represented by the prograding longshore beach bar and beach spit deposits and the strong diagenetic (evaporitic) sabkha-overprint, resulting in the growths of gypsum and anhydrite (Figure 2).

Location 4a: Site of Whale Bone Exposure

In March 2006, large bones were found weathering from the edge of the exposed eastern wall of the channel in close proximity (c. 20 m north) to measured vertical section MC-4 (Figures 1c and 2), by ADNOC geologists Khalil Al-Mehsin and Bernard Pierson. These bones were later identified as the mandible (jaw), humerus, radius and ulna (forelimbs) and the scapula (shoulder blade) of a whale (Figures 17a, 17b, and 17c) by Simon Aspinall, an ecological consultant and coordinator of the National Cetacean Database of the United Arab Emirates; most probably belonging to a baleen whale (Mysticete; Pierson et al., 2006, 2008; personal communications John Stewart, 2008).

In January 2008, the excavation and conservation of the remainder of the whale skeleton started. This effort is supported financially by ADNOC, under the supervision of the Marine Environment Research Centre of the Environmental Agency - Abu Dhabi (EAD), with assistance being provided by the Abu Dhabi Authority for Culture and Heritage, and Simon Aspinall. The excavation was carried out by two experts from the UK: John Stewart (Natural History Museum, London) and Nigel Larkin (Norwich Castle Museum, Norwich Archaeology Service), with help from Simon Aspinal. Both whale bones and whale barnacles (*Coronula diadema*, identified by Prof. Phil Rainbow) were found and preserved (Figure 17d). During the excavation, it became apparent that a large part of the whole whale skeleton was still present, more than had originally been anticipated, and a second, more comprehensive phase of excavation was planned.

The positions of the bones indicate that the whale was laid down on his back. The surrounding cerithid-rich, fine-grained to coarse-grained, bioclastic grainstones allow the interpretation that the whale was transported/stranded in a shallow tidal-channel.

The scapula (shoulder plate) directly overlies a hardground which formed at the base of a tidal-channel and also encompasses the upper part of the underlying microbial mat (Figure 17c). The shoulder plate is not cemented into the hardground. The upper surface of the hardground is pitted by burrows and borings (*Lithophaga*; Figure 17e). The cemented microbial mat shows an upward increase in cerithid gastropods towards the cemented tidal-channel deposits (cerithid-rich, bioclastic grainstone; Figure 17f). The hardground is cemented by isopachous, fibrous aragonite cement and is rich in miliolid foraminifera (*Peneroplis* sp. and *Spirolina* sp.) and worm tubes (serpulids; Figures 17g, 17h, and 17i).

At vertical section MC-4, close to the site where the whale bones were found (Figures 1c and 2), radiocarbon age-dating results of the microbial mat underlying the whale bones and the fine-grained to coarse-grained, bioclastic grainstone (tidal-channel deposits) surrounding the whale bones were age-dated at ca. 6,600 and 5,200 ^{14}C yrs BP, respectively (Figure 16a). These two radiocarbon age-dates closely bracket the age of the whale stranding and the time it took burying the whale at the Mussafah Channel site.

The finding of the whale bones at the Mussafah Channel site has added a new dimension to this location and has made it even more important and famous.

GYPSUM CRYTALS MORPHOLOGIES IN RELATION TO THEIR HOST SEDIMENT AND PALEO-GROUNDWATER TABLES

Morphology (shape), size, and color of the gypsum crystals, growing within the Pleistocene carbonate-rich, fine-grained sands, the Holocene microbial mats, and the Holocene carbonates change considerable depending on the host sediments. Morphology, size, and color of the gypsum crystals vary with the grain size and color of the host sediments. Crystal size is generally inversely related to the grain size of the host sediment. The finer-grained and more homogenous sediments contain bigger gypsum crystals. Large, 1 ft-sized, bladed gypsum crystals of dark grey color are found within the Pleistocene carbonate-rich sand, mimicking the dark sand color (Figure 18a). Gypsum crystals growing within the microbial mat are semi-translucent and lenticular, with the original microbial material still visible within the gypsum crystals (Figure 18b). Gypsum crystals growing within fine-grained, rooted and

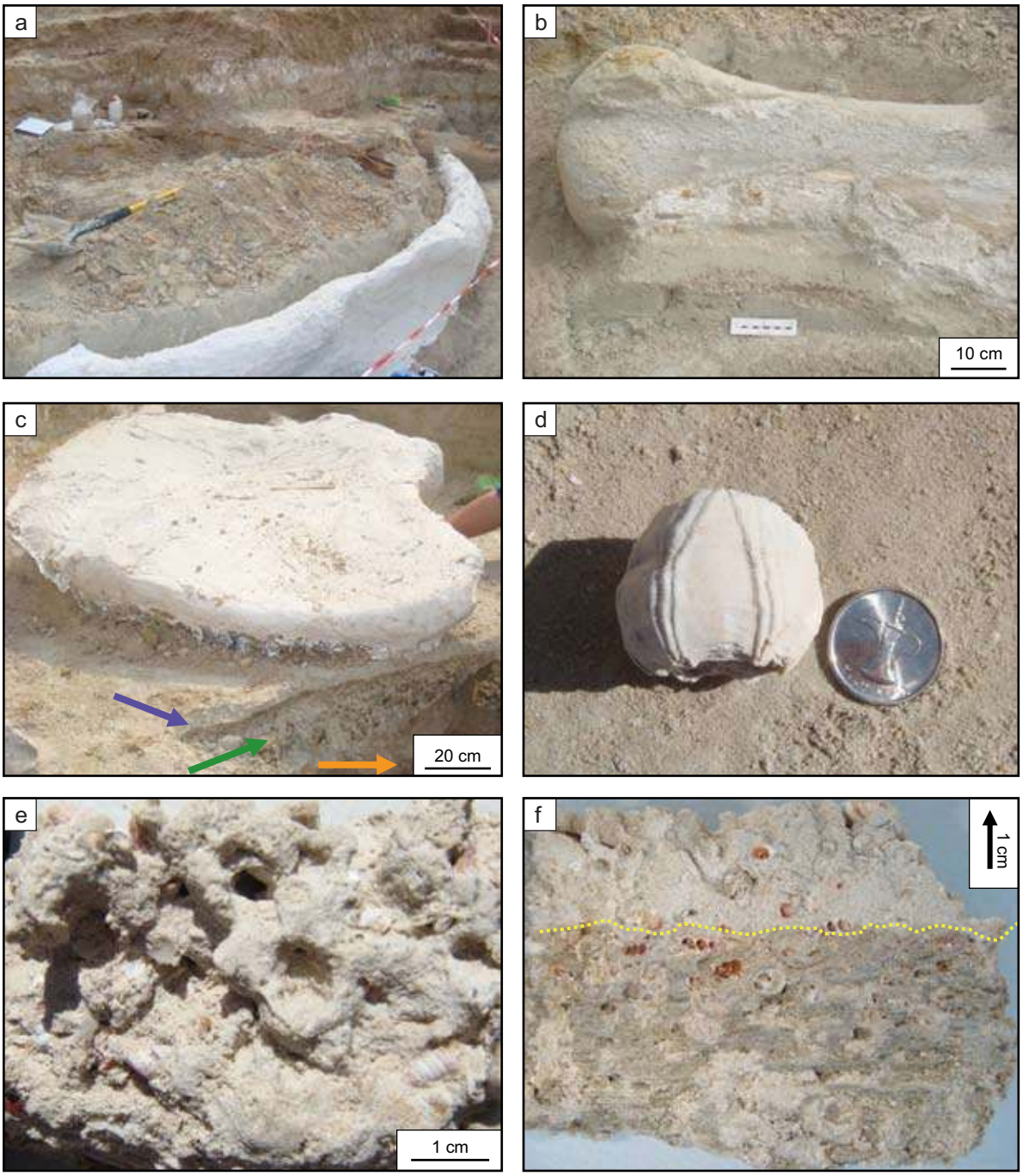

Figure 17: Photos of excavation site of large whale bones (location 4a; Figures 1c and 2), found close (c. 20 m north) to measured vertical section MC-4. (a) Large mandible (jaw bone, c. 4 m in length), covered with plaster for preservation. (b) Close-up of mandible. (c) Scapula (shoulder blade), covered with plaster for preservation on top of hardground. The hardground encompasses both tidal-channel deposits (blue arrow) and the transgressive microbial mat (green arrow, radiocarbon age ca. 6,400 ^{14}C yrs BP), overlying Pleistocene reworked aeolian dune deposits (orange arrow, radiocarbon age ca. 24,000 ^{14}C yrs BP). (d) Close-up of a whale barnacle (*Coronula diadema*, identified by Prod. Phil Rainbow). Diameter of coin is 2.3 cm. (e) Hardground showing pitted upper surface due to borings (*Lithophaga*). (f) Slabbed surface of hardground showing cemented microbial mat at the base (greenish color, below yellow stippled line) passing upward into overlying cerithid-rich, bioclastic grainstone (tidal-channel deposits showing whitish color above yellow stippled line). (g) Thin section photomicrograph (plane polarized light) of cemented microbial mat shown on Figures 17c and 17f, rich in miliolid foraminifera (*Peneroplis* sp.: white arrows) and worm tubes (serpulids: red arrows). Isopachous, fibrous aragonite cement engulfs carbonate grains.

See facing page for continuation.

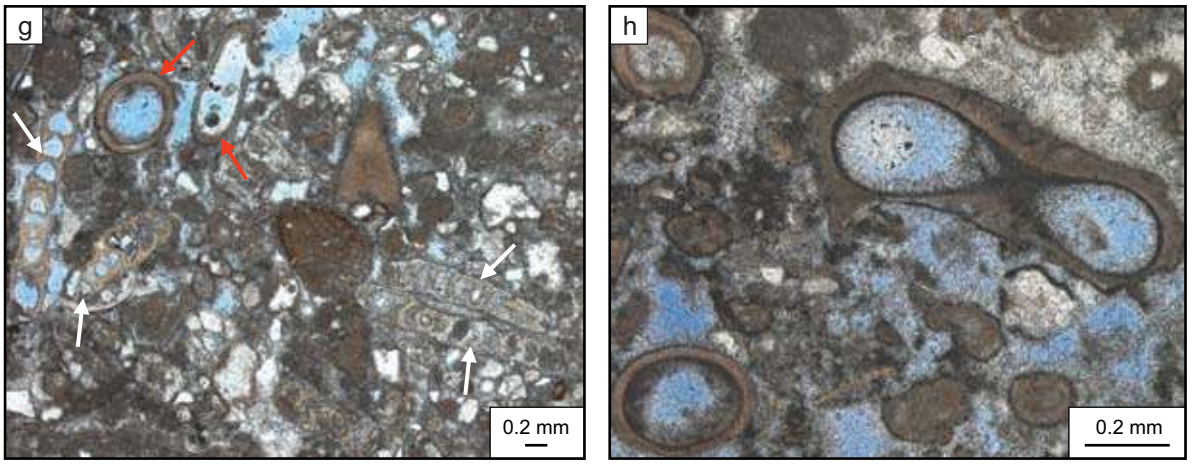

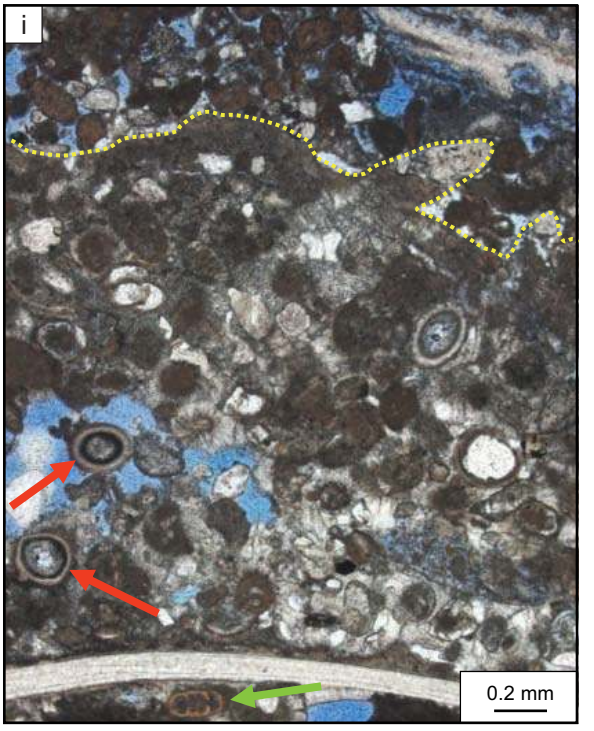

Figure 17 (continued): (h) Thin section photomicrograph (plane polarized light) of cemented microbial mat showing worm tubes (serpulids) surrounded and partly filled by isopachous, fibrous aragonite cement. (i) Thin section photomicrograph (plane polarized light) showing transition of cemented microbial mat (below yellow stippled line) to cerithid-rich, bioclastic grainstone (tidal-channel deposits, above yellow stippled line). Also displayed are worm tubes (serpulids: red arrows) and miliolid foraminifera (*Spirolina* sp.: green arrow).

microbial-laminated peloid-skeletal packstones (lagoonal deposits) are also quite large (1 ft-sized crystals) and show the same dark grey-greenish color as the enclosing carbonates (Figure 18c). In fine-grained, bioclastic carbonates (tidal-channel and tidal-channel-influenced lagoonal deposits), gypsum crystals display the light grey color like the host carbonates, showing large gypsum blades (Figure 18d) or very nice gypsum rosettes (Figure 18e). Cross-bedded, fine-grained carbonates (tidal-channel deposits) show gypsum crystals and gypsum rosettes, preserving the cross-bedding and the color of the host carbonates (Figure 18f). Gypsum crystals replacing cross-bedded, bioclastic rudstone/grainstone, rich in cerithid gastropods and pelecypods (longshore beach bar and beach spit deposits), are light colored like the host sediment and show relatively small, bladed crystals (Figure 18g).

Reddish horizons are conspicuous at various depth levels throughout the studied vertical sections (Figures 6, 7a, 8c, 8d, 9, 12a, 14a, 15c, and 16a). These oxidized horizons occur up to c. 2 m above the present-day sea level (c. 40 cm below the erosional top of the in-place studied deposits; Figures 9 and 12a) and correspond to paleo-groundwater tables, reflecting seasonal and short term sea-level fluctuations (Kirkham, 1998). Large lensoid gypsum crystals and gypsum rosettes are interpreted to have formed at and below these paleo-groundwater tables in the phreatic zone (Warren 1991, 2006; Schreiber personal communications, 2008). Smaller gypsum crystals, like the ones replacing the uppermost cross-bedded, bioclastic carbonates (Figure 18g), might, however, have also formed in the capillary zone above the paleo-groundwater table as thermalites (Wood et al., 2005). These observations, together with fact that the uppermost studied gypsum- and/or anhydrite-dominated carbonates clearly show erosion on top (overlain by construction-fill material; Figure 9), suggest that sea level was about 2–3 m higher than the present-day sea level about 5,000 years ago (the radiocarbon age of the uppermost, *in-situ* deposits; Figure 9).

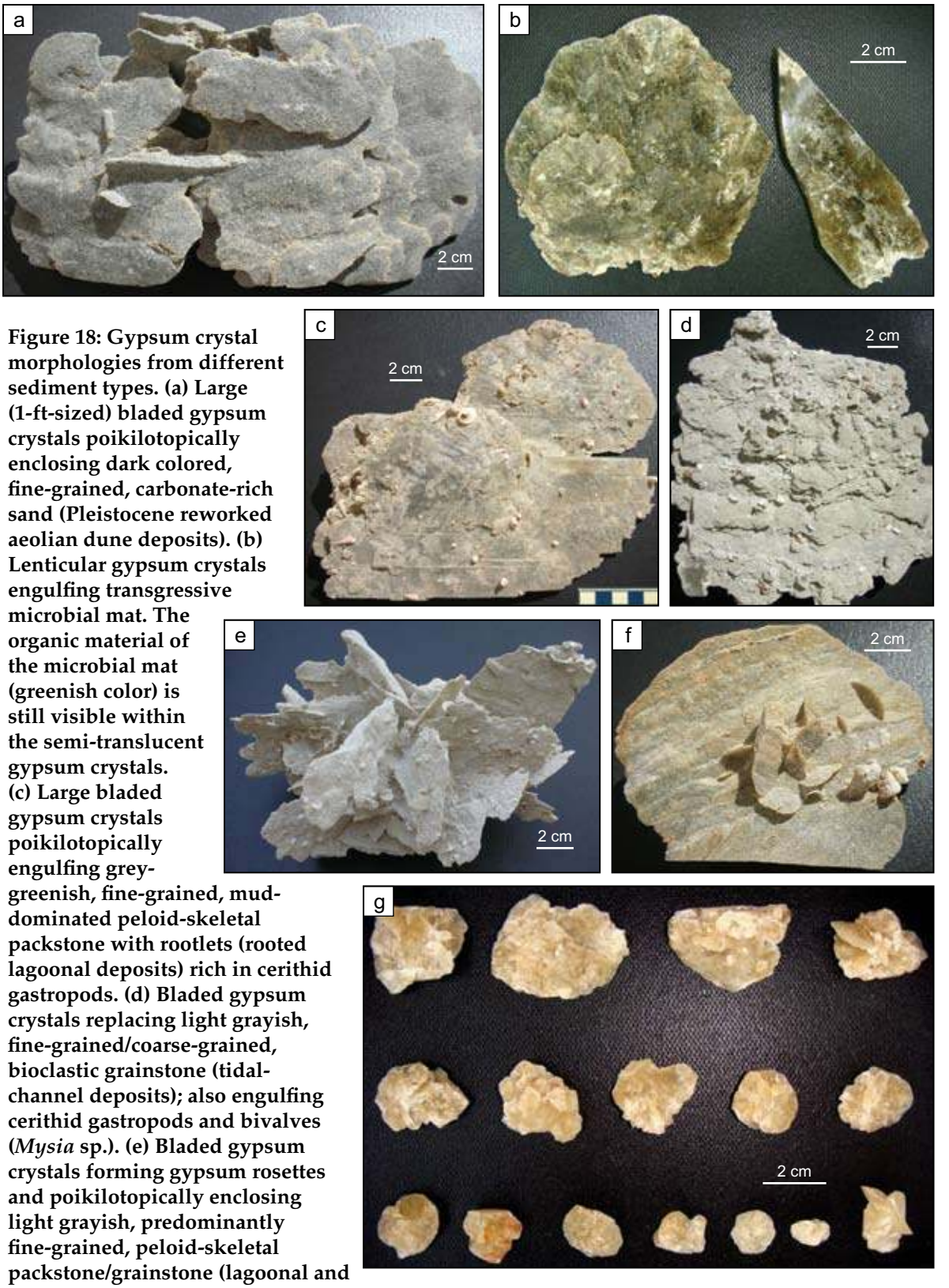

Figure 18: Gypsum crystal morphologies from different sediment types. (a) Large (1-ft-sized) bladed gypsum crystals poikilotopically enclosing dark colored, fine-grained, carbonate-rich sand (Pleistocene reworked aeolian dune deposits). (b) Lenticular gypsum crystals engulfing transgressive microbial mat. The organic material of the microbial mat (greenish color) is still visible within the semi-translucent gypsum crystals. (c) Large bladed gypsum crystals poikilotopically engulfing grey-greenish, fine-grained, mud-dominated peloid-skeletal packstone with rootlets (rooted lagoonal deposits) rich in cerithid gastropods. (d) Bladed gypsum crystals replacing light grayish, fine-grained/coarse-grained, bioclastic grainstone (tidal-channel deposits); also engulfing cerithid gastropods and bivalves (*Mysia* sp.). (e) Bladed gypsum crystals forming gypsum rosettes and poikilotopically enclosing light grayish, predominantly fine-grained, peloid-skeletal packstone/grainstone (lagoonal and tidal-channel deposits); also engulfing cerithid gastropods and bivalves (*Mysia* sp.). (f) Bladed gypsum crystals with tendency to rosette shape poikilotopically enclosing reddish stained, fine-grained, bioclastic grainstone with thin coarse-grained bands (tidal-channel deposits); also engulfing bivalves and gastropods (*Priotrochus* sp.). Cross-bedding of the fine-grained carbonate is still visible within the gypsum crystals. (g) Small flat gypsum crystals with tendency to rosette shape incorporating and replacing light colored, cross-bedded, bioclastic rudstone/grainstone (longshore beach bar and beach spit deposits).

DOLOMITE FORMATION AND DISTRIBUTION

XRD results reveal that dolomite is abundant throughout all studied vertical sections (Figures 3a, 7a, 10a, 12a, and 16a). Vertical sections MC-1 and MC-2 that are dominated by rooted lagoonal and microbial-laminated lagoonal deposits contain up to 50% of dolomite (Figures 3a and 7a). Dolomite is found in concentrations of up to 17% in the microbial mats (3a, 7a, 10a, 12a, and 16a). Up to 19% of dolomite is found in the tidal-channel and tidal-channel/lagoonal deposits (Figures 10a, 12a, 16a), and up to 20% of dolomite is found in some of the Pleistocene reworked aeolian dune deposits (Figures 3a, 12a and 16a).

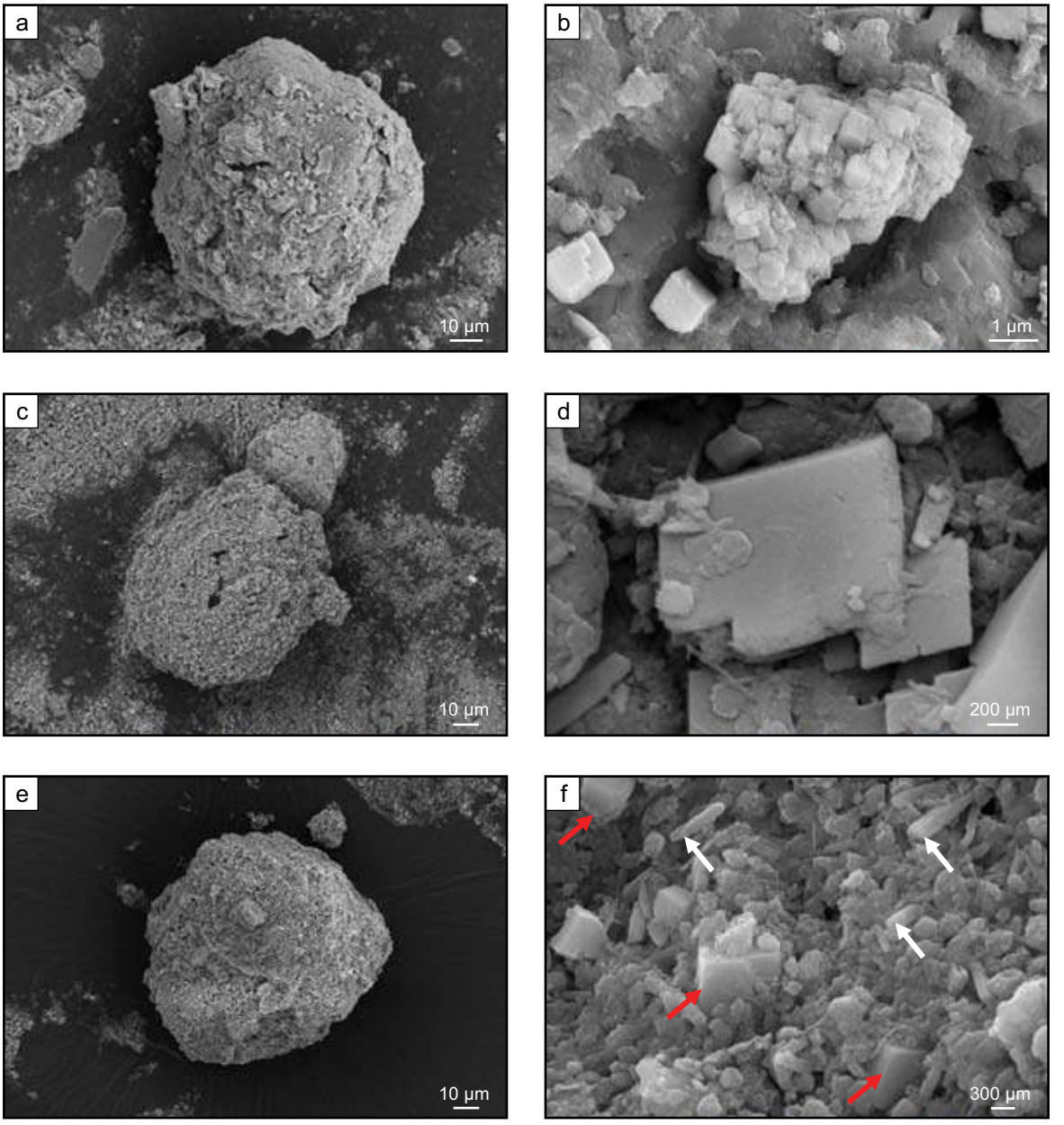

Figure 19: SEM photomicrographs of microcrystalline dolomite morphologies. SEM photomicrographs provided by Tomaso Bontognali (ETH Zurich, Switzerland). (a) Dolomite aggregate displaying spherical morphology (microbial mat, sample MC-2-2). (b) Dolomite aggregate displaying subhedral to euhedral dolomite rhombohedra (microbial mat, sample MC-2-2). (c) Dolomite aggregate displaying spherical morphology (rooted lagoon, sample MC-2-4). (d) Subhedral to euhedral dolomite rhombohedra (rooted lagoon, sample MC-2-4). (e) Dolomite aggregate displaying spherical morphology (microbial-laminated lagoon, sample MC-2-6). (f) Subhedral to euhedral dolomite rhombohedra (red arrows) between aragonite needles with blunt ends (white arrows; microbial-laminated lagoon, sample MC-2-6).

Holocene dolomite forming beneath the supratidal sabkhas of the Arabian Gulf was first reported by Wells (1962). The sabkha model (Kinsman, 1969) and its refinements which added further mechanisms to account for adequate recharge of solutes, like evaporative pumping (Hsü and Siegenthaler, 1969; McKenzie et al., 1980; Müller et al., 1990) and ascending brines (Wood et al., 2002) were based on studies of the supratidal environment along the Abu Dhabi coastline (Curtis, 1963; Wenk et al, 1993).

Microbial dolomite formation involving sulfate reducing bacteria (SRB) mediating dolomite precipitation is another model, applicable to explain the occurrence of the dolomite within the studied sediments (Vasconcelos et al., 1995, 2005; Vasconcelos and McKenzie, 1997; Warthmann et al., 2000;

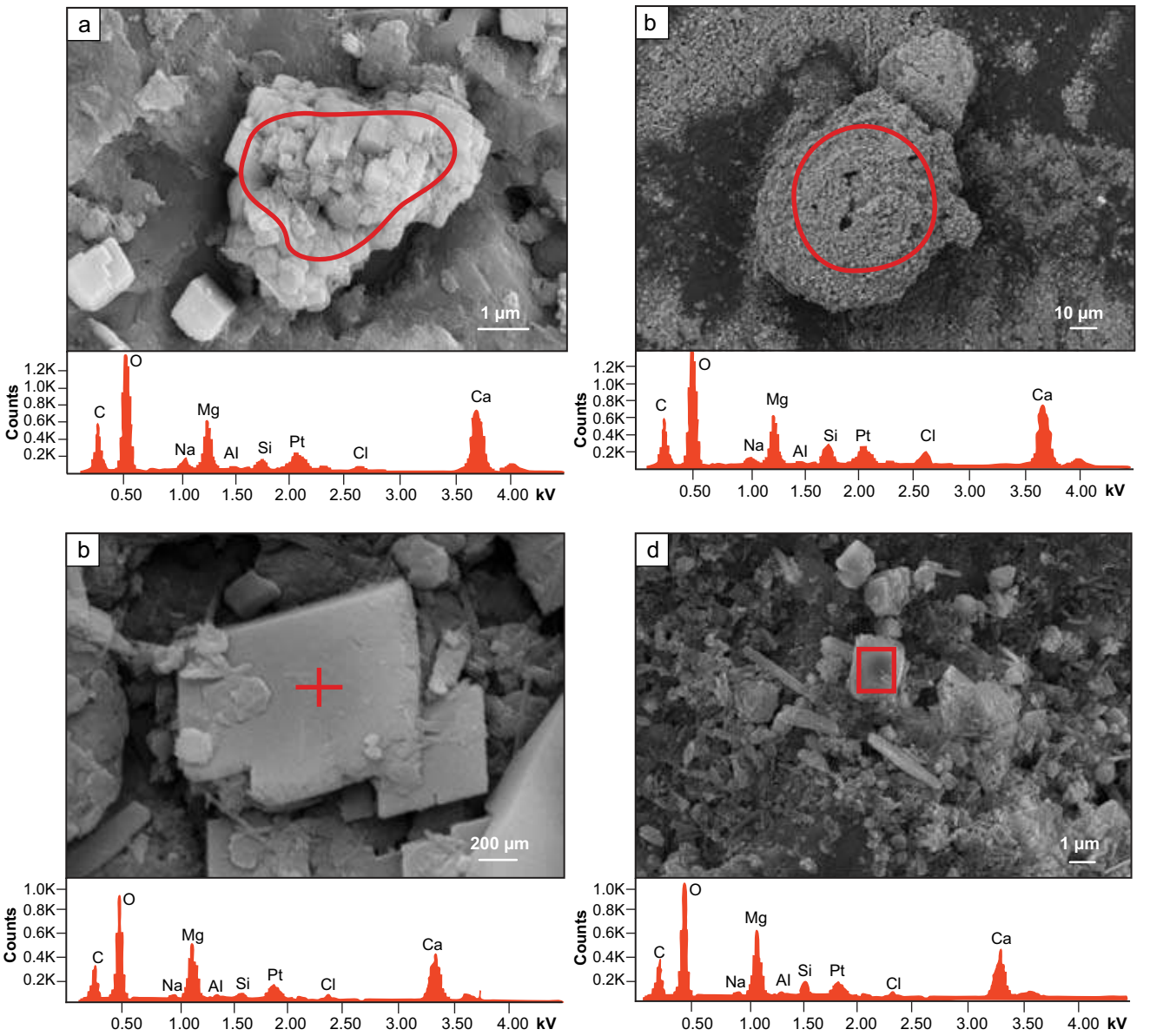

Figure 20: EDX spectra (area measured marked in red) displaying results of elemental analyses of dolomite. C-peak: carbon, O-peak: oxygen, Na-peak: sodium, Mg-peak: magnesium, Al-peak: aluminum, Si-peak: silica, Cl-peak: chlorine, and Ca-peak: calcium. Pt-peak corresponds to the coating applied during preparation. EDX analyses and SEM photomicrographs provided by Tomaso Bontognali (ETH Zurich, Switzerland). (a) EDX spectrum of dolomite aggregate displaying rhombohedral morphology (microbial mat, sample MC-2-2). (b) EDX spectrum of dolomite aggregate displaying spherical morphology (rooted lagoon, sample MC-2-4). (c) EDX spectrum of rhombohedral dolomite crystal (rooted lagoon, sample MC-2-4). (d) EDX spectrum of rhombohedral dolomite crystal within aragonite crystals (microbial-laminated lagoon, sample MC-2-6).

van Lith et al., 2003a, b; Wright and Wacey, 2005; Strohmenger et al., 2010). Most recently, Bontognali (2008) and Bontognali et al. (2010) studying microbial dolomite formation within the recent and buried microbial mats of the Abu Dhabi sabkha in the vicinity of Al-Qanatir Island (Al-Dabbiya area), demonstrated that dolomite precipitates as a consequence of mineral nucleation and growth within the extracellular polymeric substances (EPS) constituting the microbial mats (Bontognali, 2008; Bontognali et al., 2008). Microbial communities commonly live and grow in aggregates composed of EPS, a broad term which groups a large variety of organic polymers (Decho, 1990).

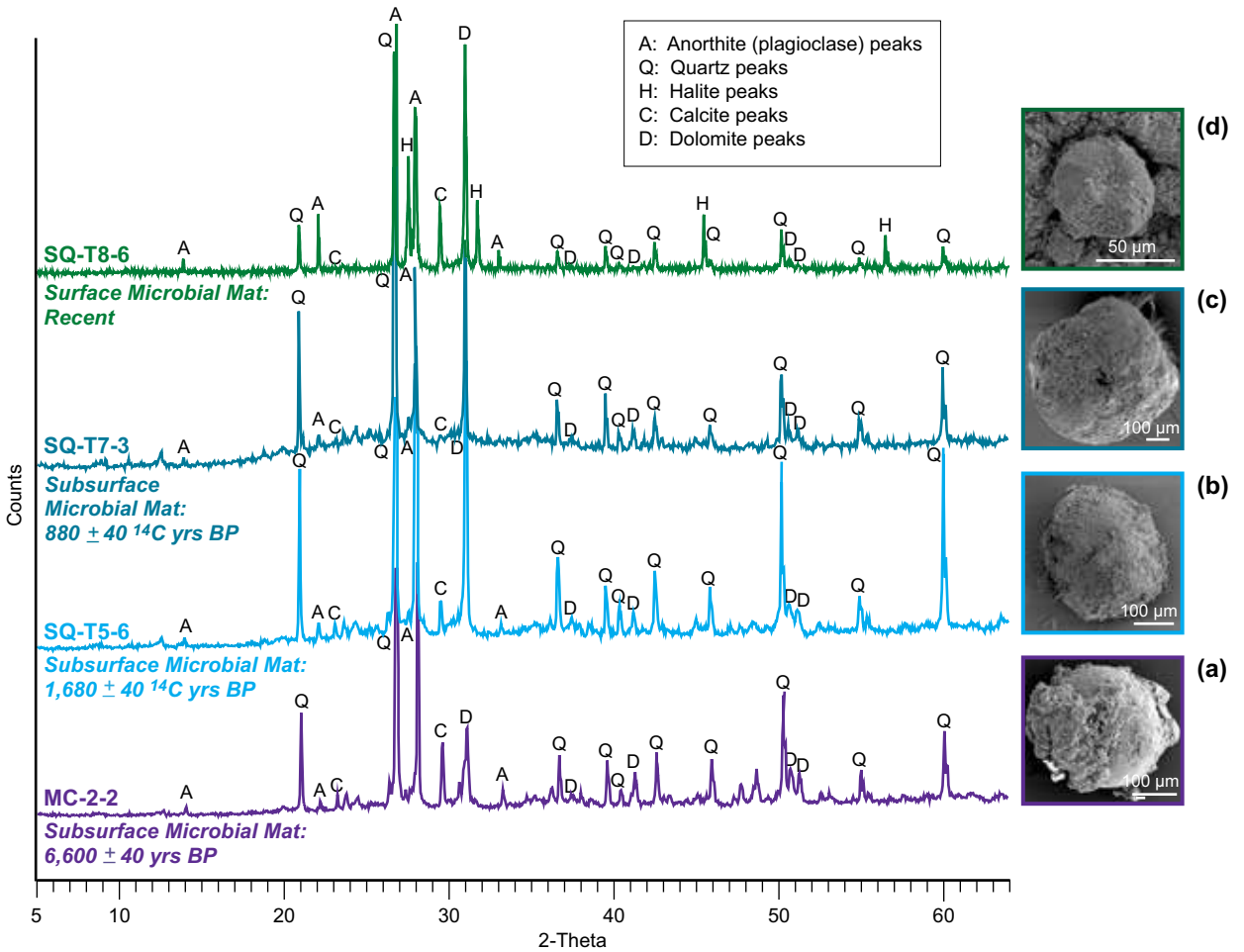

Figure 21: XRD spectra and SEM photomicrographs (modified after Bontognali, 2008, and Bontognali et al., 2010) comparing dolomite spheroids identified by SEM within the microbial mat studied at Mussafah Channel vertical section MC-2 (sample MC-2-2) with dolomite spheroids identified by SEM within two subsurface microbial mats (samples SQ-T5-6 and SQ-T7-3) and the present-day surface microbial mat (sample SQ-T8-6); studied in the vicinity of Al-Qanatir Island (Al-Dabbiya area), c. 80 km west of Abu Dhabi City (Strohmenger et al., 2010; Bontognali, 2008; Bontognali et al., 2010; see Figure 1b for location). All microbial mat samples show the same XRD spectra, no matter of the age or the amount of burial of the samples. XRD analyses and SEM photomicrographs provided by Tomaso Bontognali (ETH Zurich, Switzerland). For detailed description of trenches and cores SQ-T5, SQ-T7, and SQ-T8 see Strohmenger et al. (2010).

(a) Subsurface microbial mat (sample MC-2-2). Radiocarbon age: ca. 6,600 ^{14}C yrs BP. Depth: c. 75–85 cm below surface.

(b) Subsurface microbial mat (sample SQ-T5-6). Radiocarbon age: ca. 1,700 ^{14}C yrs BP. Depth: c. 15–30 cm below surface.

(c) Subsurface microbial mat (sample SQ-T7-3). Radiocarbon age: ca. 900 ^{14}C yrs BP. Depth: c. 10–35 cm below surface.

(d) Surface microbial mat (sample SQ-T8-6). Age: Recent. Depth: c. 0–5 cm below surface. Note that the dolomite spheroid is slightly smaller compared to those of the buried, older microbial mats (Figures 21a, 21b, and 21c).

The dolomite found within carbonates at Mussafah Channel is microcrystalline and below resolution by conventional petrogrographic thin section analysis (Figure 7e). Scanning electron microscope (SEM) and X-ray diffraction (XRD) analyses detect dolomite in samples from the microbial mat (sample MC-2-2; Figures 19a and 19b), the rooted lagoon (sample MC-2-4; Figures 19c and 19d), and the microbial-laminated lagoon (sample MC-2-6; Figures 19e and 19f). The dolomite displays authigenic spheroids composed of subhedral to euhedral dolomite rhombohedra. Dolomite mineralogy of both speroids and rhombohedra is proven by energy-dispersive X-ray spectrometer (EDX) analyses (Figures 20a, 20b, 20c, and 20d). XRD analyses and SEM photomicrographs comparing dolomite spheroids from the microbial mat of section MC-2 (sample MC-2-2) with dolomite spheroids studied by Bontognali (2008) and Bontognali et al. (2010; see Figure 1b for location) within two subsurface microbial mats (samples SQ-T5-6 and SQ-T7-3) and the present-day surface microbial mat (SQ-T8-6) in the vicinity of Al-Qanatir Island (Al-Dabbiya area), show the same XRD spectra and spherical morphologies (Figures 21a, 21b, 21c, and 21d). Like the dolomite identified in the modern day sabkha at Al-Qanatir Island (Strohmenger et al., 2004, 2007, 2008b, 2008c, 2010; Bontognali, 2008; Bontognali et al., 2010; see Figure 1b for location), the dolomite found at Mussafah Channel is interpreted to have precipitated as a consequence of mineral nucleation and growth within the extracellular polymeric substances (EPS) constituting the microbial mats (Bontognali, 2008; Bontognali et al., 2010). A microbial origin is inferred for the dolomite found in the microbial mat and the lagoonal deposits, but, most probably, also for the dolomite occurring in tidal-channel deposits and reworked Pleistocene dune deposits.

RESERVOIR QUALITY DISTRIBUTION AND CONNECTIVITY

The observed variations in texture and facies found at Mussafah Channel provide a rough analogue for lateral and vertical variations in reservoir quality observed in subsurface settings. Assuming that the primary variations in porosity and permeability are preserved in the subsurface, the textural and facies variations observed at the Mussafah Channel are a guide to reservoir continuity and quality. Figure 22 schematically displays the lateral and vertical texture and facies variations without the evaporitic (sabkha) overprint. The inferred reservoir quality of the different facies types are shown using hypothetical gamma-ray (GR) and neutron porosity (NPHI) log-curves. High-energy, coarse-grained, grain-dominated carbonate facies (grainstones and rudstones: tidal-channel, tidal-delta, and longshore beach bar and beach spit deposits) are interpreted to have low GR and high NPHI values due to low clay content and high interparticle porosity, respectively. Low energy, fine-grained, mud-dominated facies (packstones: rooted lagoonal and microbial-laminated lagonnal deposits) are interpreted to have higher GR and lower NPHI values due to higher clay/organic content and reduced interparticle porosity, respectively. The microbial mat deposits have high GR and high NPHI values due to the high organic content and bounded water, respectively. The fine-grained, carbonate-rich sandstones (reworked aeolian dune deposits) are interpreted to have low GR and higher NPHI values due to low clay content and high interparticle porosity, respectively. The hardgrounds are interpreted to have low GR and low NPHI values due to low clay content and cementation, respectively.

The grain-dominated facies at locations A (tidal-delta and tidal-bar deposits) and C, D, and E (tidal-channel and longshore beach bar and beach spit deposits) is expected to have good to excellent primary porosity (Figure 22). At location B, mud-dominated, rooted lagoonal and microbial-laminated lagoonal deposits (laterally intercalated between tidal-delta and tidal-bar deposits at location A and tidal-channel deposits at location C) show inferred low reservoir quality (Figure 22). Lateral connectivity between the good to excellent reservoir facies at location A and at locations C, D, and E is reduced due to the intercalated mud-dominated, rooted lagoonal and microbial-laminated lagoonal deposits (location B; Figure 22). Lateral connectivity also might be reduced between the juxtaposed tidal-channel deposits at location C and location E due to the occurrence of shingled hardgrounds and early cementation along the channel-cut (location D; Figure 22). The channel-cut surface might act as a baffle between positions C and E, as indicated by the low porosity peak displayed by the NPHI log-curve at location D (Figure 22).

Vertical connectivity is inferred to be reduced between the fine-grained tidal-channel deposits and the overlaying longshore beach bar and beach spit deposits (location E) due to the occurrence of a hardground at the boundary between the two grain-dominated deposits (Figure 22). The microbial mat as well as the hardground is interpreted to act as baffles or even barriers between the underlying

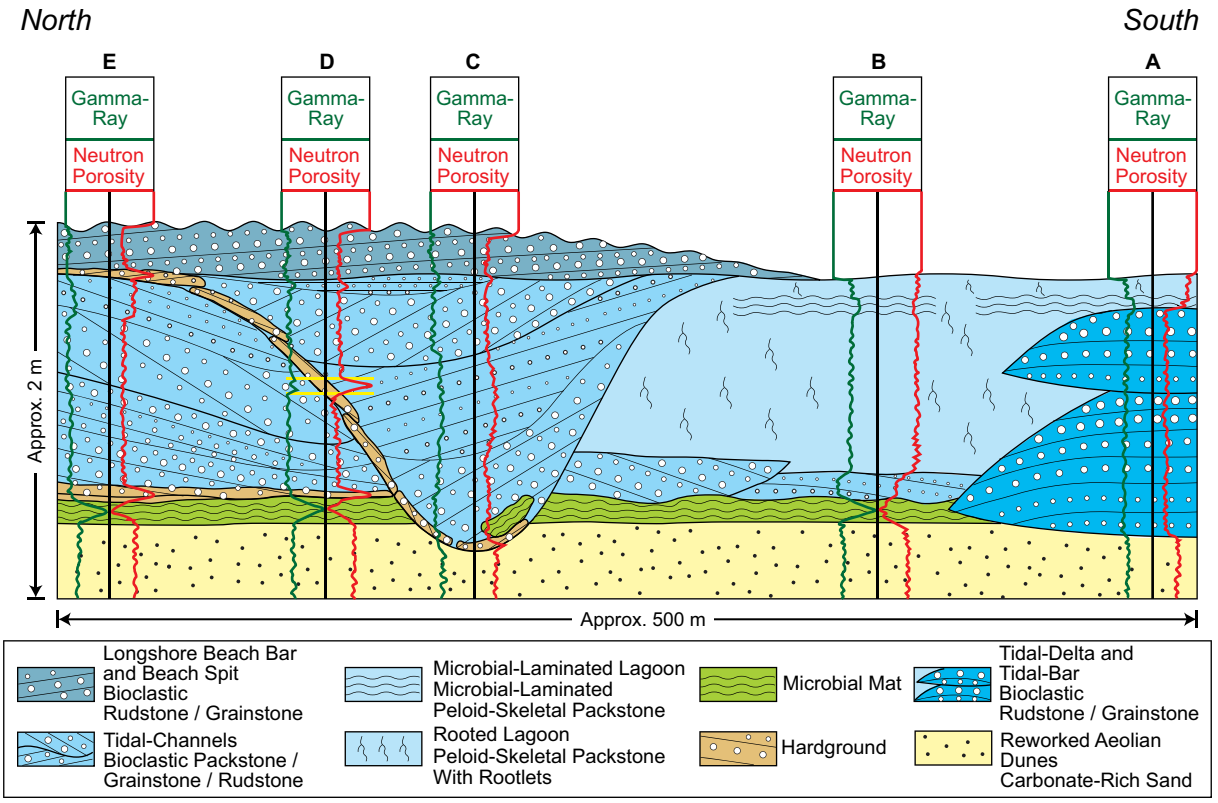

Figure 22: Sketch showing the facies-related reservoir quality distribution along the east wall of the Mussafah Channel. Hypothetical gamma-ray (increasing to the right) and neutron porosity (increasing to the left) log-curves, derived from exposure descriptions, are also displayed at locations A, B, C, D, and E. Displayed is the primary depositional facies without evaporitic (sabkha) overprint. See Figure 2 and text for further explanations.

porous carbonate-rich Pleistocene sands and the overlying porous Holocene grain-rich carbonates (locations D and E; Figure 19). Reduced connectivity might, however, exist between the Pleistocene carbonate-rich sands and the Holocene grain-rich carbonates of the tidal-channel that cuts into the underlying sands (location C). The connectivity would depend on the continuity/discontinuity of the intercalated hardground (Figure 22).

Of course, considering the evaporitic (sabkha) overprint (gypsum and anhydrite precipitation), the carbonate section above the microbial mat will act as a perfect seal for the underlying carbonate-rich sand after burial. All the gypsum will be likely transformed to anhydrite during burial (dewatering) when ambient temperature rises above 50–60 °C. In a hydrological open system with normal geothermal gradient this process is completed at a burial depth of c. 1,000 m (Warren, 1989, 1999, 2006).

The sketch displayed on Figure 22 only represents a snapshot in time but demonstrates the spatial complexity of modern shallow water carbonate systems, an important aspect to be considered for geological facies and reservoir quality modeling.

CONCLUSIONS

The man-made Mussafah Channel, southwest of the city of Abu Dhabi (Figure 1), is often cited as showing classical, text book like, sabkha anhydrite and gypsum exposures (Kening et al., 1990; Kening, 1990, 2009; Kirkham, 1997; Evans and Kirkham, 2002; Warren, 2006). This study concludes that most of the sediments are marine and formed during a Holocene sea-level rise c. 2–3 m above present-day sea level. The sediments have been extensively modified by evaporite growth, likely related to paleo-groundwater tables established during falling sea level (Figure 2).

Pleistocene reworked aeolian carbonate-rich sands (radiocarbon age: ca. 24,800–23,500 ^{14}C yrs BP) are unconformable overlain by a Holocene microbial mat (radiocarbon age: ca. 6,600–6,200^{14}C yrs BP), formed during the post-glacial Flandrian transgression that started around 18,000 ^{14}C yrs BP (Kassler, 1973; Lambeck, 1996; Lambeck et al., 2002). Above the microbial mat are sediments interpreted as rooted and microbial-laminated lagoonal, tidal-delta, and tidal-channel deposits, passing upward into longshore beach bar and beach spit deposits. The oldest Holocene sediments show a radiocarbon age of ca. 6,600 ^{14}C yrs BP (microbial mat deposits). The youngest Holocene sediments show a radiocarbon age of ca. 5,000 ^{14}C yrs BP (longshore beach bar and beach spit deposits) and are presently 2–3 m above mean sea level. During falling sea level, the succession was diagenetically overprinted by gypsum and anhydrite (sabkha-overprint; Figures 3, 6, 7, 8, 9, 10, 12, 14, 15, and 16).

The vertical facies successions, the lateral facies variations, and the diagenetic (evaporitic) overprint displayed at Mussafah Channel correspond to the shallow subtidal to supratidal arid depositional environments that can be observed along the present-day Abu Dhabi coastline (Figures 1c and 2). Thus, the sabkha sequence at Mussafah Channel represents a perfect training ground for teaching the importance of facies analysis (facies stacking patterns: "Walter's Law"; Walter 1893-94), diagenesis (cementation and dolomite, gypsum, and anhydrite formation) and stratigraphy/sequence stratigraphy (radiocarbon age-dating analysis/chronostratigraphic correlation).

Gypsum crystals are found within the Holocene carbonates, the microbial mat, and the underlying Pleistocene carbonate-rich sands (Figures 4b, 14a, 15a, 15b, 15c, 16a and 18). Gypsum crystals vary in size, shape, and color depending on the host sediment (Figure 18). They are interpreted as having formed at various paleo-groundwater tables, preserved as horizontal reddish horizons. These reddish (oxidized) horizons occur at different levels throughout the studied sections (up to c. 2 m above the present-day sea level) and are interpreted as reflecting seasonal and short term sea-level fluctuations (Figures 6, 7a, 8c, 8d, 9, 12a, 14a, 15c, and 16a). Thus supporting the interpretation that sea level was 2–3 m above present-day sea level ca. 5,000 years ago (radiocarbon age of the uppermost exposed carbonates, showing erosion on top; Figure 9).

Nodular anhydrite is present within the upper beds of the section (longshore beach bar and beach spit deposits), replacing previously precipitated gypsum crystals (Figure 14a). Displacive anhydrite forms folds (contorted or enterolithic/ptygmatic anhydrite; Figure 14b, and 15d) and teepee structures (Figure 14c).

Abu Dhabi sabkha evaporites were often used as analogues for ancient carbonate-evaporite dominated formations such as the Arab Formation (Wood and Wolfe, 1969; Leeder and Zeidan, 1977; Alsharhan and Kendall, 1994, 2002). However, thick bedded anhydrite deposits like those of the Upper Permian (Khuff and Zechstein formations) and the Upper Jurassic (Arab Formation) mostly represent salina- or saltern-type (Warren, 1983, 1989, 1999; Warren and Kendall, 1985; Kendall, 1992; Schreiber, 1988) rather than sabkha-type deposits (Al Silwadi et al., 1996; Strohmenger et al., 1996; Steinhoff and Strohmenger, 1999; Kirkham, 2004). Sabkha-type evaporites, like the ones described at the Mussafah Channel, are forming within the host rock (sediment-dominated), whereas salina-type evaporites represent subaqueous precipitations (evaporite-dominated), often containing vertically-oriented chevron-type crystals ("swallow-tail" anhydrite-after-gypsum).

High amounts of dolomite were found within rooted lagoonal and microbial-laminated lagoonal deposits (vertical sections MC-1 and MC-2: up to 50%; Figures 3a, 7a, 19c, 19d, 19e, and 19f). Dolomite is also quite abundant in all microbial mats (up to 17%; Figures 3a, 7a, 10a, 12a, 16a, 19a, and 19b), in most of the tidal-channel and tidal-channel/lagoonal deposits (up to 20%; Figures 10a, 12a, and 16a), and in some of the Pleistocene reworked carbonate-rich sands (up to 19%; Figures 3a, 12a, and 16a). SEM and EDX analyses (Figures 19 and 20) indicate that the dolomite occurs as authigenic spheroids composed of subhedral to euhedral dolomite rhombohedra (Figures 19 and 20). The dolomite identified within the microbial mat of studied section MC-2 (sample MC-2-2) shows the same XRD spectra and spherical morphologies (Figures 21a, 21b, 21c, and 21d) as the dolomite identified within two subsurface microbial mats (samples SQ-T5-6 and SQ-T7-3) and the present-day surface microbial mat (SQ-T8-6); previously studied in the vicinity of Al-Qanatir Island (Al-Dabbiya area; Strohmenger et al., 2010; Bontognali, 2008, Bontognali et al., 2010). Like the dolomite identified in the modern day

sabkha at Al-Qanatir Island (Strohmenger et al., 2004, 2007, 2008b, 2008c, 2010; Bontognali, 2008; Bontognali et al., 2010), the dolomite found at Mussafah Channel is interpreted to have precipitated as a consequence of mineral nucleation and growth within the extracellular polymeric substances (EPS) constituting the microbial mats (Bontognali, 2008; Bontognali et al., 2010). Furthermore, it is postulated that also the authigenic dolomite identified within the rooted and microbial-laminated lagoonal deposits, as well as the dolomite identified within the tidal-channel deposits and the reworked Pleistocene carbonate-rich sands is of microbial origin.

Facies-controlled reservoir quality varies considerably vertically and laterally along the studied channel walls (Figure 22). Excellent reservoir facies like tidal-delta and tidal-bar, as well as tidal-channel deposits (bioclastic grainstones and rudstones) grade laterally into rooted lagoonal and microbial-laminated lagoonal deposits (mud-dominated packstones) of low primary reservoir potential (Figure 22). In addition, intercalated hardgrounds may act as baffles or barrier to vertical and lateral reservoir connectivity (Figure 22). The observed facies and primary reservoir quality heterogeneities are important factors to be considered for geological facies and reservoir quality modeling of subsurface shallow water carbonates.

The discovery of whale bones at the Mussafah Channel site (Pierson et al., 2006; 2008) has added a new dimension to this location and has made it even more important and famous than before (Figure 17). Efforts should be taken to protect this Mussafah Channel site for future visits and studies. The unique geologic and palaeo-environmental importance of this site to geoscientists all over the world truly makes it a national treasure of the United Arab Emirates.

ACKNOWLEDGEMENTS

The authors gratefully acknowledge the management of Abu Dhabi Company for Onshore Oil Operations (ADCO), Zakum Development Company (ZADCO), and Abu Dhabi National Oil Company (ADNOC), Abu Dhabi for permission to publish this paper. Yousef A. Hamade, John Danial, and Issam Al-Haj (ADCO Drafting Department) are thanked for drafting the figures. Ozair A. Khan (ADCO Geodetics Department) is thanked for providing the satellite images.

We express our sincere appreciation to the management of ADCO for granting us the time and for financing this project.

We thank Tomaso Bontognali (ETH Zurich, Switzerland) for performing the dolomite XRD and EDX analyses and for providing the dolomite SEM photomicrographs. We extend our thanks to Chegjie Liu (EMEC, Houston, USA) for identifying the foraminifera and for identifying and photographing the sampled gastropods and pelecypods. Prof. Phil Rainbow (Natural History Museum, London, UK) is thanked for identifying the whale barnacles.

For very valuable discussions we would like to thank J.A. McKenzie and T. Bontognali (Zurich, Switzerland), C.G.St.C. Kendall (Columbia, USA), B.C. Schreiber (Seattle, USA), G. Evans (Jersey, UK), J.K. Warren (Muscat, Oman), F. Kenig (Chicago, USA), G. Shinn (St. Petersburg, USA), J. Jameson (Doha, Qatar), A. Kirkham (Safron Walden, UK), J. Stewart (London, UK), N. Larkin (Norwich, UK), S. Aspinall (Abu Dhabi, UAE), M. Beech (Abu Dhabi, UAE), and P. Hellyer (Abu Dhabi, UAE).

The paper benefited from the careful and constructive initial reviews of William L. Soroka (Abu Dhabi, UAE) and Jeremy Jameson (Doha, Qatar). We are also grateful to Nestor A. Buhay II for designing the final graphics and two anonymous GeoArabia reviewers for their comments and suggestions.

REFERENCES

Alsharhan, A.S. and C.G.St.C. Kendall 1994. Depositional setting of the Upper Jurassic Hith anhydrite of the Arabian Gulf: An analog to Holocene evaporites of the United Arab Emirates and Lake MacLeod of Western Australia. American Association of Petroleum Geologists Bulletin, v. 78, p. 1075-1096.

Alsharhan, A.S. and C.G.St.C. Kendall 2002. Holocene carbonate/evaporites of Abu Dhabi, and their Jurassic ancient analogs. In H.-J. Barth and B. Böer (Eds.), Sabkha Ecosystems. Volume I: The Arabian Peninsula and Adjacent Countries. Kluwer Academic Publishers, Dordrecht, p. 187-202.

Alsharhan, A.S., C.G.St.C. Kendall and G.L. Whittle 1998. Field trip guide to examine the Holocene carbonate/evaporites of Abu Dhabi, United Arab Emirates. UAE University Publications Department, Al Ain, 46 p.

Al Silwadi M.S., A. Kirkham, M.D. Simmons and B.N. Twombley 1996. New insights into regional correlation and sedimentology, Arab Formation (Upper Jurassic), offshore Abu Dhabi. GeoArabia, v. 1, no. 1, p. 6-27.

Baltzer F., F. Kenig, R. Boichard, J.-C. Plaziat and B.H. Purser 1994. Organic matter distribution, water circulation and dolomitization beneath the Abu Dhabi sabkha (United Arab Emirates). In B. Purser, M. Tucker and D. Zenger (Eds.), Dolomites. A Volume in Honour of Dolomieu. International Association of Sedimentologists, Special Publication 21, p. 409-427.

Bontognali, T.R.R. 2008. Microbial dolomite formation within exopolymeric substances. PhD Thesis, ETH Zurich, no. 17775, 139 p.

Bontognali, T.R.R., C. Vasconcelos, R.J.Warthmann, C. Dupraz, S.M. Bernasconi and J.A. McKenzie 2008. Microbes produce nanobacteria-like structures, avoiding cell entombment. Geology, v. 36, no. 8, p. 663-666.

Bontognali, T.R.R., C. Vasconcelos, R.J. Warthmann, S.M. Bernasconi, C. Dupraz, C.J. Strohmenger and J.A. McKenzie 2010. Dolomite formation within microbial mats in the coastal sabkha of Abu Dhabi, United Arab Emirates. Sedimentology (in press).

Butler, G.P. 1969. Modern evaporite deposition and geochemistry of co-existing brines, the sabkha, Trucial Coast, Arabian Gulf. Journal of Sedimentary Petrology, v. 39, no. 1, p. 70-89.

Butler, G.P. 1970. Holocene gypsum and anhydrite of the Abu Dhabi sabkha, Trucial coast: An alternative explanation of origin. Third Symposium on Salt. North Ohio Geological Society, v. 1, p. 120-152.

Butler, G.P., P.M. Harris and C.G.St.C. Kendall 1982. Recent evaporites from the Abu Dhabi coastal flats. In C.R. Handford, R.G. Loucks and G.R. Davies (Eds.), Depositional and Diagenetic Spectra of Evaporites – A Core Workshop. SEPM (Society for Sedimentary Geology), Core Workshop 3, p. 33-64.

Curtis R., G. Evans, D.J.J. Kinsman and D.J. Shearman 1963. Association of dolomite and anhydrite in the recent sediments of the Persian Gulf. Nature, v. 197, p. 679-680.

Decho, A.W. 1990. Microbial exopolymer secretions in ocean environments: Their role(s) in food webs and marine processes. Oceanography and marine biology: An annual review, v. 28, p. 73 -153.

Dunham, R.J. 1962. Classification of carbonate rocks according to depositional texture. In W.E Ham. (Ed.), Classification of Carbonate Rocks. American Association of Petroleum Geologists, Memoir 1, p. 108-121.

Embry, A.F. and J.E. Klovan 1971. A Late Devonian reef tract on Northeastern Banks Island, NWT. Canadian Petroleum Geology Bulletin, v. 19, p. 730-781.

Evans, G. 1995. The Arabian Gulf: A modern carbonate-evaporite factory; a review. Cuadernos de Geología Ibérica, v. 19, p. 61-96.

Evans, G. and A. Kirkham 2002. The Abu Dhabi sabkha. In H.-J. Barth and B. Böer (Eds.), Sabkha Ecosystems. Volume I: The Arabian Peninsula and Adjacent Countries. Kluwer Academic Publishers, Dordrecht, p. 7-20.

Evans, G., V. Schmidt, P. Bush and H. Nelson 1969. Stratigraphy and geologic history of the Sabkha, Abu Dhabi, Persian Gulf. Sedimentology, v. 12, no. 1-2, p. 145-159.

Homewood, P., V. Vahrenkamp, M. Mettraux, J. Mattner, B. Vlaswinkel, H. Droste and A. Kwarteng 2007. Bar Al Hikman: A modern carbonate and outcrop analogue in Oman for Middle East Cretaceous fields. First Break, v. 25, no. 11, p. 55-61.

Hsü, K.J. and C. Siegenthaler 1969. Preliminary experiments on hydrodynamic movement induced by evaporation and their bearing on the dolomite problem. Sedimentology, v. 12, no. 1-2 , p. 11-25.

Jameson J., C.J. Strohmenger and M. Kozar 2008. A comparative study of facies and diagenesis of Arabian Plate sabkhas (Abstract). GEO 2008 Middle East Conference and Exhibition, Bahrain, GeoArabia, v. 13, no. 1, 178 p.

Kassler, P. 1973. The structural and geomorphic evolution of the Persian Gulf. In B.H. Purser (Ed.), The Persian Gulf. Holocene Carbonate Sedimentation and Diagenesis in a Shallow Epicontinental Sea. Springer-Verlag, Berlin, p. 11-32.

Kendall, A.C. 1992. Evaporites. In R.G. Walker and N.P. James (Eds.), Facies Models. Response to Sea-Level Change. Geological Association of Canada, St. John's, p. 375-409.

Kendall, C.G.St.C. and P.A. d'E. Skipwith 1968. Recent algal mats of a Persian Gulf lagoon. Journal of Sedimentary Petrology, v. 38, no. 4, p. 1040-1058.

Kendall, C.G.St.C. and P.A. d'E. Skipwith 1969. Geomorphology of a recent shallow-water carbonate province: Khor Al Bazam, Trucial Coast, Southwest Persian Gulf. Geological Society of America Bulletin, v. 80, no. 5, p. 865-892.

Kendall, C.G.St.C. and J.K. Warren 1988. Peritidal evaporites and their sedimentary assemblages. In B.C. Schreiber (Ed.), Evaporites and Hydrocarbons. Columbia University Press, New York, p. 66-138.

Kendall, C.G.St.C., A.S. Alsharhan and A. Cohen, 2002. The Holocene tidal flat complex of the Arabian Gulf coast of Abu Dhabi. In H.-J. Barth and B. Böer (Eds.), Sabkha Ecosystems. Volume I: The Arabian Peninsula and Adjacent Countries. Kluwer Academic Publishers, Dordrecht, p. 21-35.

Kendall, C.G.St.C., J.L. Sadd and A. Alsharhan 1994. Holocene marine cement coatings on beach-rocks of the Abu Dhabi coastline (UAE); analogs for cement fabrics in ancient limestones. Carbonates and Evaporites, v. 9, no. 2, p. 119-131.

Kenig, F. 1991. Sédimentation, distribution et diagenèse de la matière organique dans un environnement carbonaté hypersalin: Le système lagune-sabkha d'Abu Dhabi. PhD Thesis, Université d'Orléans, Orleans, 327 p.

Kenig, F. 2010. Distribution of organic matter in the transgressive and regressive Holocene sabkha sediments of Abu Dhabi, United Arab Emirates. In A. Alsharhan and C.G.St.C Kendall (Eds.), Quaternary Carbonate and Evaporite Sedimentary Facies and their Ancient Analogues. International Association of Sedimentologists, Special Publication (in press).

Kenig, F., A.Y. Huc, B.H. Purser and J.L. Oudin 1990. Sedimentation, distribution and diagenesis of organic-matter in a recent carbonate environment, Abu-Dhabi, UAE. Organic Geochemistry, v. 16, p. 735-747.

Kinsman, D.J.J. 1969. Modes of the formation, sedimentary associations, and diagnostic features of shallow-water and supratidal evaporites. American Association of Petroleum Geologists Bulletin, v. 53, no. 4, p. 30-840.

Kinsman, D.J.J. and R.K. Park 1976. Algal belt and coastal sabkha evolution, Trucial Coast, Persian Gulf. In M.R. Walter (Ed.), Stromatolites. Developments in Sedimentology, v. 20, p. 421-433.

Kirkham, A. 1997. Shoreline evolution, aeolian deflation and anhydrite distribution of the Holocene, Abu Dhabi. GeoArabia, v. 2, no. 4, p. 403-416.

Kirkham, A. 1998. A Quaternary proximal foreland ramp and its continental fringe, Arabian Gulf, UAE. In V.P. Wright and T.P. Burchette (Eds.), Carbonate Ramps. Geological Society London, Special Publication 149, p. 15-41.

Kirkham, A. 2004. Patterned dolomites: Microbial origins and clues to vanished evaporites in the Arab Formation, Upper Jurassic, Arabian Gulf. In C.J.R. Braithwaite, G. Rizzi and G. Darke (Eds.), The Geometry and Petrogenesis of Dolomite Hydrocarbon Reservoirs. Geological Society, London, Special Publication 235, p. 301-308.

Leeder, M.R. and R. Zeidan 1977. Giant late Jurassic sabkhas of Arabian Tethys. Nature, v. 268, p. 42-44.

McKenzie, J.A. 1981. Holocene dolomitization of calcium carbonate sediments from the coastal sabkhas of Abu Dhabi, UAE: A stable isotope study. Journal of Geology, v. 89, p. 185-198.

Lambeck, K. 1996. Shoreline reconstructions for the Persian Gulf since the last glacial maximum. Earth and Planetary Science Letters, 142, p. 43-57.

Lambeck, K., T.M. Esat and E.-K. Potter 2002. Links between climate and sea levels for the past three million years. Nature, 419, p. 199-206.

McKenzie, J.A., K.J. Hsü and J.F. Schneider 1980. Movement of subsurface waters under the sabkha, Abu Dhabi, UAE, and its relation to evaporative dolomite genesis. In D.H. Zenger, J.B. Dunham and R.L. Ethington (Eds.), Concepts and Models of Dolomitization, SEPM (Society for Sedimentary Geology), Special Publication 28, p. 11-30.

Müller, D.W., J.A. McKenzie and P.A. Mueller 1990. Abu Dhabi sabkha, Persian Gulf, revisited: Application of strontium isotopes to test an early dolomitization model. Geology, v. 18, no. 7, p. 618-621.

Park, P.K. 1977. The preservation potential of some recent stromatolites. Sedimentology, v. 24, no. 4, p. 485-506.

Patterson, R.J. and D.J.J. Kinsman 1977. Marine and continental groundwater sources in a Persian Gulf coastal sabkha. In S.H. Frost, M.P. Weiss and J.B. Saunders (Eds.), Reefs and Related Carbonates – Ecology and Sedimentology. American Association of Petroleum Geologists, Studies in Geology 4, p. 381-397.

Patterson, R.J. and D.J.J. Kinsman 1981. Hydrologic framework of a sabkha along Arabian Gulf. American Association of Petroleum Geologists Bulletin, v. 65, no. 8, p. 1457-1475.

Patterson, R.J. and D.J.J. Kinsman 1982. Formation of diagenetic dolomite in coastal sabkha along Arabian (Persian) Gulf. American Association of Petroleum Geologists Bulletin, v. 66, no. 1, p. 28-43.

Peebles, R.G., M. Shaner and A. Kirkham 1995. Arid coastline depositional environments. An American Association of Petroleum Geologists International Field Seminar. A fieldguide to the Abu Dhabi Coast, United Arab Emirates, 45 p.

Pierson, B.J., S. Aspinall and K. Al-Mehsin 2006. Fossil whale bones in Abu Dhabi's coastal sabkha. First Break, v. 24, no. 11, p. 3-4.

Pierson, B.J., S. Aspinall and K. Al-Mehsin 2008. Fossil whale skeleton in Abu Dhabi's coastal sabkha. Abstracts of the First and Second International Conference on Evaporites, 2004 and 2006, Abu Dhabi, United Arab Emirates. GeoArabia, v. 13, no. 2, p. 170.

Purser, B.H. 1973. The Persian Gulf. Holocene carbonate sedimentation and diagenesis in a shallow epicontinental sea. Springer-Verlag, Berlin, 471 p.

Sanford, W.E. and W.W. Wood 2001. Hydrology of the coastal sabkhas of Abu Dhabi, United Arab Emirates. Hydrogeological Journal, v. 9, p. 358-366.

Schneider, F.J. 1975. Recent tidal deposits, Abu Dhabi, UAE, Arabian Gulf. In R.N. Ginsburg (Ed.), Tidal Deposits. A Casebook of Recent Examples and Fossil Counterparts. Springer-Verlag, Berlin, p. 209-214.

Schreiber, B.C. 1988. Sabaqueous evaporite deposition. In B.C. Schreiber (Ed.), Evaporites and Hydrocarbons. Columbia University Press, New York, p. 182-255.

Shearman, D.J. 1983. Syndepositional and late diagenetic alteration of primary gypsum to anhydrite. Sixth International Symposium on Salt, Toronto, v. 1, p. 41-50.

Shinn, E.A. 1973. Carbonate coastal accretion in the area of longshore transport, NE Qatar. In B.H. Purser (Ed.), The Persian Gulf. Holocene Carbonate Sedimentation and Diagenesis in a Shallow Epicontinental Sea. Springer-Verlag, Berlin, p. 179-191.

Shinn, E.A. 1983. Tidal flat environment. In P.A. Scholle, D.G. Bebout and C.H. Moore (Eds.), Carbonate Depositional Environments. American Association of Petroleum Geologists, Memoir 33, p. 171-210.

Shinn, E.A. 2008. Spits, beaches, beachrock, tidal channels, evaporitic carbonates, and longshore-currents: Return to Qatar. Abstracts of the First and Second International Conference on Evaporites, 2004 and 2006, Abu Dhabi, United Arab Emirates. GeoArabia, v. 13, no. 2, p. 174-175.

Steinhoff, I. and C. Strohmenger 1999. Facies differentiation and sequence stratigraphy in ancient evaporite basins – an example from the Basal Zechstein (Upper Permian of Germany). Carbonates and Evaporites, v. 14, no. 2, p. 146-181.

Strohmenger, C., M. Antonini, G Jäger, K. Rockenbauch and C. Strauss 1996. Zechstein 2 carbonate reservoir facies prediction in relation to Zechstein sequence stratigraphy (Upper Permian, Northwest Germany): An integrated approach. Bulletin des Centres de Recherches Exploration-Production Elf-Aquitaine, v. 20, no. 1, p. 1-35.

Strohmenger, C.J., A. Al-Mansoori, H. Shebl, O. Al-Jeelani, I. Al-Hosani, K. Al-Mehsin and A. Al-Shamry 2004. Modern carbonate-evaporite depositional environments of Abu Dhabi (UAE). Unpublished field trip guide book, 11th ADIPEC Meeting, First International Evaporite Conference, Abu Dhabi.

Strohmenger, C.J., H. Shebl, A. Al-Mansoori, K. Al-Mehsin, O. Al-Jeelani, I. Al-Hosani, A. Al-Shamry and S. Al-Baker 2007. Depositional environment and sea-level history of the Abu Dhabi sabkha in the vicinity of Al-Qanatir Island, United Arab Emirates (Abstract). GEO 2006 Middle East Conference and Exhibition, Bahrain. GeoArabia, v. 12, no. 2, p. 219 p.

Strohmenger, C.J., A. Al-Mansoori, O. Al-Jeelani, A. Al-Shamry, I. Al-Hosani, H. Shebl and K. Al-Mehsin 2008a. The vertical sabkha sequence at Mussafah Channel, Abu Dhabi, United Arab Emirates (Abstract). GEO 2008 Middle East Conference and Exhibition, Bahrain. GeoArabia, v. 13, no. 1, p. 241.

Strohmenger, C.J., H. Shebl, A. Al-Mansoori, K. Al-Mehsin, O. Al-Jeelani and I. Al-Hosani 2008b. Facies stacking patterns and sea-level history of the Abu Dhabi sabkha in the vicinity of Al-Qanatir Island, United Arab Emirates. Abstracts of the First and Second International Conference on Evaporites, 2004 and 2006, Abu Dhabi, United Arab Emirates. GeoArabia, v. 13, no. 2, p. 176.

Strohmenger, C.J., A. Al-Mansoori, O. Al-Jeelani, I. Al-Hosani, A. Al-Shamry, H. Shebl, K. Al-Mehsin and S. Al-Baker 2008c. The arid supratidal to shallow subtidal environment: A case study from the Abu Dhabi sabkha (United Arab Emirates). American Association of Petroleum Geologists 2008 Annual Convention and Exhibition, San Antonio, Abstracts, v. 17, p. 197.

Strohmenger C.J., H. Shebl, A. Al-Mansoori, K. Al-Mehsin, O. Al-Jeelani, I. Al-Hosani, A. Al-Shamry and S. Al-Baker 2010. Facies stacking patterns in a modern arid environment: A case study of the Abu Dhabi sabkha in the vicinity of Al-Qanatir Island, United Arab Emirates. In A. Alsharhan and C.G.St.C Kendall (Eds.), Quaternary Carbonate and Evaporite Sedimentary Facies and their Ancient Analogues. International Association of Sedimentologists, Special Publication (in press).

van Lith, Y., R. Warthmann, C. Vasconcelos and J.A. McKenzie 2003a. Microbial fossilization in carbonate sediments: A result of the bacterial surface involvement in dolomite precipitation. Sedimentology, v. 50, no. 2, p. 237-245.

van Lith, Y, R., Warthmann, C. Vasconcelos and J.A. McKenzie 2003b. Sulphate-reducing bacteria induce low-temperature Ca-dolomite and high Mg-calcite formation. Geobiology, v. 1, p. 71-79.

Vasconcelos, C. and J.A. McKenzie 1997. Microbial mediation of modern dolomite precipitation and diagenesis under anoxic conditions (Lagoa Vermelha, Rio de Janeiro, Brazil). Journal of Sedimentary Research, v. 67, no. 3, p. 378-390.

Vasconcelos, C., J.A. McKenzie, S. Bernasconi, D. Grujic and A.J. Tien 1995. Microbial mediation as a possible mechanism for natural dolomite formation at low temperatures. Nature, v. 377, p. 220-222.

Vasconcelos, C., J.A. McKenzie, R. Warthmann and S.M. Bernasconi 2005. Calibration of the $\delta^{18}O$ paleothermometer for dolomite precipitated in microbial cultures and natural environments. Geology, v. 33, no. 4, p. 317-320.

Walther, J. 1893-94. Einleitung in die Geologie als historische Wissenschaft. Gustav Fischer Verlag, Jena, v. 1-3, 1055 p.

Wanless, H.R., E.A. Burton and J. Dravis 1981. Hydrodynamics of carbonate fecal pellets. Journal of Sedimentary Research, v. 51, no. 1, p. 27-36.

Warren, J.K. 1983. On the significance of evaporite lamination. Sixth International Symposium on Salt, Toronto, v. 1, p. 161-170.

Warren, J.K. 1989. Evaporite sedimentology. Prentice Hall Advanced Reference Series, New Jersey, 285 p.

Warren, J.K. 1991. Sulfate dominated sea-marginal and platform evaporative settings. In J.L. Melvin (Ed.), Evaporites, Petroleum and Mineral Resources. Developments in Sedimentology, v. 50, Elsevier, Amsterdam, p. 477-533.

Warren, J.K. 1999. Evaporites. Their evolution and economics. Blackwell Science Ltd., Oxford, 438 p.

Warren, J.K. 2006. Evaporites: Sediments, resources and hydrocarbons. Springer-Verlag, Berlin, 1035 p.

Warren, J.K. and C.G.St.C. Kendall 1985. Comparison of sequences formed in marine sabkha (subaerial) and salina (subaqueous) settings – modern and ancient. American Association of Petroleum Geologists Bulletin, v. 69, no. 6, p. 1013-1023.

Warthmann, R., Y. van Lith, C. Vasconcelos, J.A. McKenzie and A.M. Karpoff 2000. Bacterially induced dolomite precipitation in anoxic culture experiments. Geology, v. 28, no. 12, p. 1091-1094.

Wells, A.J. 1962, Recent Dolomite in the Persian Gulf: Nature, v. 194, p. 274-275.

Wenk, H.R., M. Hu and S. Frisia 1993. Partially disordered dolomite; microstructural characterization of Abu Dhabi sabkha carbonates. American Mineralogist, v. 78, p. 769-774.

Wood, W.W. and W.E. Sanford 2002. Hydrology and solute chemistry of the coastal-sabkha aquifer in the Emirate of Abu Dhabi. In H.-J. Barth and B. Böer (Eds.), Sabkha Ecosystems. Volume I: The Arabian Peninsula and Adjacent Countries. Kluwer Academic Publishers, Dordrecht, p. 173-185.
Wood, W.W., W.E. Sanford and A.R.S. Al Habshi 2002. Source of solutes to the coastal sabkha of Abu Dhabi. Geological Society of America Bulletin, v. 114, p. 259-268.
Wood, W.W., W.E. Sanford and S.K. Frape 2005. Chemical openness and potential for misinterpretation of the solute environment of coastal sabkhat. Chemical Geology, v. 215, p. 361-372.
Wood, G.V. and M.J. Wolfe 1969. Sabkha cycles in the Arab/Darb Formation off the Trucial Coast of Arabia. Sedimentology, v. 12, p. 165-191.
Wright, D.T. and D. Wacey 2005. Precipitation of dolomite using sulphate-reducing bacteria from the Coorong Region, South Australia: Significance and implications. Sedimentology, v. 52, no. 5, p. 987-1008.

ABOUT THE AUTHORS

Christian J. Strohmenger *received a Diploma in Geology from the University of Giessen (1983) and a PhD in Sedimentology from the University of Heidelberg, Germany (1988). From 1989 to 1990 he worked as a Research Assistant in carbonate sedimentology and sequence stratigraphy at the University of Geneva, Switzerland. He joined BEB Erdgas und Erdoel GmbH, Hanover, Germany (now ExxonMobil Production Germany, EMPG) in 1990 working as a Carbonate Sedimentologist and Seismic Interpreter. From 1996 to 2002 he was with ExxonMobil Exploration Company in Houston, Texas where he worked on Mesozoic and Paleozoic carbonate and sandstone reservoirs of Kuwait and Saudi Arabia. Christian was seconded to Abu Dhabi Company for Onshore Oil Operations (ADCO), United Arab Emirates in 2002 working as a Carbonate Stratigraphy Specialist until 2009. Since early 2009 Christian has been working for ExxonMobil Oil Indonesia, Jakarta as a Carbonate Advisor. His main interests are carbonate sequence stratigraphy, sedimentology, and reservoir quality prediction. Christian is a member of AAPG, SEPM, GSA, IAS, and ESG.*

christian.j.strohmenger@exxonmobil.com

Abdulla Al-Mansoori *graduated from the Al-Ain University, United Arab Emirates, with a BSc in Geology in 1995. During this time he also worked as a Core Store Supervisor for Abu Dhabi Company for Onshore Oil Operations (ADCO). After his graduation, Abdulla was appointed to ADCO's Petroleum Development Department (PDD) as a Geologist. From 1995 to 1999 he carried out various assignments pertinent to well-site geological operations, covering vertical, deviated and horizontal wells, both in exploration and production. Since 1999 Abdulla has worked as a Reservoir Geologist on various reservoir characterization studies. During an eighteen month cross-posting with ExxonMobil Exploration and Research Companies in Houston, USA (2005 to 2006), he worked on regional, high-resolution sequence stratigraphic correlations of Cretaceous reservoirs, integrating subsurface, outcrop, and 3-D seismic data. Abdulla is currently involved in a PhD program at the University of Tuebingen, Germany. His main interests are carbonate sequence stratigraphy, reservoir characterization, and regional geology. Abdulla is a member of AAPG, SPE, and ESG.*

amansoori@adco.ae

Omar Al-Jeelani *received a BSc in Geology from the University in Al-Ain, United Arab Emirates (1993). He joined Abu Dhabi National Oil Company (ADNOC) in 1993 and was seconded to Abu Dhabi Company for Onshore Oil Operation (ADCO) in 1995, working as an Operation Geologist in the Exploration and Production Department. From 1995 to 2002 he worked as a Reservoir Geologist and from 2002 to 2005 as a Geological Modeler in ADCO's Petroleum Development Department (PDD). Omar spent one year on temporary assignment with Shell E&P International in The Hague, Netherlands (2000 to 2001) where he was involved in 3-D modeling and well-log evaluation. Since 2007 he has been Team Leader with the Reserves Development Division (RDD). His main interests are carbonate sequence stratigraphy and carbonate reservoir modeling. Omar is a member of AAPG, SPE, and ESG.*

ojeelani@adco.ae

Ali Al-Shamry *graduated from the Al-Ain University, United Arab Emirates with a BSc in Geology in 1982 and joined Abu Dhabi Company for Onshore Oil Operations (ADCO) the same year. He was appointed to the Geology Department as Operation and Review Geologist and took various assignments pertinent to well site geological operations covering vertical, deviated, and horizontal wells in both exploration and production from 1987 to 1997. Since 1997 Ali has been working as a Senior Operation Geologist. He supports all ADCO Teams in the Reserves Development Division (RDD) as a specialist for coring and SCAL analyses. His main interests are well-site operation, carbonate sedimentology, and regional geology. Ali is a member of SPE and ESG.*

ashamry@adco.ae

Ismail A. Al-Hosani *is a Reservoir Geologist with the Reserves Development Division (RDD) of the Abu Dhabi Company for Onshore Oil Operations (ADCO), United Arab Emirates. He holds a BSc in Geology from the University of Al-Ain, United Arab Emirates (1995) and a MSc in Science Education from the Ohio University, USA (1998). Ismail joined ADCO in 1999 working as an Operation Geologist. Since 2002 he has worked as a reservoir geologist with focus on sequence stratigraphy, sedimentology, and reservoir quality prediction of Cretaceous reservoirs. Currently Ismail is involved in 3-D geologic modeling of Cretaceous reservoirs. His main interests are carbonate sedimentology and sequence stratigraphy. He is a member of AAPG, SPE, and ESG.*

alhosani@adco.ae

Khalil Al-Mehsin *has 17 years of experience in the petroleum industry and is currently working as a Manager for the Geoscience Department (Exploration Division) at Abu Dhabi National Oil Company (ADNOC). He received a BSc in Geology from Al-Ain University, United Arab Emirates in 1990 and joined ADNOC the same year. Khalil was seconded to Abu Dhabi Company for Onshore Oil Operations (ADCO) from 1991 to 2004. During this period he worked as operation geologist (1991 to 1995), reservoir geologist (1995 to 1998), and carbonate sedimentologist (2000 to 2004). From 1998 to 2000 Khalil was on a temporary assignment with Shell E&P International in The Hague, Netherlands. He worked with the technology applications and research group, as well as with the carbonate team. In 2004 he returned to ADNOC working in the Exploration Division. His main interests are carbonate sequence stratigraphy and reservoir characterization. Khalil is a member of AAPG, SPE, and ESG.*

kalmehsin@adnoc.com

Hesham Shebl *is a Sedimentologist with Zakum Development Company (ZADCO), Abu Dhabi, United Arab Emirates. He received a BSc degree from the Ain Shams University of Cairo, Egypt in 1980 and a MSc from the King Fahd University of Petroleum and Minerals of Dhahran, Saudi Arabia in 1989. Prior to joining ZADCO in 2000, Hesham worked with Core Laboratories as a Senior Sedimentologist from 1993 to 2000. His main areas of interest are carbonate reservoir characterization and sequence stratigraphy. Hesham is a member of AAPG, SPE, SCA, and ESG.*

hshebl@zadco.ae

Manuscript Received December 31, 2008

Revised June 3, 2009

Accepted June 6, 2009

Press version proofread by the authors on December 11, 2009